# CLIMATE DIAGNOSTICS BULLETIN

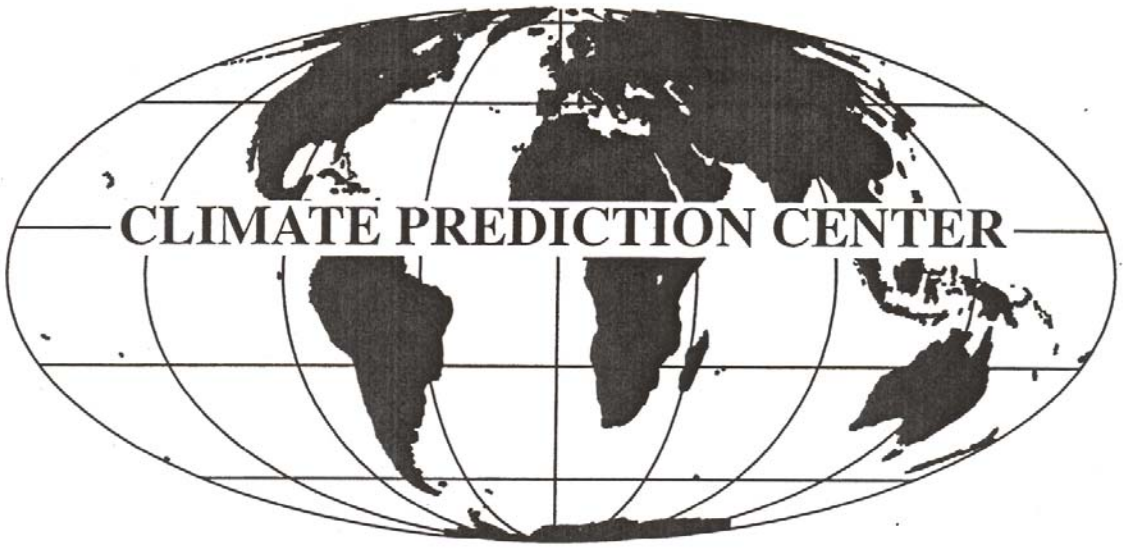


# FEBRUARY 2018

## NEAR REAL-TIME OCEAN / ATMOSPHERE

## Monitoring, Assessments, and Prediction

**U.S. DEPARTMENT OF COMMERCE**
**National Oceanic and Atmospheric Administration**
**National Weather Service**

**National Centers for Environmental Prediction**

# CLIMATE DIAGNOSTICS BULLETIN


## CLIMATE PREDICTION CENTER
**Attn: Climate Diagnostics Bulletin**
**Room 3116, NCWCP**
**5830 University Research Court**
**College Park, MD 20740**



**Chief Editor:** Gerald D. Bell
**Editors:** Wei Shi, Michelle L'Heureux, and Michael Halpert
**Bulletin Production:** Wei Shi

**ExternalCollaborators:**

Center for Ocean-Atmospheric Prediction Studies (COAPS)
Cooperative Institute for Research in the Atmosphere (CIRA)
Earth & Space Research
International Research Institute for Climate and Society (IRI)
Joint Institute for the Study of the Atmosphere and Ocean (JISAO)
Lamont-Doherty Earth Observatory (LDEO)
NOAA-CIRES, Climate Diagnostics Center
NOAA-AOML, Atlantic Oceanographic and Meteorological Laboratory
NOAA-NESDIS-STAR, Center for Satellite Applications and Research
NOAA-NDBC, National Data Buoy Center
Scripps Institution of Oceanography


**Software:** Most of the bulletin figures generated at CPC are created using the Grid Analysis and Display System (GrADS).

**- Climate Diagnostics Bulletin available on the World Wide Web**

The CDB is available on the World Wide Web. The address of the online version of the CDB is:

**http://www.cpc.ncep.noaa.gov/products/CDB**

If you have any problems accessing the bulletin, contact Dr. Wei Shi by E-mail:

*Wei.Shi@noaa.gov*

# Table of Contents

FIGURE

# Tropical Highlights - February 2018

Sea surface temperatures (SSTs) during February 2018 remained below-average across the central and eastern equatorial Pacific (Fig. T18, Table T2). The latest monthly Niño indices were -0.2°C for the Niño 4 region, -0.9°C for the Niño 3.4 region, and -0.6°C for the Niño 1+2 region (Table T2, Fig. T5). The depth of the oceanic thermocline (measured by the depth of the 20°C isotherm) was slightly below-average over the eastern equatorial Pacific (Figs. T15, T16), and the corresponding sub-surface temperatures were 0-1°C below average (Fig. T17).

Also during February, the lower-level wind anomalies were westerly across the western and central equatorial Pacific while the upper-level westerly winds were above-average over the eastern equatorial Pacific (Table T1, Figs. T20, T21). Meanwhile, convection was suppressed over Indonesia and east-central equatorial Pacific and enhanced over the far western and west-central equatorial Pacific (Figs. T25, E3). Collectively, these oceanic and atmospheric anomalies reflect weakening La Niña conditions.

For the latest status of the ENSO cycle see the ENSO Diagnostic Discussion at:
http://www.cpc.ncep.noaa.gov/products/analysis_monitoring/enso_advisory/index.html

| Month | SLP Anomalies | | Tahiti minus Darwin SOI | 850-hPa Zonal Wind Index | | | 200-hPa Wind Index | OLR Index |
|---|---|---|---|---|---|---|---|---|
| | Tahiti | Darwin | | 5N-5S 135E-180 | 5N-5S 175W-140W | 5N-5S 135W-120W | 5N-5S 165W-110W | 5N-5S 160E-160W |
| FEB 18 | -0.8 | 0.2 | -0.5 | -1.2 | -0.3 | 0.1 | 0.7 | 0.0 |
| JAN 18 | 0.1 | -1.9 | 1.1 | 1.4 | 0.8 | 0.1 | 0.9 | 1.8 |
| DEC 17 | -0.3 | -0.1 | -0.1 | 0.5 | 0.4 | -0.1 | 0.3 | 0.9 |
| NOV 17 | 0.2 | -1.5 | 0.9 | 0.8 | 0.9 | 0.2 | 1.0 | 1.1 |
| OCT 17 | 0.3 | -1.4 | 0.9 | 0.6 | 0.3 | -0.4 | 1.0 | 0.7 |
| SEP 17 | 1.2 | 0.1 | 0.6 | 1.2 | 0.2 | 0.0 | -0.3 | 0.8 |
| AUG 17 | 0.6 | -0.4 | 0.5 | 0.8 | 0.0 | -0.4 | -0.3 | 0.3 |
| JUL 17 | 1.2 | -0.2 | 0.8 | 0.9 | 0.3 | -0.7 | -0.2 | -0.4 |
| JUN 17 | -0.3 | 0.6 | -0.4 | 0.4 | -0.4 | -0.8 | -0.4 | 0.6 |
| MAY 17 | 0.7 | 0.2 | 0.3 | 1.0 | 0.0 | -0.6 | -0.3 | 0.1 |
| APR 17 | -0.5 | -0.2 | -0.2 | 0.3 | -0.1 | -0.5 | -0.4 | 0.4 |
| MAR 17 | 0.7 | -0.9 | 0.9 | 1.5 | 0.9 | 0.0 | 0.8 | 1.1 |
| FEB 17 | 0.1 | 0.3 | -0.1 | 0.6 | 0.4 | -1.4 | -0.2 | 1.4 |

TABLE T1 - Atmospheric index values for the most recent 12 months. Indices are standardized by the mean annual standard deviation, except for the Tahiti and Darwin SLP anomalies which are in units of hPa. Positive (negative) values of 200-hPa zonal wind index imply westerly (easterly) anomalies. Positive (negative) values of 850-hPa zonal wind indices imply easterly (westerly) anomalies. Anomalies are departures from the 1981-2010 base period means.

| Month | PACIFIC SST | | | | | | | | ATLANTIC SST | | | | GLOBAL | |
|---|---|---|---|---|---|---|---|---|---|---|---|---|---|---|
| | Niño 1+2 0-10S 90W-80W | | Niño 3 5N-5S 150W-90W | | Niño 3.4 5N-5S 170W-120W | | Niño 4 5N-5S 160E-150W | | N.ATL 5N-20N 60W-30W | | S. ATL 0-20S 30W-10E | | TROPICS 10N-10S 0-360 | |
| FEB 18 | -0.6 | 25.6 | -1.0 | 25.4 | -0.9 | 25.8 | -0.2 | 27.9 | -0.0 | 25.6 | -0.3 | 26.3 | -0.1 | 27.7 |
| JAN 18 | -0.8 | 23.7 | -1.1 | 24.5 | -0.8 | 25.8 | -0.3 | 28.0 | 0.3 | 26.3 | -0.1 | 25.6 | -0.1 | 27.5 |
| DEC 17 | -1.5 | 21.3 | -1.1 | 24.0 | -0.8 | 25.8 | -0.3 | 28.2 | 0.6 | 27.4 | -0.3 | 24.4 | -0.1 | 27.6 |
| NOV 17 | -1.2 | 20.4 | -1.0 | 23.9 | -0.9 | 25.8 | -0.2 | 28.5 | 0.2 | 27.9 | 0.0 | 24.0 | 0.1 | 27.7 |
| OCT 17 | -1.3 | 19.5 | -0.6 | 24.3 | -0.5 | 26.2 | -0.1 | 28.6 | 0.2 | 28.3 | 0.2 | 23.6 | 0.1 | 27.5 |
| SEP 17 | -0.7 | 19.7 | -0.7 | 24.2 | -0.4 | 26.3 | 0.0 | 28.7 | 0.4 | 28.5 | 0.1 | 23.2 | 0.1 | 27.4 |
| AUG 17 | -0.5 | 20.2 | -0.2 | 24.8 | -0.2 | 26.7 | 0.2 | 28.9 | 0.5 | 28.3 | 0.3 | 23.4 | 0.3 | 27.4 |
| JUL 17 | -0.1 | 21.5 | 0.2 | 25.9 | 0.4 | 27.6 | 0.4 | 29.2 | 0.6 | 27.8 | 0.1 | 23.9 | 0.3 | 27.8 |
| JUN 17 | 0.1 | 23.0 | 0.3 | 26.8 | 0.6 | 28.2 | 0.6 | 29.4 | 0.5 | 27.3 | 0.5 | 25.5 | 0.3 | 28.3 |
| MAY 17 | 0.8 | 25.1 | 0.5 | 27.6 | 0.5 | 28.3 | 0.3 | 29.1 | 0.5 | 26.9 | 0.2 | 26.4 | 0.3 | 28.8 |
| APR 17 | 0.9 | 26.5 | 0.6 | 28.1 | 0.3 | 28.1 | 0.2 | 28.6 | 0.3 | 26.2 | 0.2 | 27.2 | 0.3 | 28.9 |
| MAR 17 | 2.0 | 28.6 | 0.5 | 27.7 | 0.1 | 27.3 | -0.1 | 28.1 | 0.1 | 25.7 | 0.1 | 27.2 | 0.3 | 28.6 |
| FEB 17 | 1.6 | 27.7 | 0.6 | 27.0 | 0.1 | 26.9 | -0.1 | 28.0 | 0.3 | 25.9 | 0.0 | 26.6 | 0.3 | 28.1 |

TABLE T2. Mean and anomalous sea surface temperature (°C) for the most recent 12 months. Anomalies are departures from the 1981–2010 adjusted OI climatology (Smith and Reynolds 1998, *J. Climate*, **11**, 3320-3323).

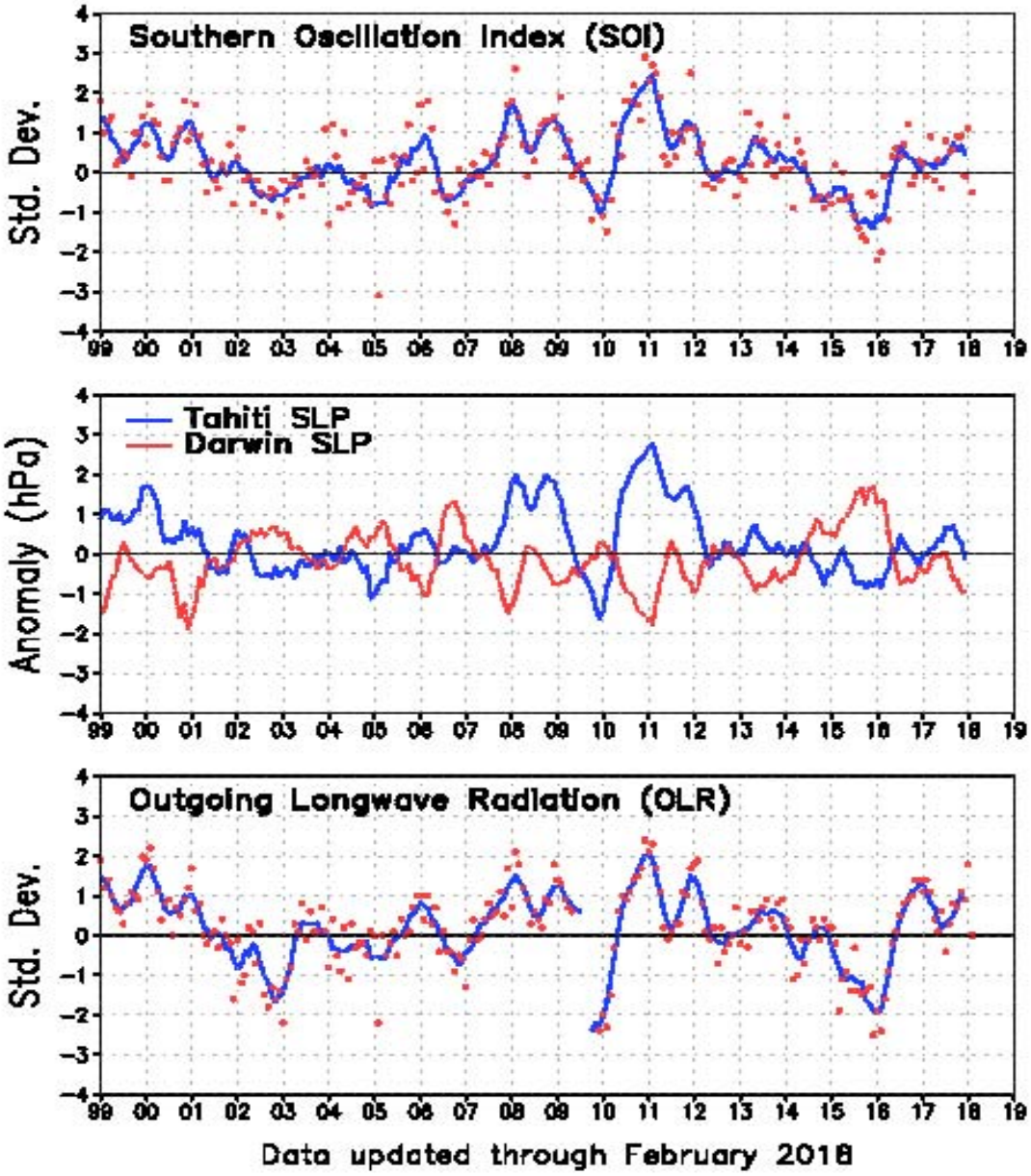


FIGURE T1. Five-month running mean of the Southern Oscillation Index (SOI) (top), sea-level pressure anomaly (hPa) at Darwin and Tahiti (middle), and outgoing longwave radiation anomaly (OLR) averaged over the area 5N-5S, 160E-160W (bottom). Anomalies in the top and middle panels are departures from the 1981-2010 base period means and are normalized by the mean annual standard deviation. Anomalies in the bottom panel are departures from the 1981-2010 base period means. Individual monthly values are indicated by "x"s in the top and bottom panels. The x-axis labels are centered on July.

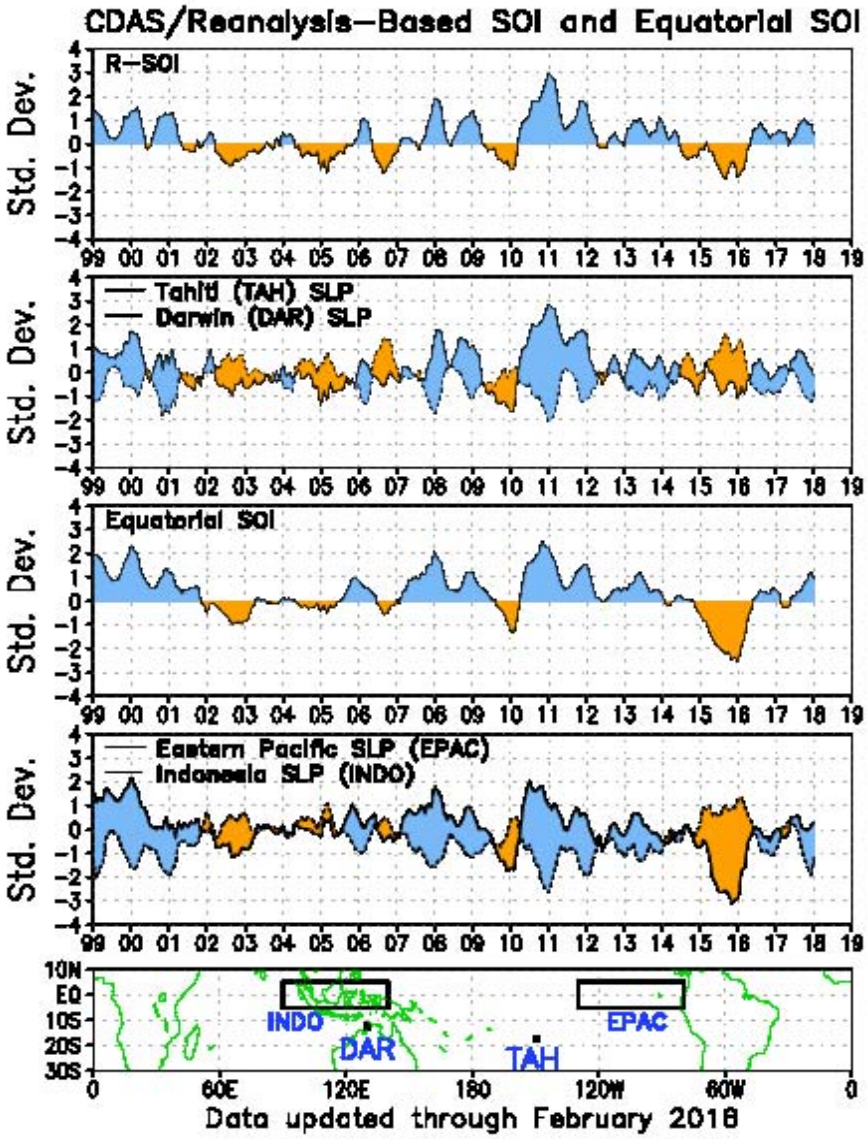


FIGURE T2. Three-month running mean of a CDAS/Reanalysis-derived (a) Southern Oscillation Index (RSOI), (b) standardized pressure anomalies near Tahiti (solid) and Darwin (dashed), (c) an equatorial SOI ([EPAC] - [INDO]), and (d) standardized equatorial pressure anomalies for (EPAC) (solid) and (INDO) (dashed). Anomalies are departures from the 1981-2010 base period means and are normalized by the mean annual standard deviation. The equatorial SOI is calculated as the normalized difference between the standardized anomalies averaged between 5°N–5°S, 80°W–130°W (EPAC) and 5°N–5°S, 90°E–140°E (INDO).

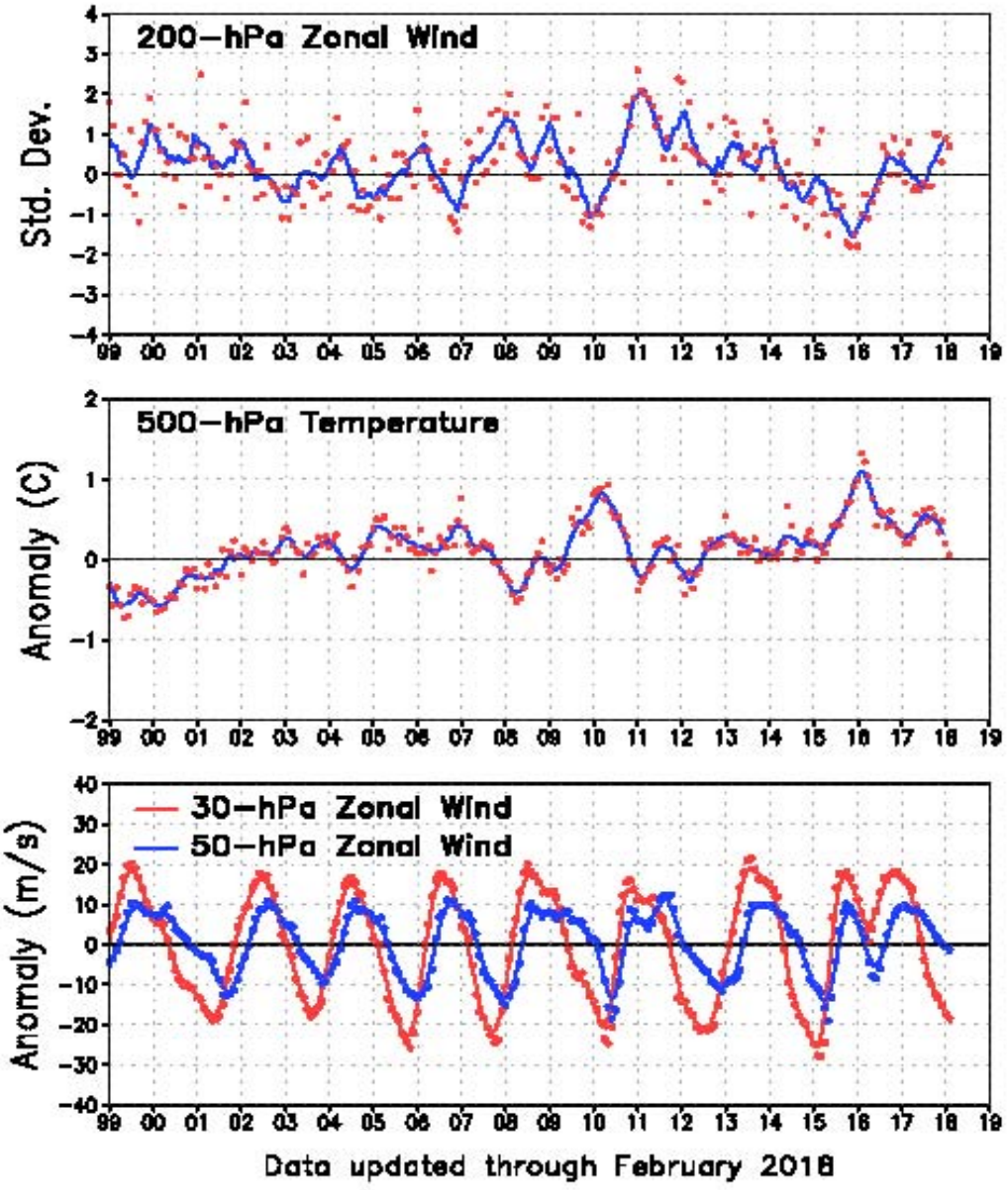


FIGURE T3. Five-month running mean (solid lines) and individual monthly mean (dots) of the 200-hPa zonal wind anomalies averaged over the area 5N-5S, 165W-110W (top), the 500-hPa virtual temperature anomalies averaged over the latitude band 20N-20S (middle), and the equatorial zonally-averaged zonal wind anomalies at 30-hPa (red) and 50-hPa (blue) (bottom). In the top panel, anomalies are normalized by the mean annual standard deviation. Anomalies are departures from the 1981-2010 base period means. The x-axis labels are centered on January.

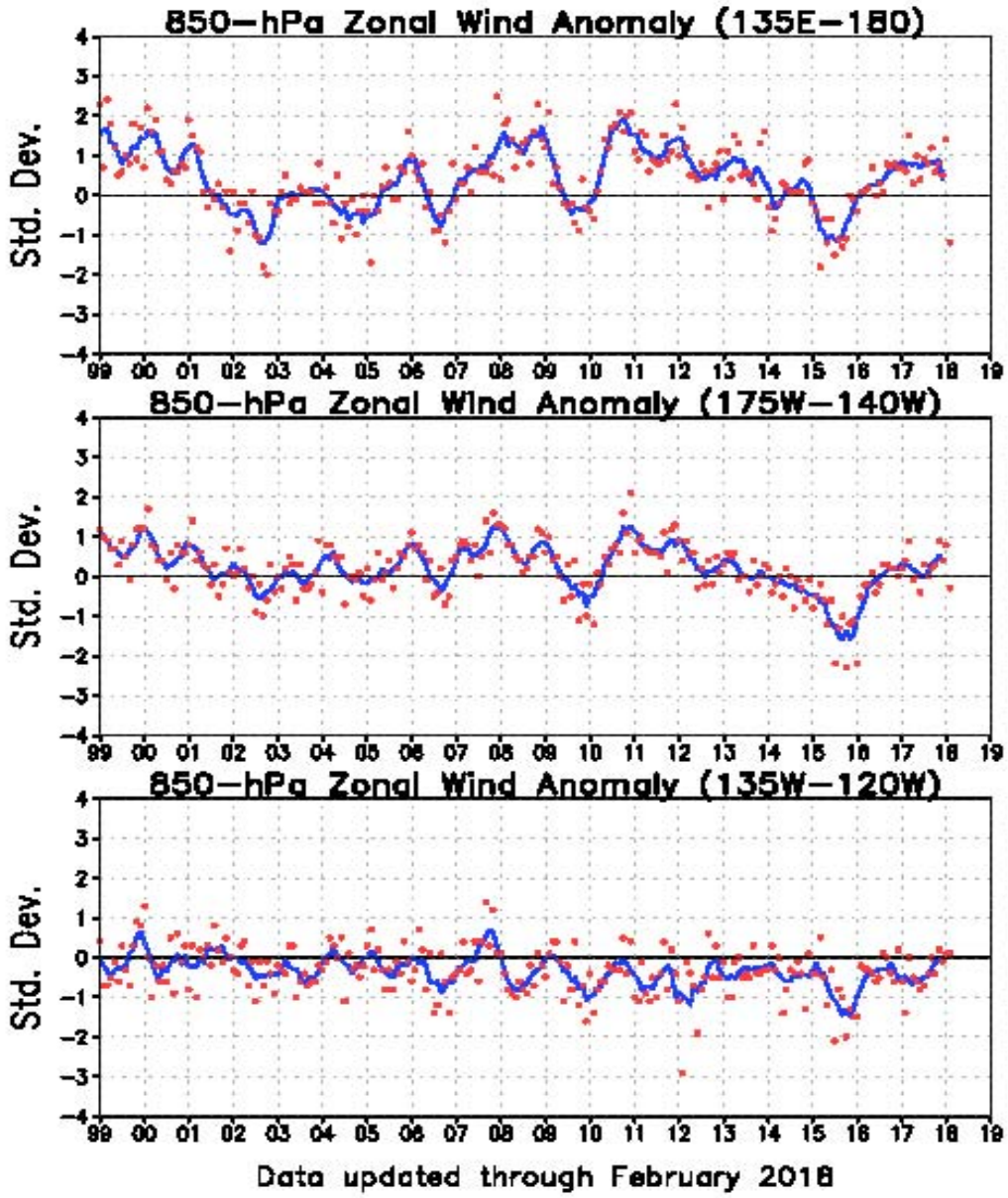


FIGURE T4. Five-month running mean (solid line) and individual monthly mean (dots) of the standardized 850-hPa zonal wind anomaly index in the latitude belt 5N-5S for 135E-180 (top), 175W-140W (middle) and 135W-120W (bottom). Anomalies are departures from the 1981-2010 base period means and are normalized by the mean annual standard deviation.The x-axis labels are centered on January. Positive (negative) values indicate easterly (westerly) anomalies.

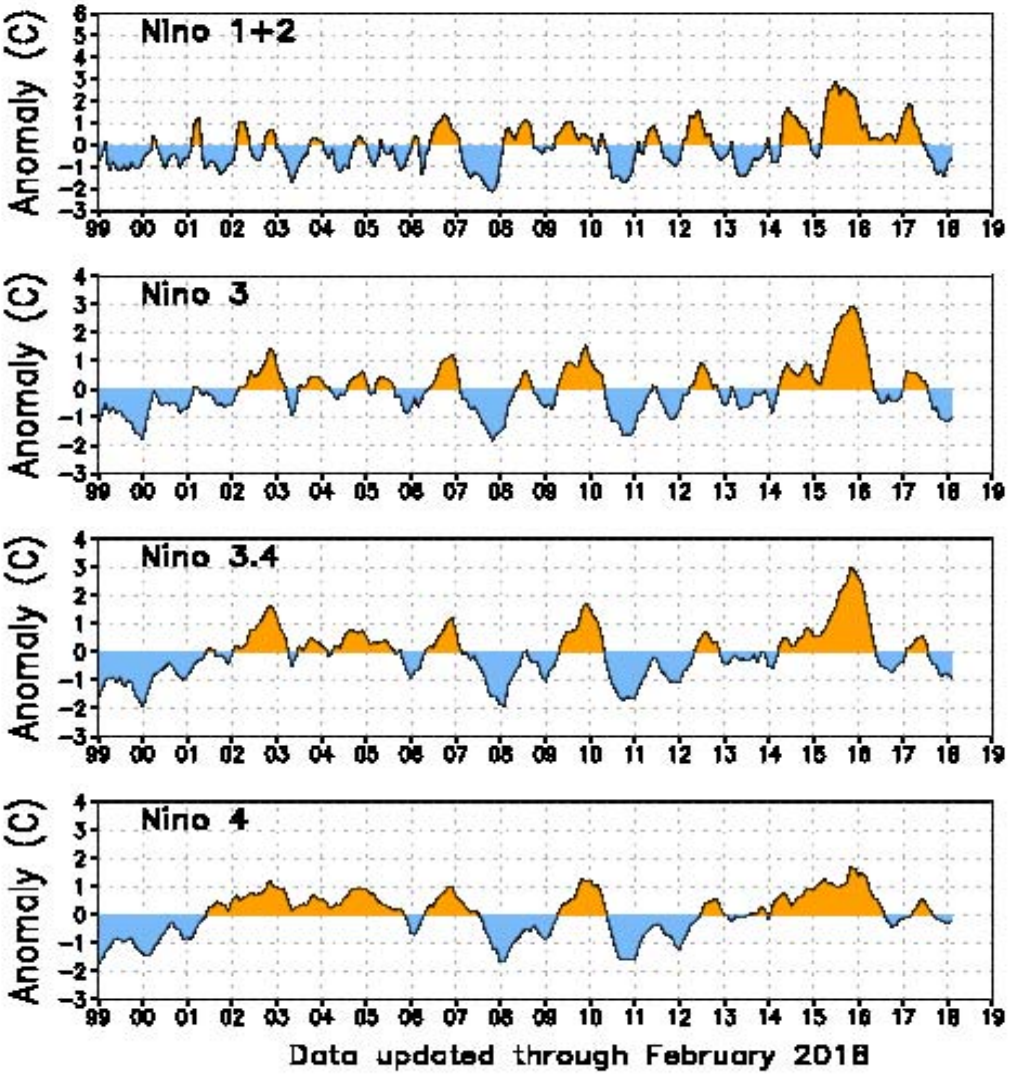


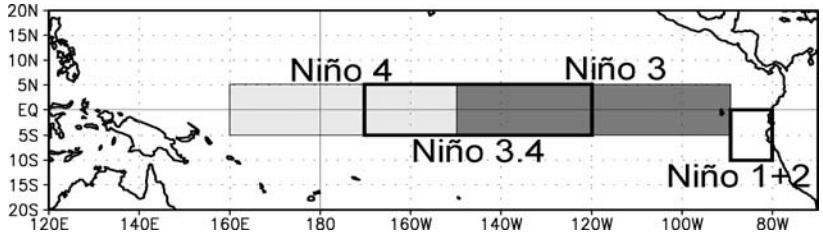


FIGURE T5. Nino region indices, calculated as the area-averaged sea surface temperature anomalies (C) for the specified region. The Nino 1+2 region (top) covers the extreme eastern equatorial Pacific between 0-10S, 90W-80W. The Nino-3 region (2nd from top) spans the eastern equatorial Pacific between 5N-5S, 150W-90W. The Nino 3.4 region 3rd from top) spans the east-central equatorial Pacific between 5N-5S, 170W-120W. The Nino 4 region (bottom) spans the date line and covers the area 5N-5S, 160E-150W. Anomalies are departures from the 1981-2010 base period monthly means *(Smith and Reynolds 1998, J. Climate, 11, 3320-3323)*. Monthly values of each index are also displayed in Table 2.

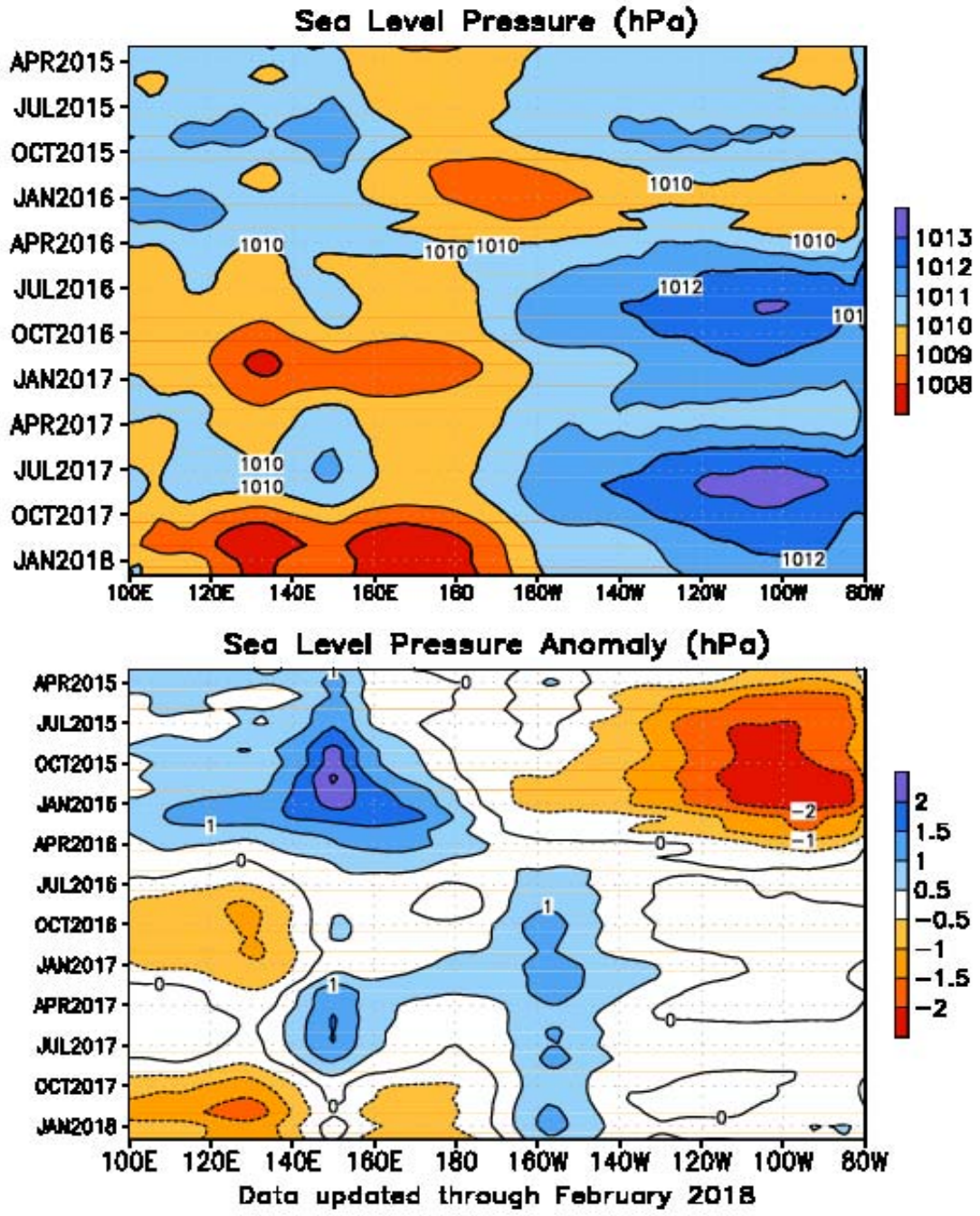


FIGURE T6. Time-longitude section of mean (top) and anomalous (bottom) sea level pressure (SLP) averaged between 5N-5S (CDAS/Reanalysis). Contour interval is 1.0 hPa (top) and 0.5 hPa (bottom). Dashed contours in bottom panel indicate negative anomalies. Anomalies are departures from the 1981-2010 base period monthly means. The data are smoothed temporally using a 3-month running average.

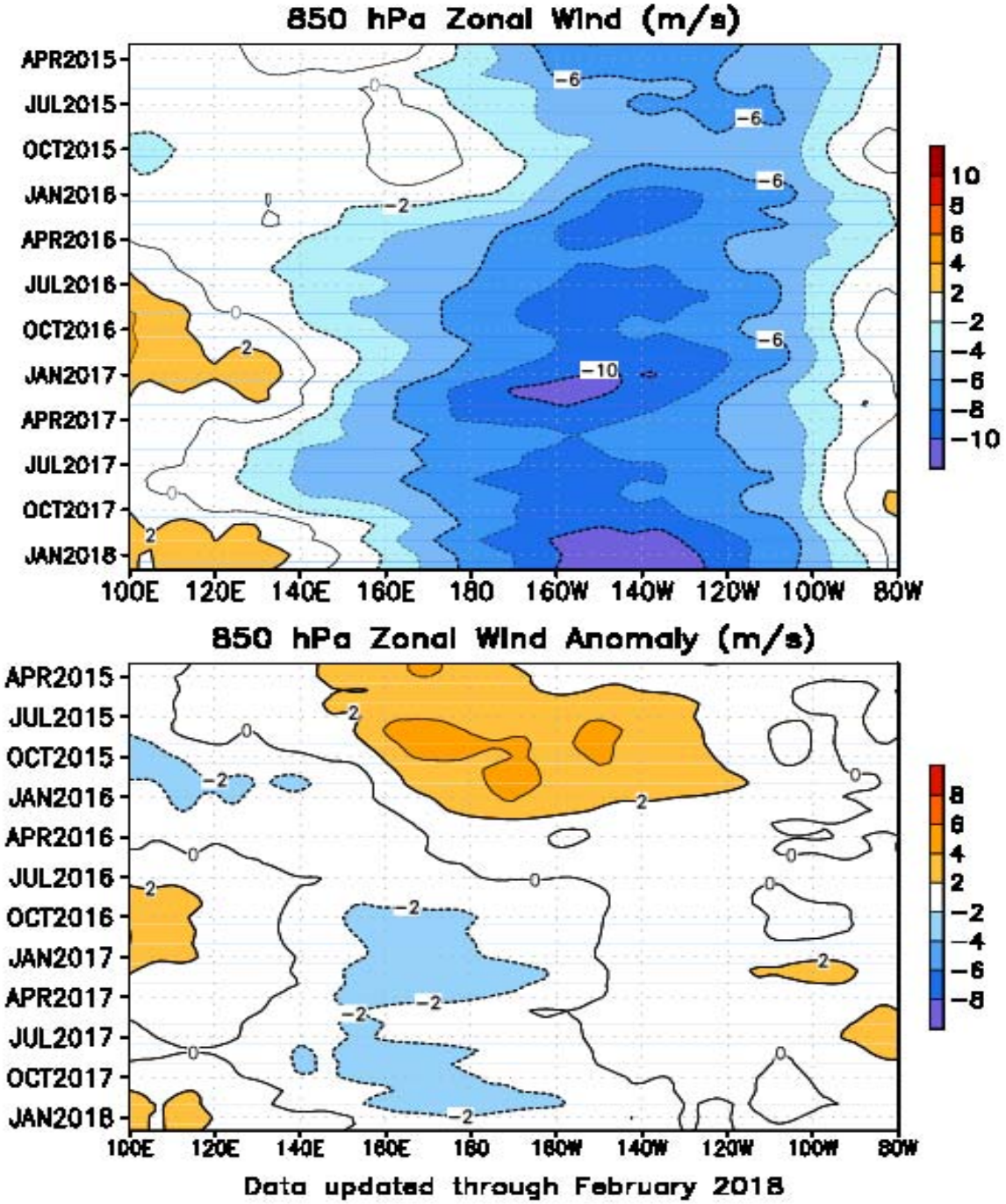


FIGURE T7. Time-longitude section of mean (top) and anomalous (bottom) 850-hPa zonal wind averaged between 5N-5S (CDAS/Reanalysis). Contour interval is 2 $ms^{-1}$. Blue shading and dashed contours indicate easterlies (top) and easterly anomalies (bottom). Anomalies are departures from the 1981-2010 base period monthly means. The data are smoothed temporally using a 3-month running average.

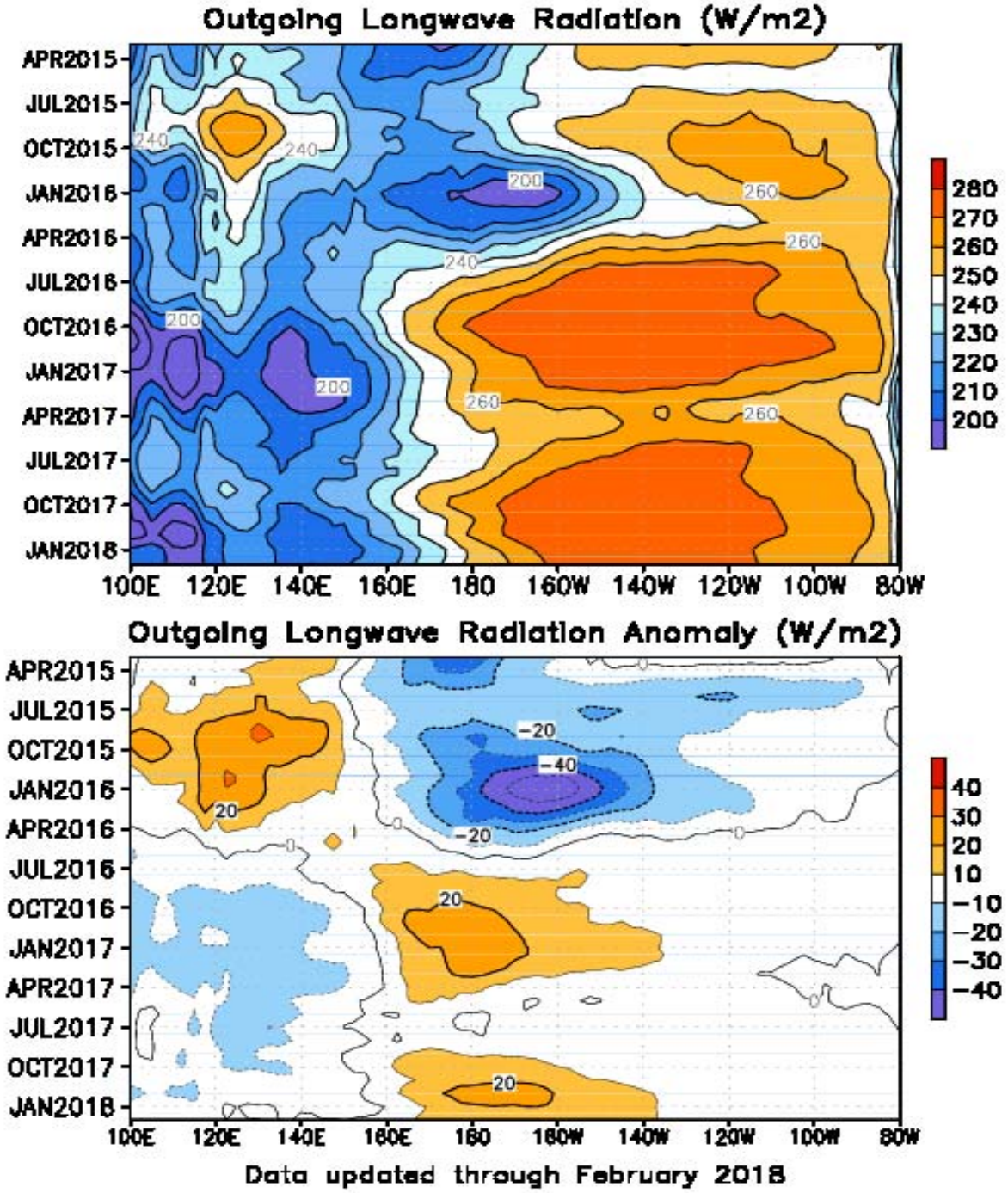


FIGURE T8. Time-longitude section of mean (top) and anomalous (bottom) outgoing longwave radiation (OLR) averaged between 5N-5S. Contour interval is 10 $Wm^{-2}$. Dashed contours in bottom panel indicate negative OLR anomalies. Anomalies are departures from the 1981-2010 base period monthly means. The data are smoothed temporally using a 3-month running average.

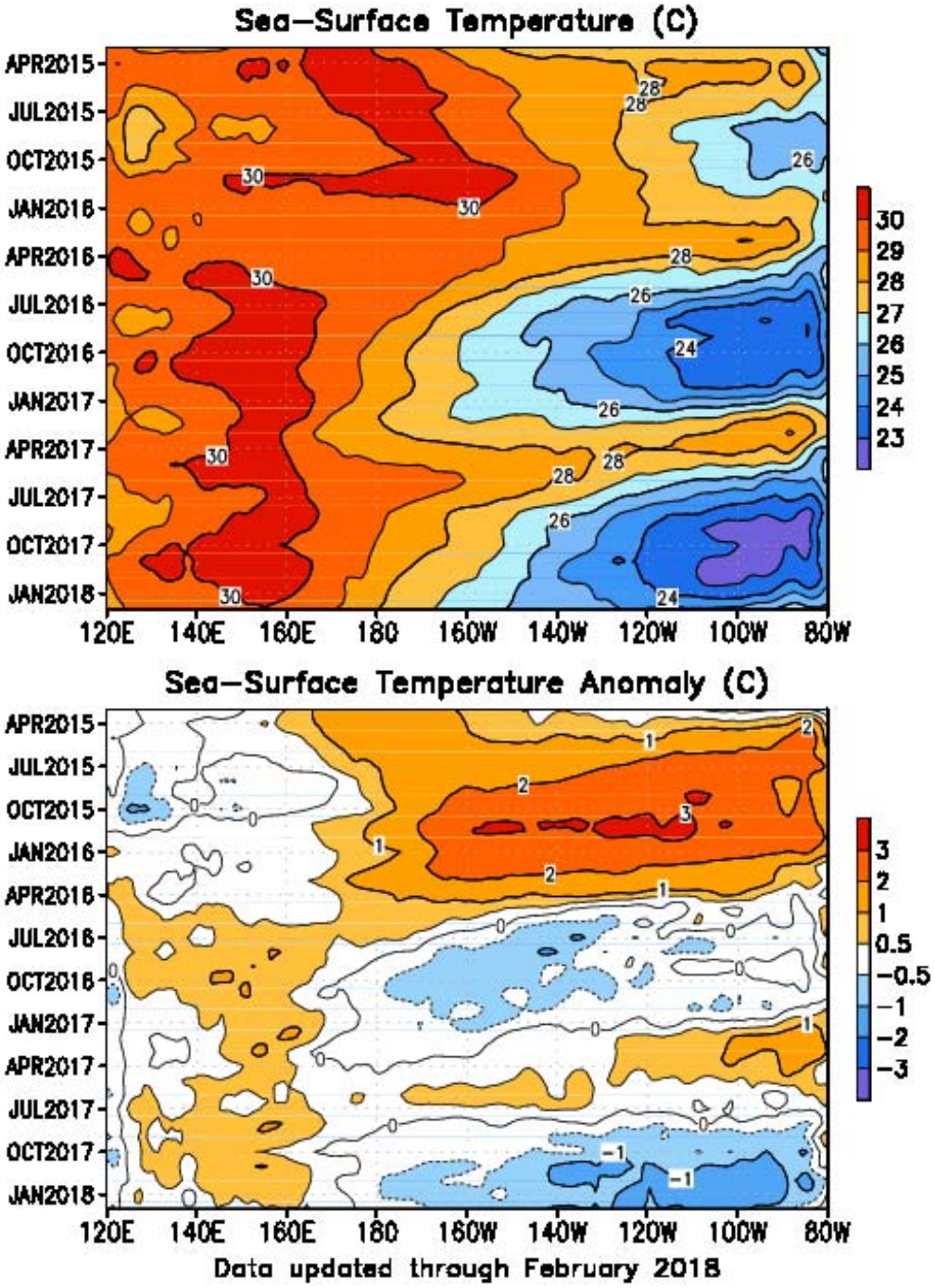


FIGURE T9. Time-longitude section of monthly mean (top) and anomalous (bottom) sea surface temperature (SST) averaged between 5N-5S. Contour interval is 1C (top) and 0.5C (bottom). Dashed contours in bottom panel indicate negative anomalies. Anomalies are departures from the 1981-2010 base period means (Smith and Reynolds 1998, *J. Climate*, **11**, 3320-3323).

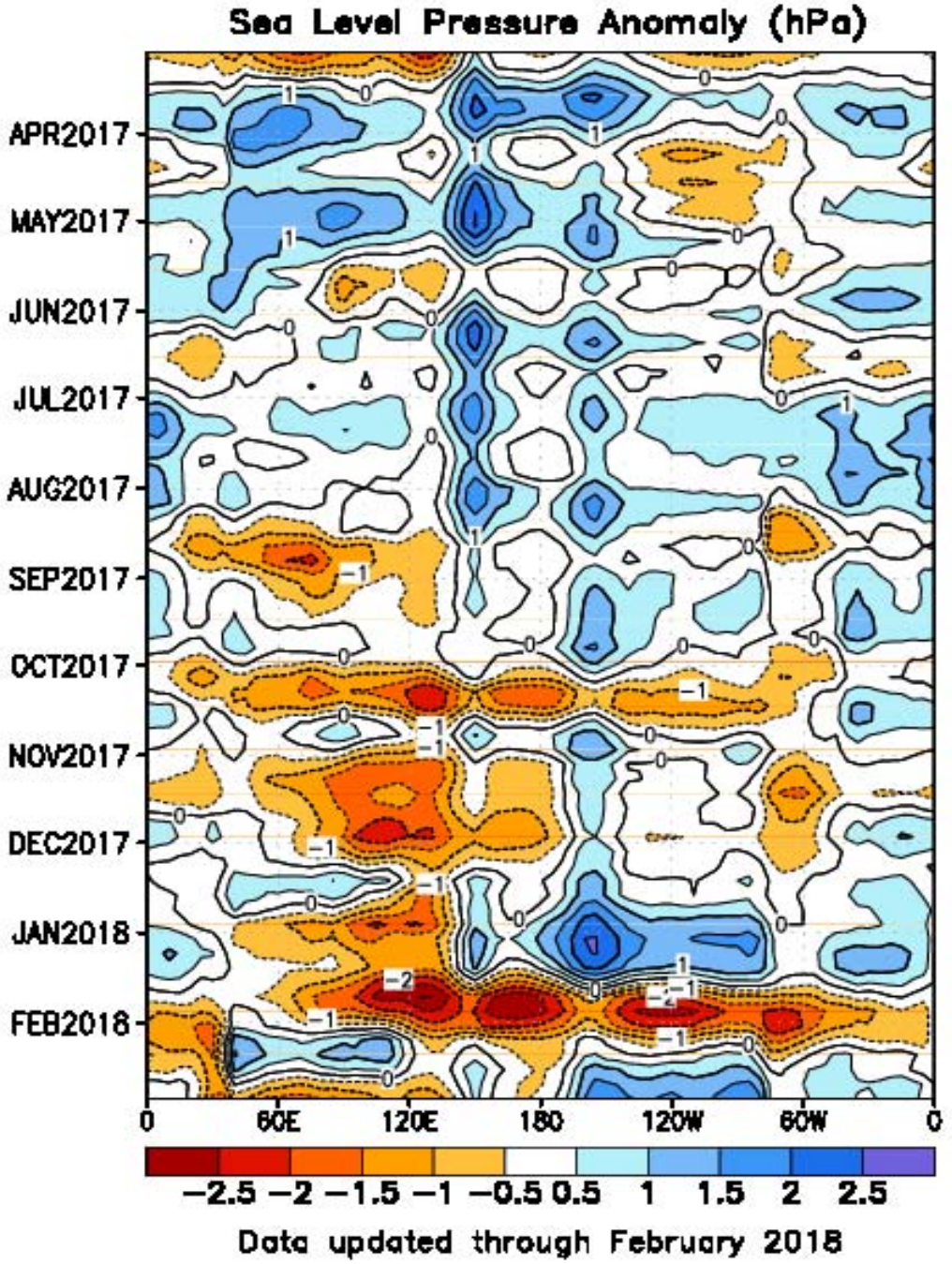


FIGURE T10. Time-longitude section of anomalous sea level pressure (hPa) averaged between 5N-5S (CDAS/Reanaysis). Contour interval is 1 hPa. Dashed contours indicate negative anomalies. Anomalies are departures from the 1981-2010 base period pentad means. The data are smoothed temporally using a 3-point running average.

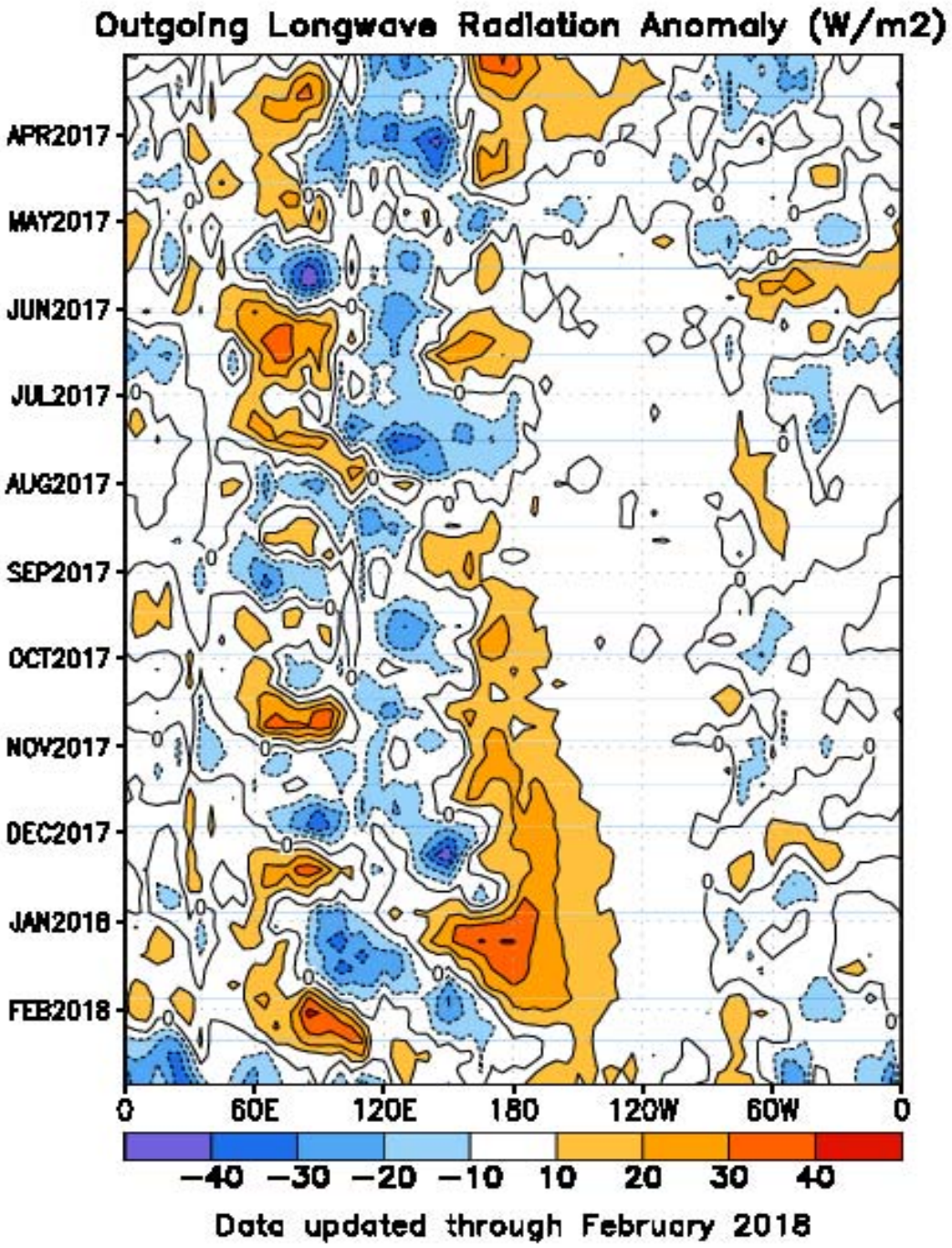


FIGURE T11. Time-longitude section of anomalous outgoing longwave radiation averaged between 5N-5S. Contour interval is 15 $Wm^{-2}$. Dashed contours indicate negative anomalies. Anomalies are departures from the 1981-2010 base period pentad means. The data are smoothed temporally using a 3-point running average.

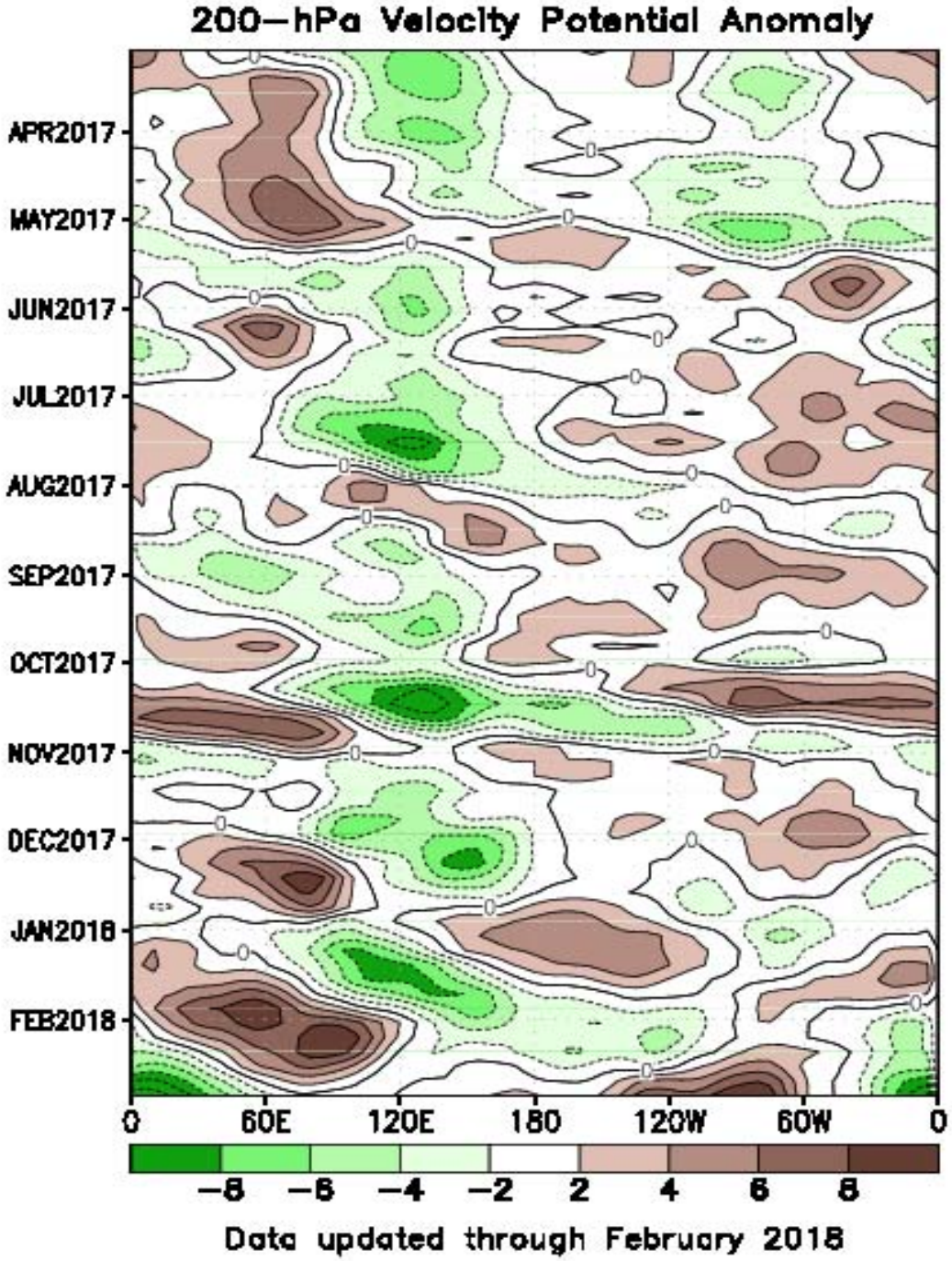


FIGURE T12. Time-longitude section of anomalous 200-hPa velocity potential averaged between 5N-5S (CDAS/Reanalysis). Contour interval is 3 x $10^6$ $m^2s^{-1}$. Dashed contours indicate negative anomalies. Anomalies are departures from the 1981-2010 base period pentad means. The data are smoothed temporally using a 3-point running average.

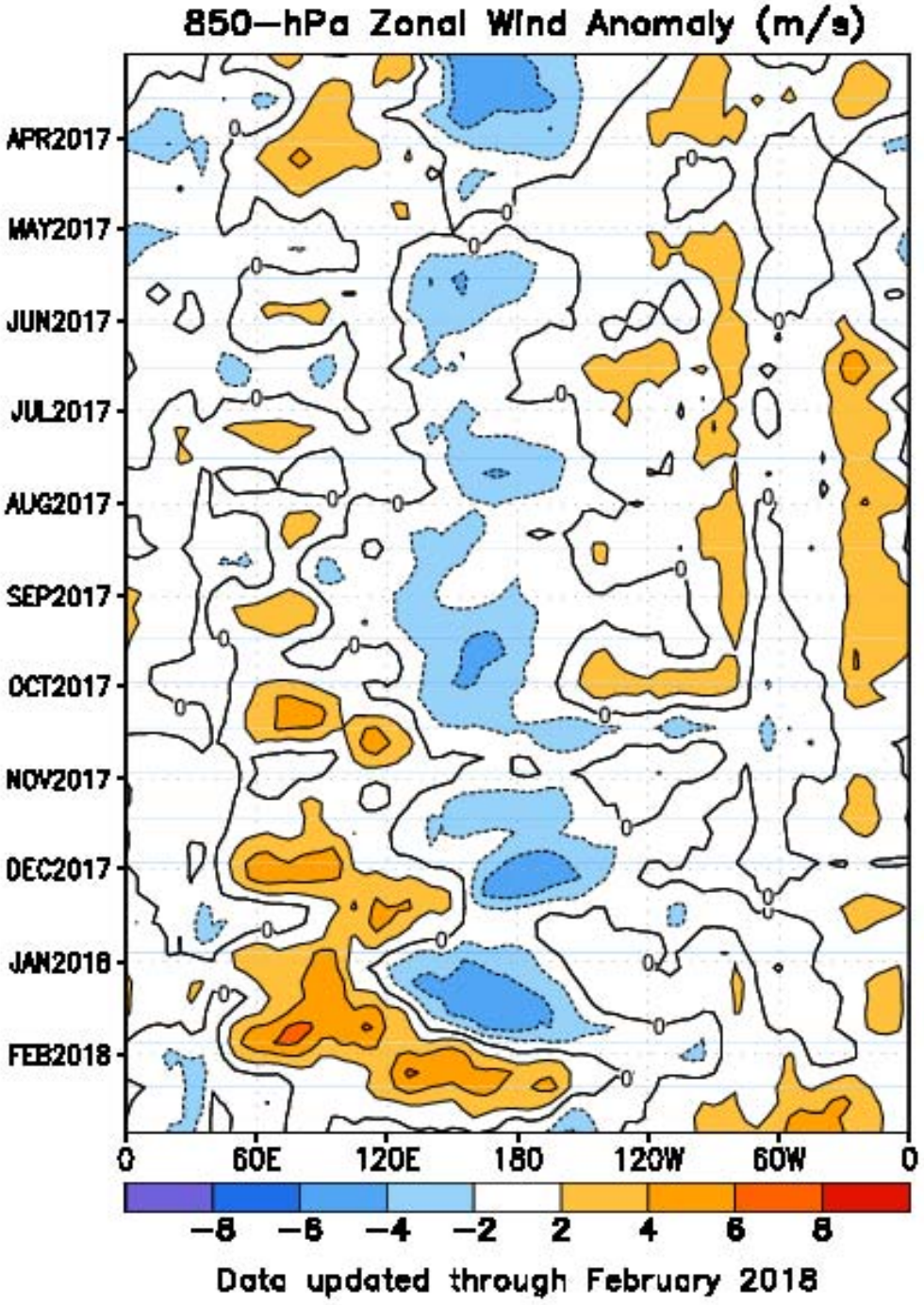


FIGURE T13. Time-longitude section of anomalous 850-hPa zonal wind averaged between 5N-5S (CDAS/Reanalysis). Contour interval is 2 $ms^{-1}$. Dashed contours indicate negative anomalies. Anomalies are departures from the 1981-2010 base period pentad means. The data are smoothed temporally by using a 3-point running average.

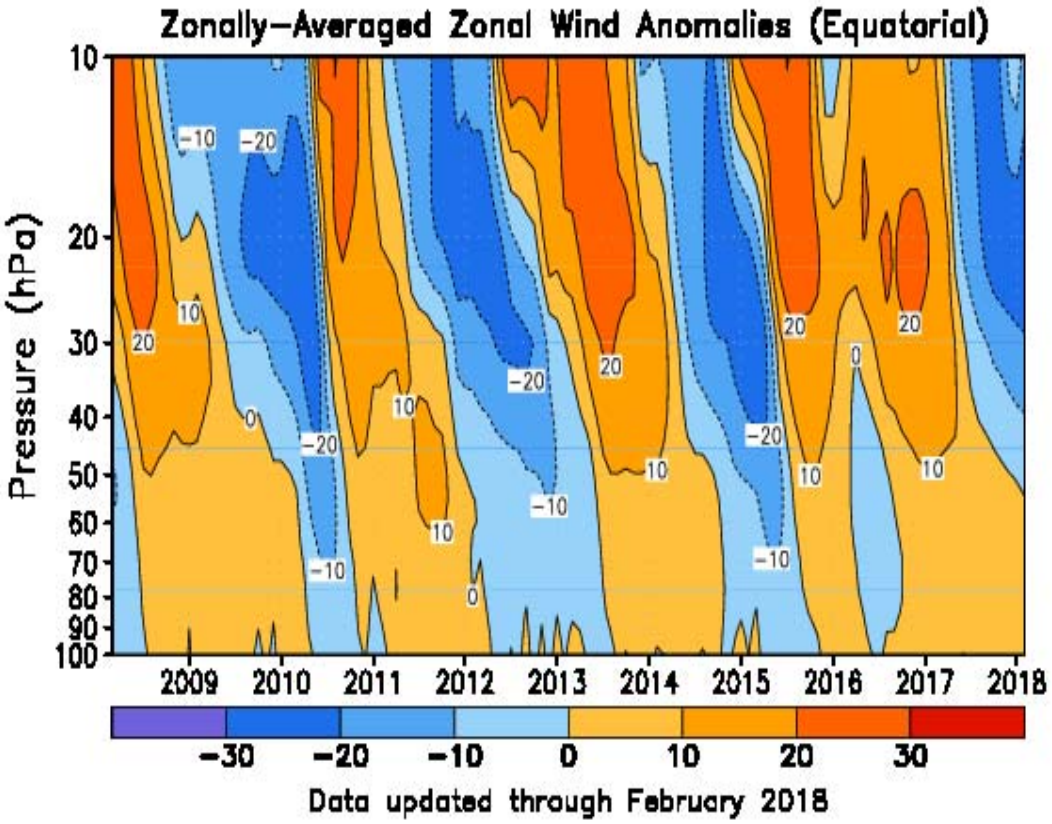


FIGURE T14. Equatorial time-height section of anomalous zonally-averaged zonal wind (m $s^{-1}$) (CDAS/Reanalysis). Contour interval is 10 $ms^{-1}$. Anomalies are departures from the 1981-2010 base period monthly means.

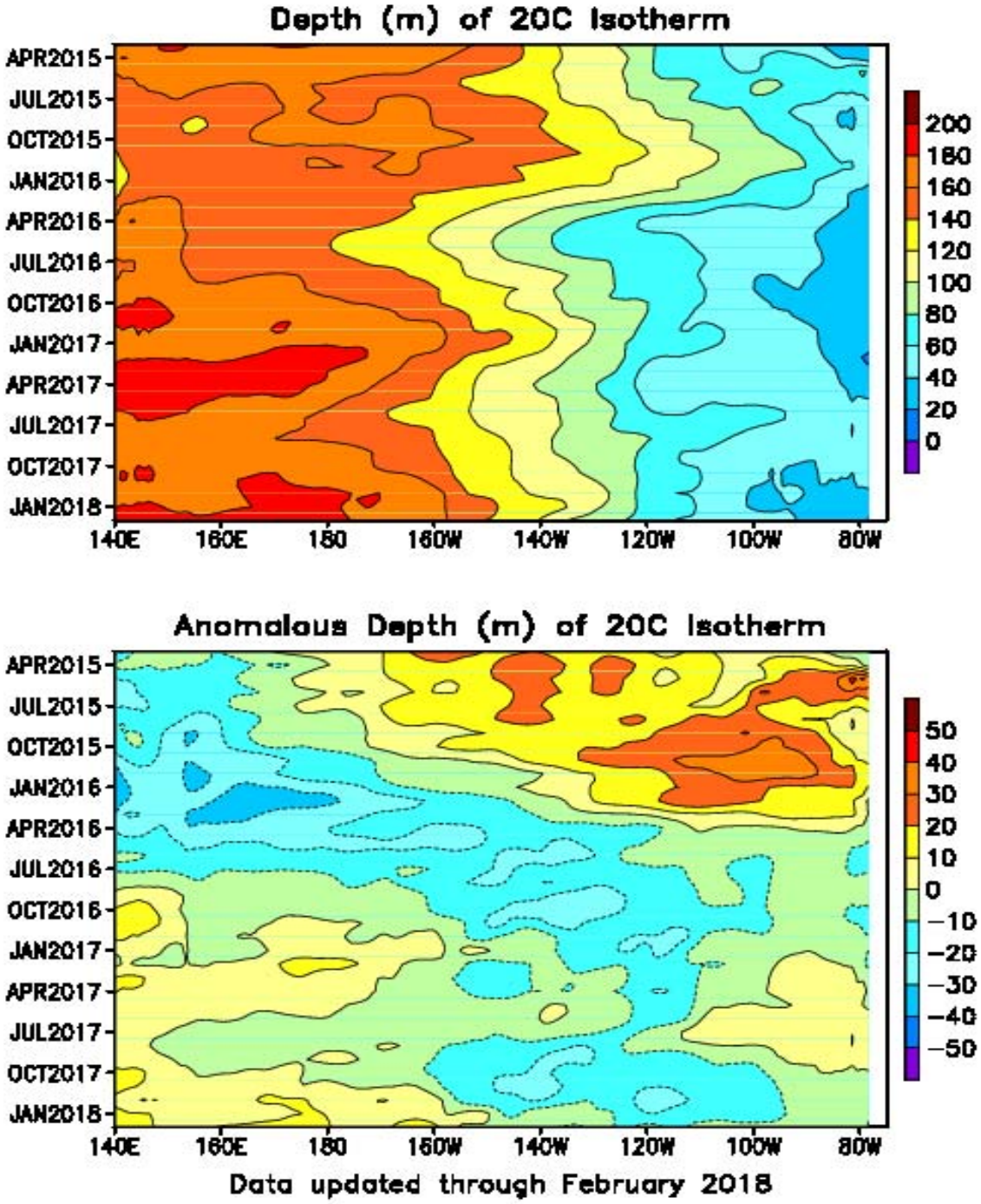


FIGURE T15. Mean (top) and anomalous (bottom) depth of the 20C isotherm averaged between 5N-5S in the Pacific Ocean. Data are derived from the NCEP's global ocean data assimilation system which assimilates oceanic observations into an oceanic GCM (Behringer, D. W., and Y. Xue, 2004: Evaluation of the global ocean data assimilation system at NCEP: The Pacific Ocean. AMS 84th Annual Meeting, Seattle, Washington, 11-15). The contour interval is 10 m. Dashed contours in bottom panel indicate negative anomalies. Anomalies are departures from the 1981-2010 base period means.

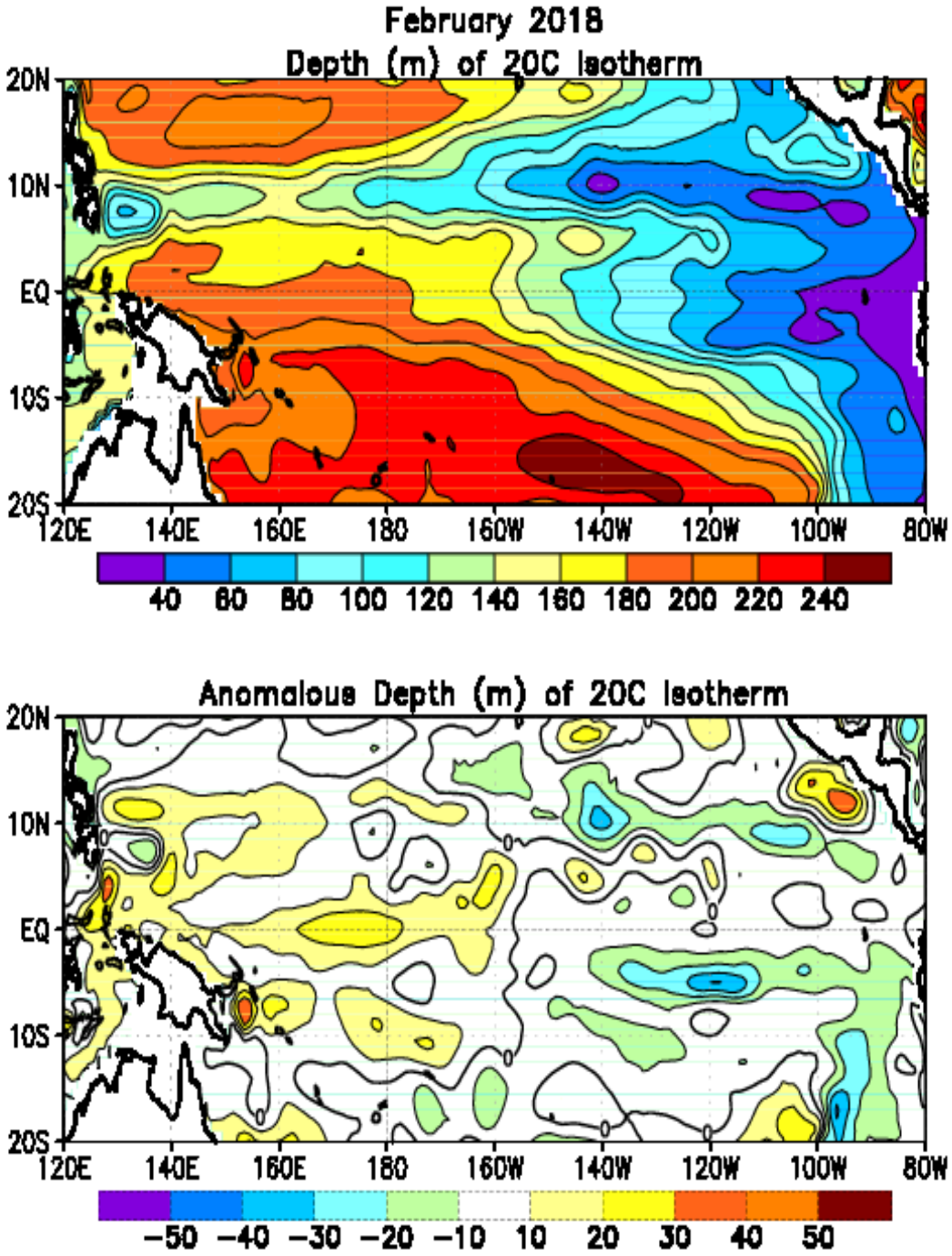


FIGURE T16. Mean (top) and anomalous (bottom) depth of the 20°C isotherm for FEB 2018. Contour interval is 40 m (top) and 10 m (bottom). Dashed contours in bottom panel indicate negative anomalies. Data are derived from the NCEP's global ocean data assimilation system version 2 which assimilates oceanic observations into an oceanic GCM (Xue, Y. and Behringer, D.W., 2006: Operational global ocean data assimilation system at NCEP, to be submitted to BAMS). Anomalies are departures from the 1981–2010 base period means.

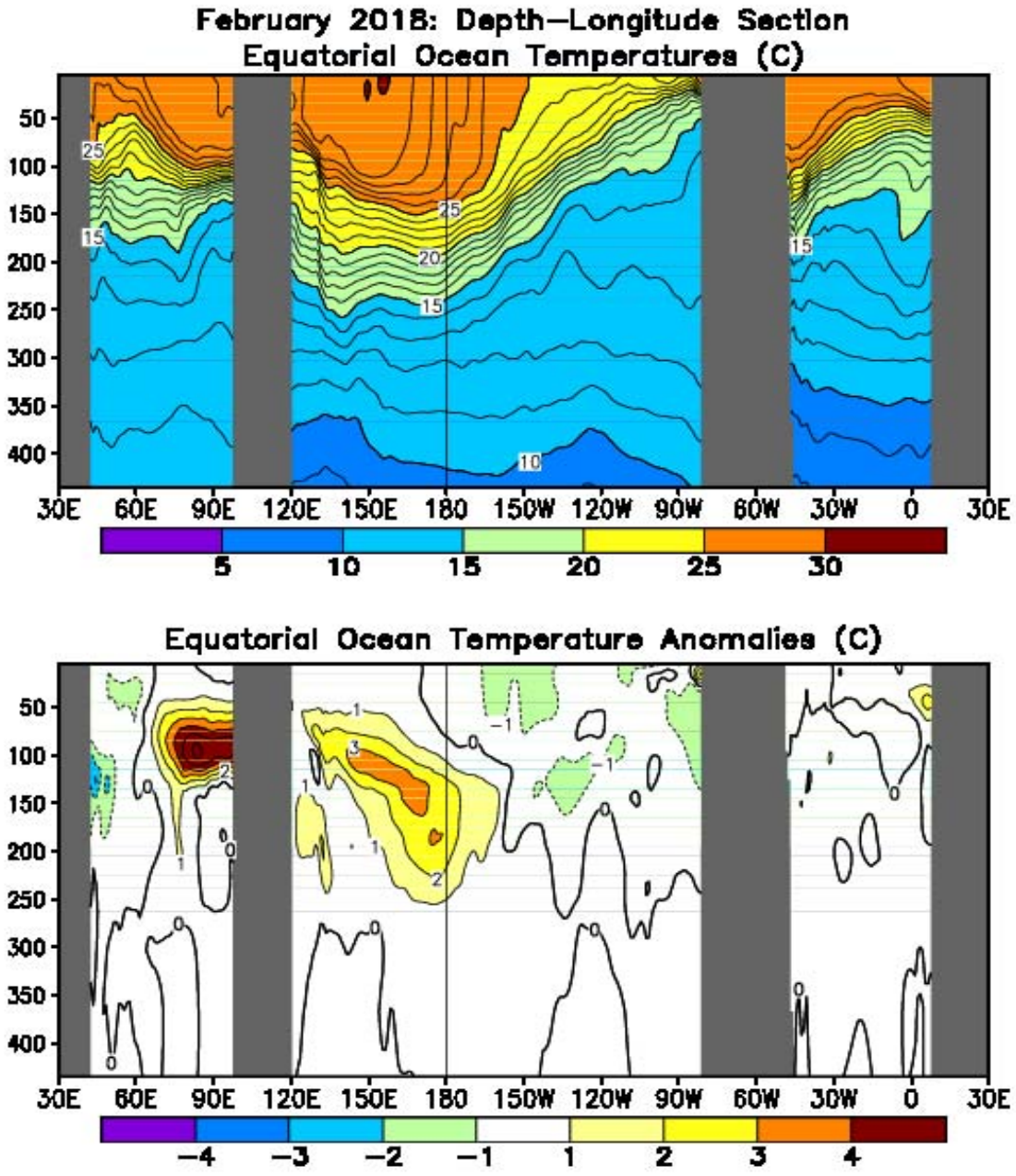


FIGURE T17. Equatorial depth-longitude section of ocean temperature (top) and ocean temperature anomalies (bottom) for FEB 2018. Contour interval is 1°C. Dashed contours in bottom panel indicate negative anomalies. Data are derived from the NCEP's global ocean data assimilation system version 2 which assimilates oceanic observations into an oceanic GCM (Xue, Y. and Behringer, D.W., 2006: Operational global ocean data assimilation system at NCEP, to be submitted to BAMS). Anomalies are departures from the 1981–2010 base period means.

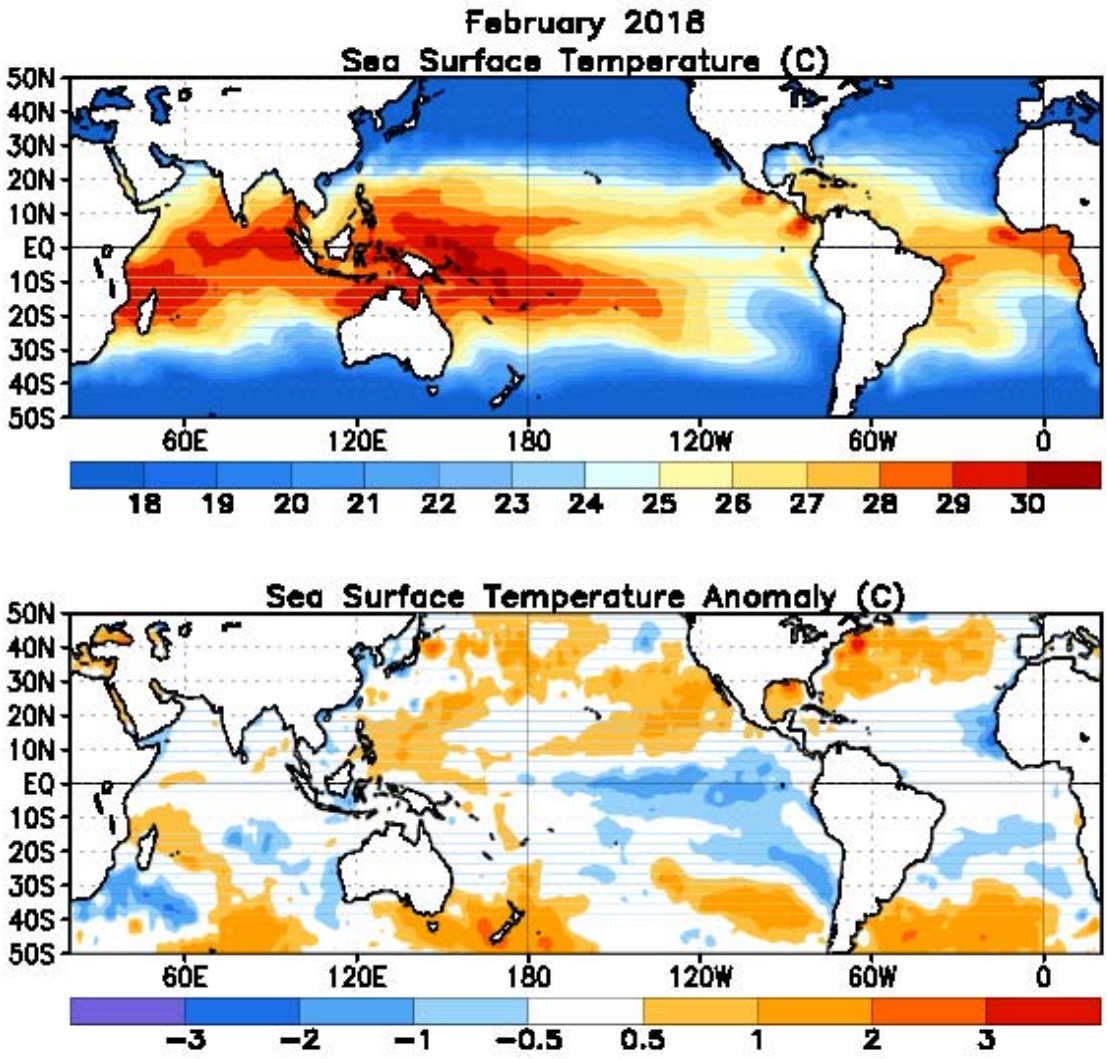


FIGURE T18. Mean (top) and anomalous (bottom) sea surface temperature (SST). Anomalies are departures from the 1981-2010 base period monthly means (Smith and Reynolds 1998, *J. Climate*, **11**, 3320-3323).

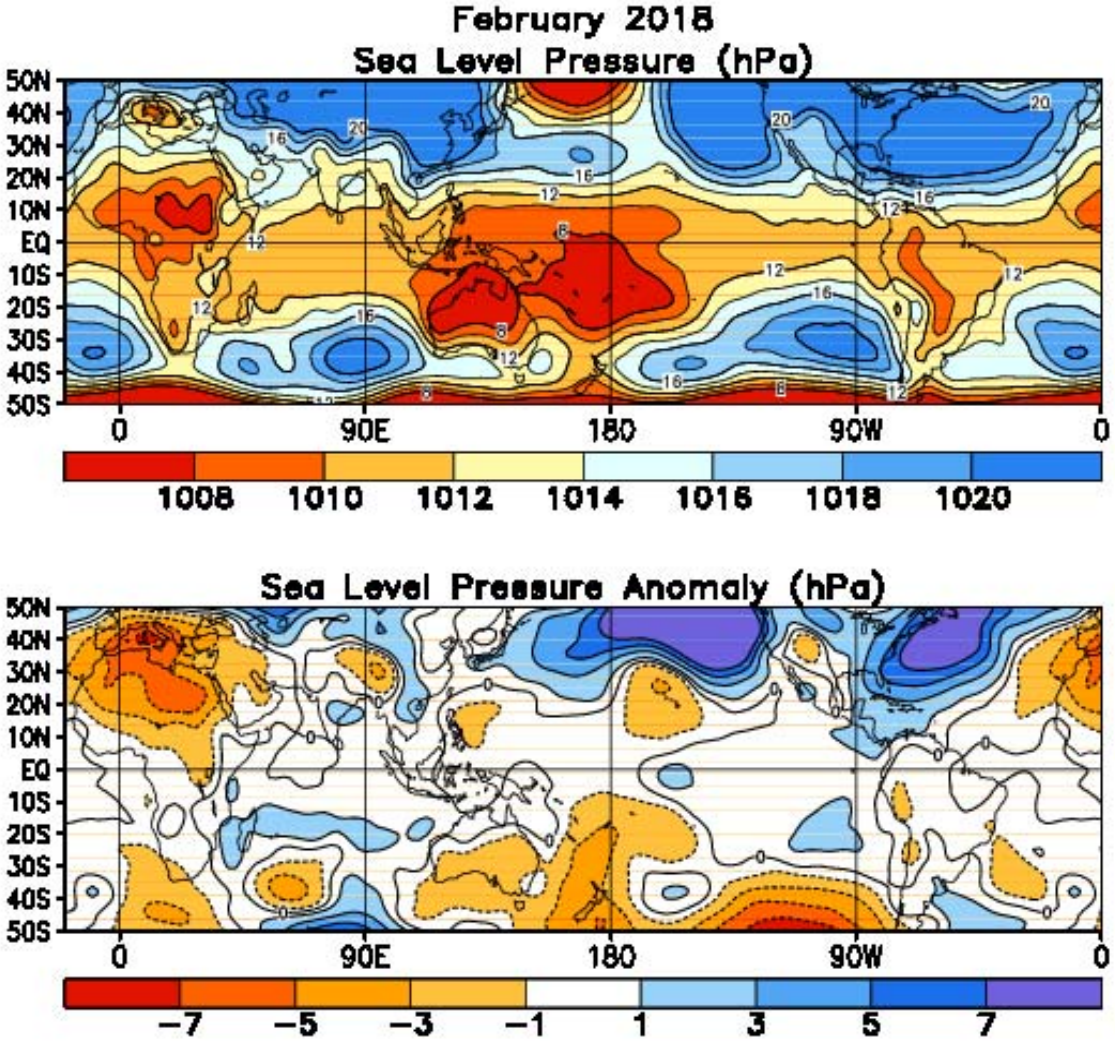


FIGURE T19. Mean (top) and anomalous (bottom) sea level pressure (SLP) (CDAS/Reanalysis). In top panel, 1000 hPa has been subtracted from contour labels, contour interval is 2 hPa, and values below 1000 hPa are indicated by dashed contours. In bottom panel, anomaly contour interval is 1 hPa and negative anomalies are indicated by dashed contours. Anomalies are departures from the 1981-2010 base period monthly means.

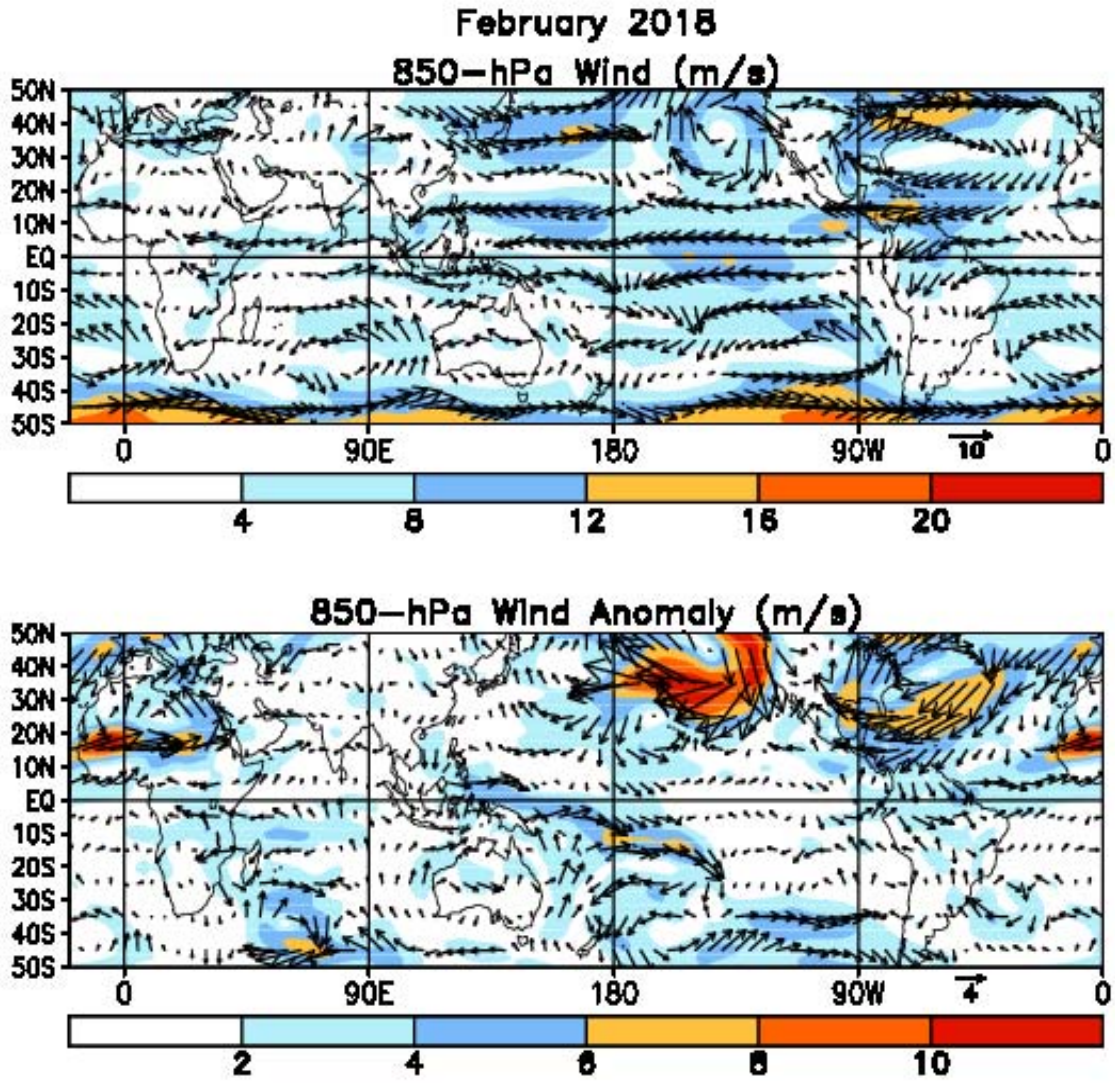


FIGURE T20. Mean (top) and anomalous (bottom) 850-hPa vector wind (CDAS/Reanaysis) for FEB 2018. Contour interval for isotachs is 4 $ms^{-1}$ (top) and 2 $ms^{-1}$ (bottom). Anomalies are departures from the 1981-2010 base period monthly means.

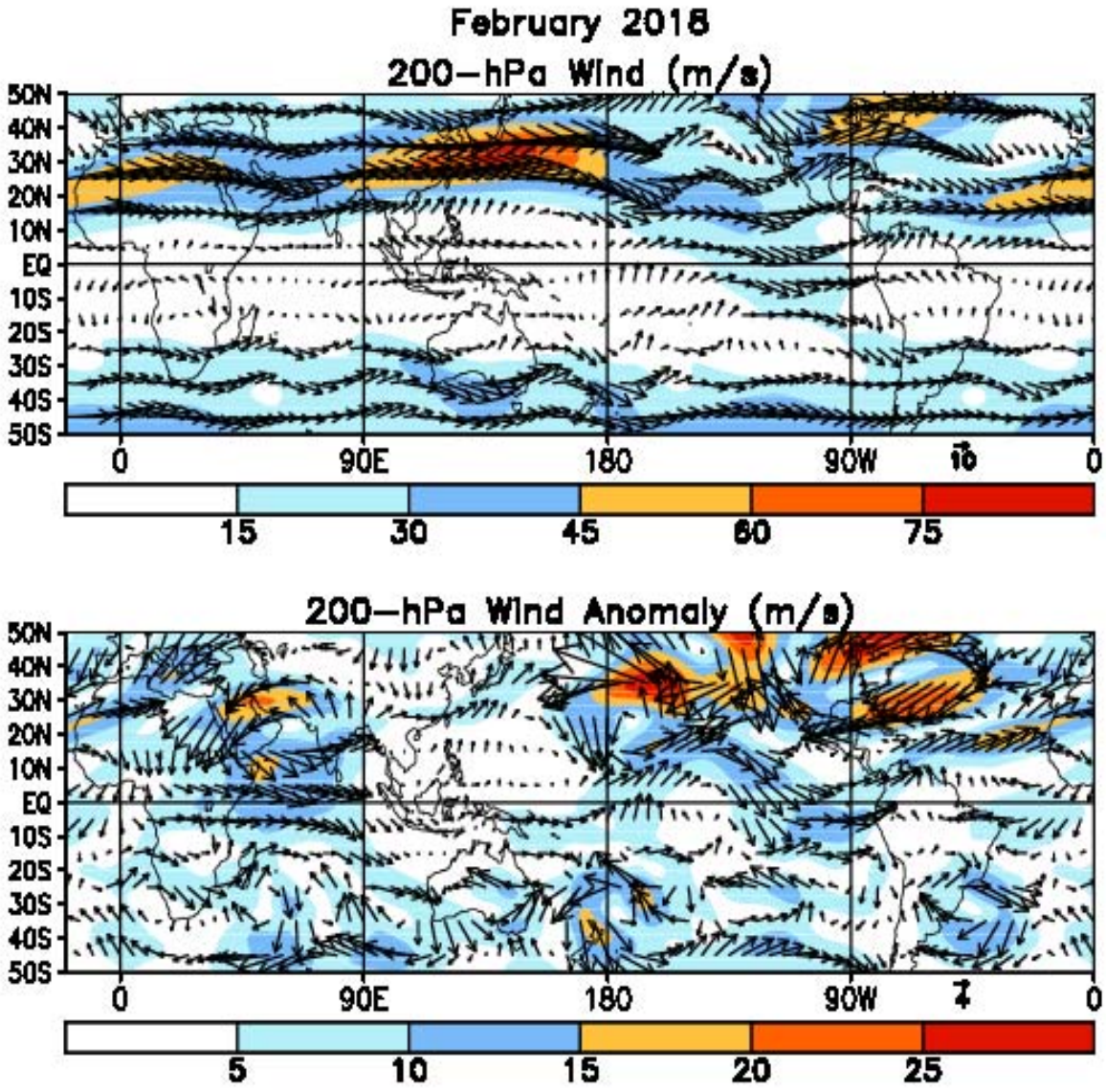


FIGURE T21. Mean (top) and anomalous (bottom) 200-hPa vector wind (CDAS/Reanalysis) for FEB 2018. Contour interval for isotachs is 15 $ms^{-1}$ (top) and 5 $ms^{-1}$ (bottom). Anomalies are departures from 1981-2010 base period monthly means.

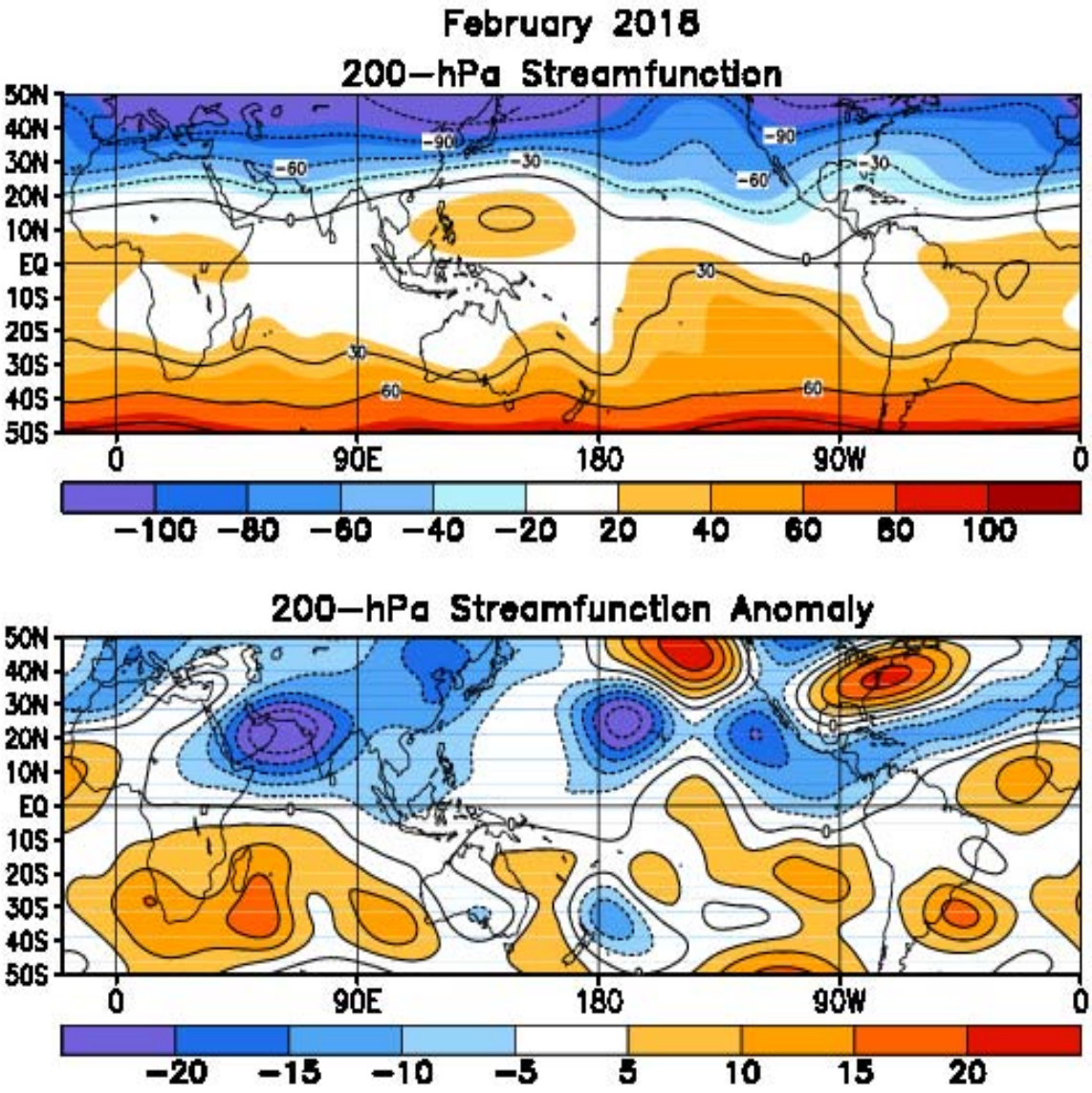


FIGURE T22. Mean (top) and anomalous (bottom) 200-hPa streamfunction (CDAS/Reanalysis). Contour interval is 20 x $10^6$ $m^2s^{-1}$ (top) and 5 x $10^6$ $m^2s^{-1}$ (bottom). Negative (positive) values are indicated by dashed (solid) lines. The non-divergent component of the flow is directed along the contours with speed proportional to the gradient. Thus, high (low) stream function corresponds to high (low) geopotential height in the Northern Hemisphere and to low (high) geopotential height in the Southern Hemisphere. Anomalies are departures from the 1981-2010 base period monthly means.

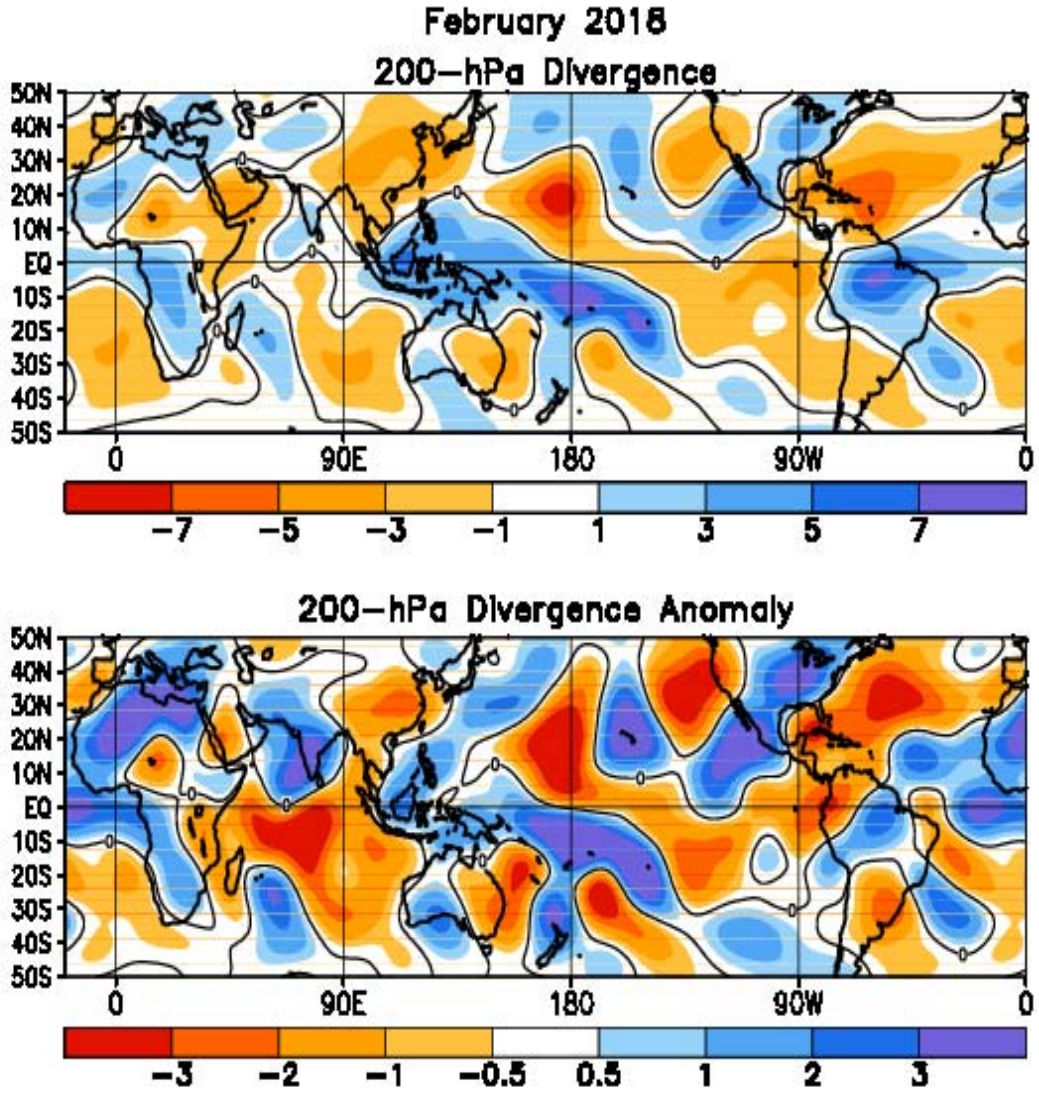


FIGURE T23. Mean (top) and anomalous (bottom) 200-hPa divergence (CDAS/Reanalysis). Divergence and anomalous divergence are shaded blue. Convergence and anomalous convergence are shaded orange. Anomalies are departures from the 1981-2010 base period monthly means.

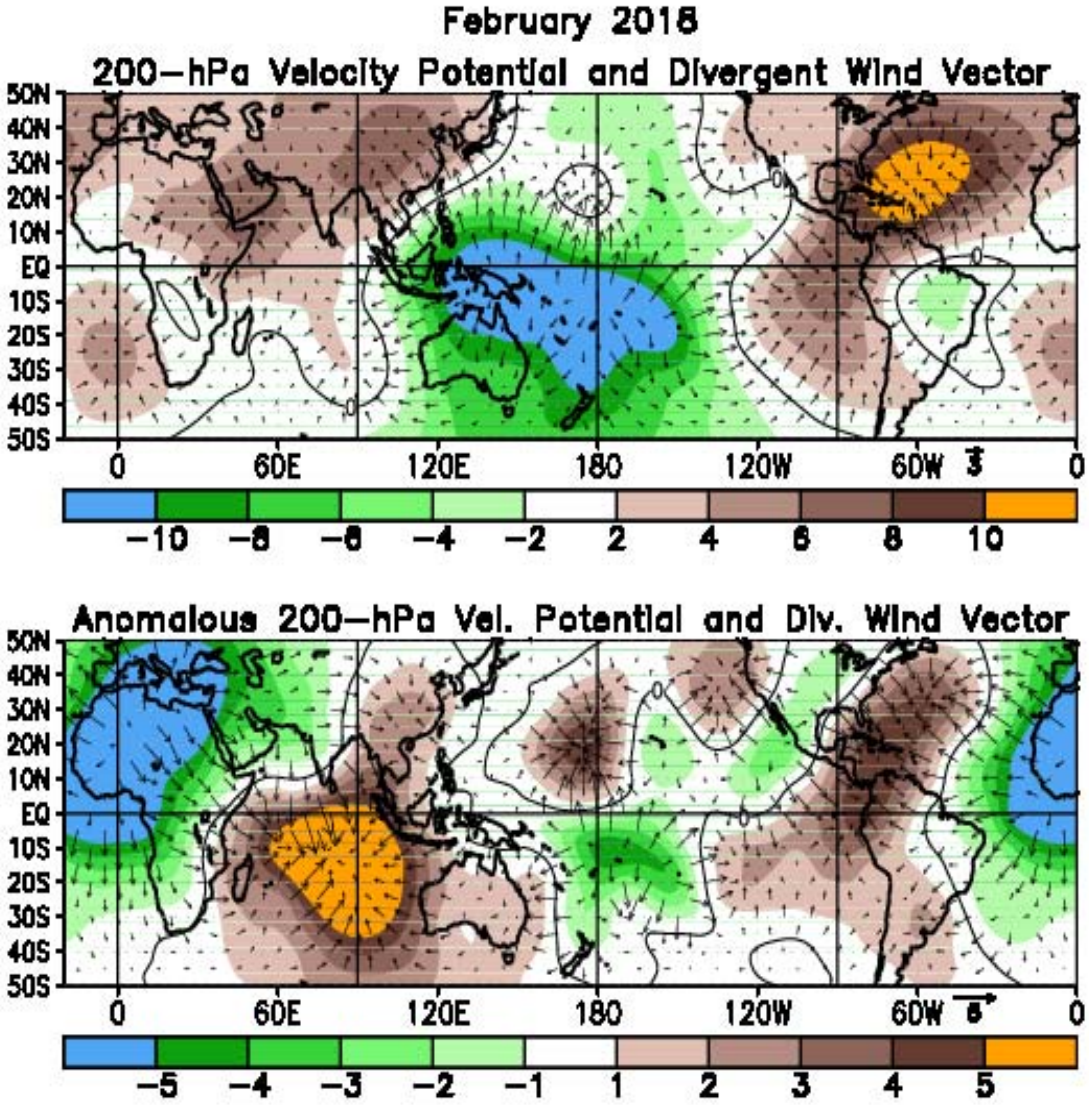


FIGURE T24. Mean (top) and anomalous (bottom) 200-hPa velocity potential ($10^6 m^2 s$) and divergent wind (CDAS/ Reanalysis). Anomalies are departures from the 1981-2010 base period monthly means.

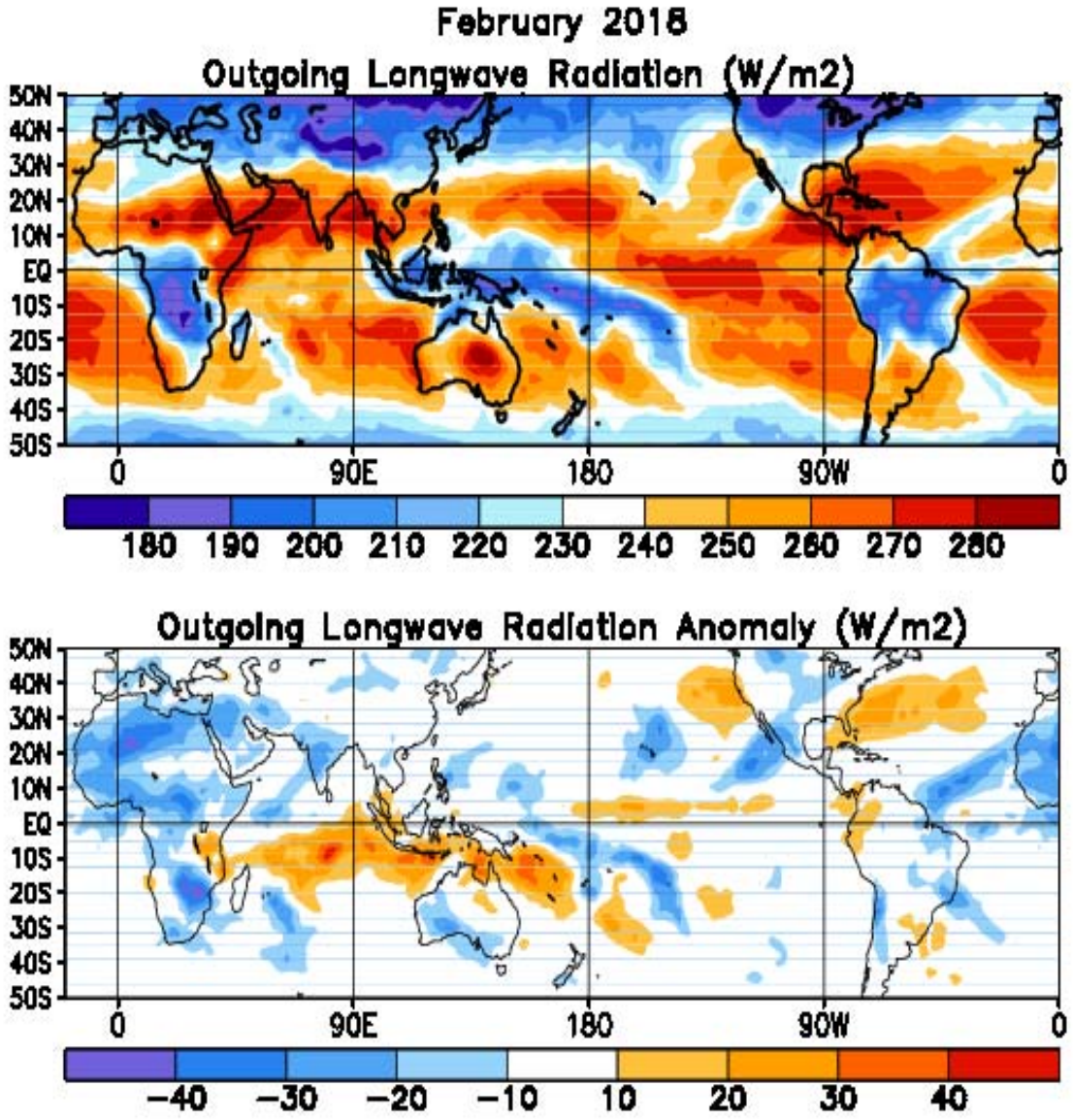


FIGURE T25. Mean (top) and anomalous (bottom) outgoing longwave radiation for FEB 2018 (NOAA 18 AVHRR IR window channel measurements by NESDIS/ORA). OLR contour interval is 20 $Wm^{-2}$ with values greater than 280 $Wm^{-2}$ indicated by dashed contours. Anomaly contour interval is 15 $Wm^{-2}$ with positive values indicated by dashed contours and light shading. Anomalies are departures from the 1981-2010 base period monthly means.

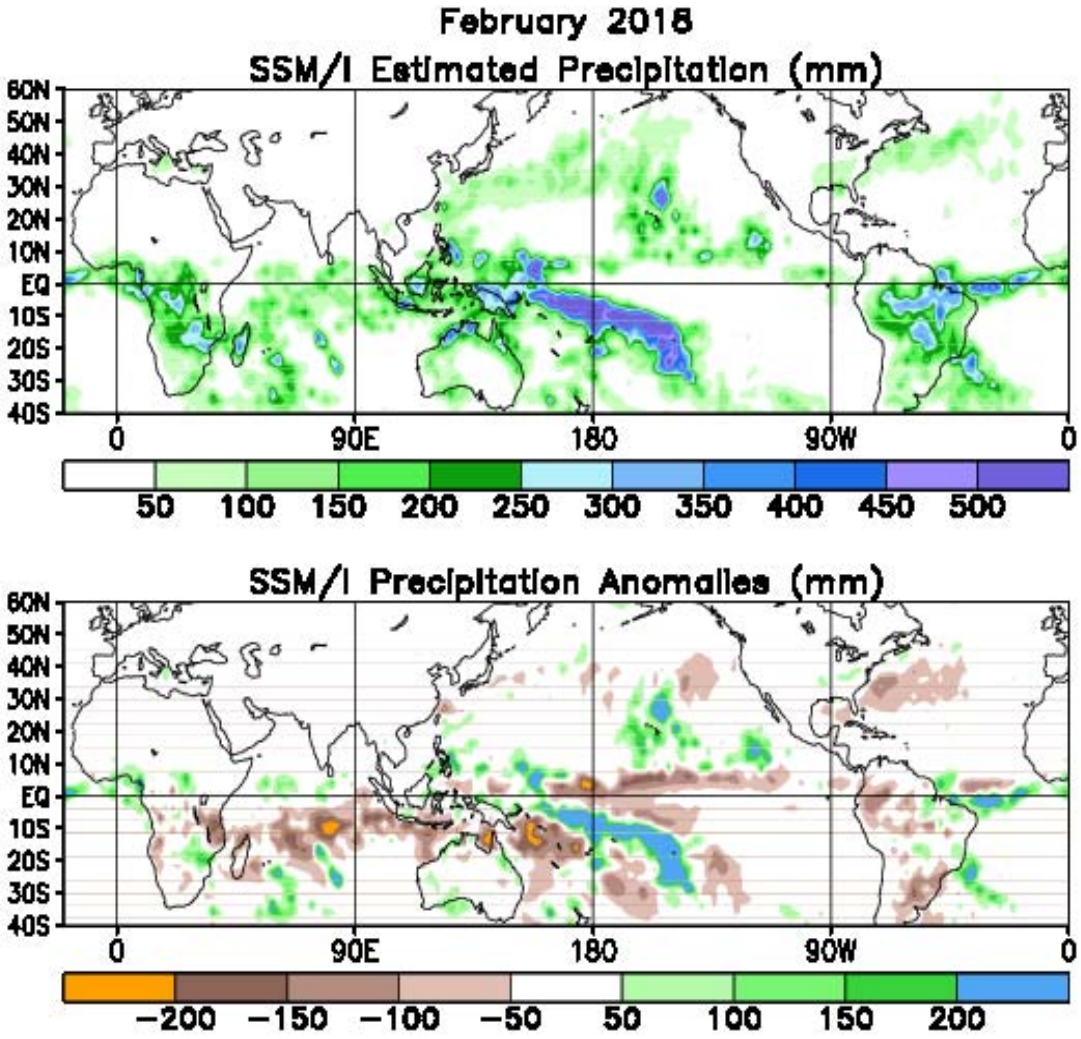


FIGURE T26. Estimated total (top) and anomalous (bottom) rainfall (mm) based on the Special Sensor Microwave/ Imager (SSM/S) precipitation index (Ferraro 1997, *J. Geophys. Res.*, **102**, 16715-16735). Anomalies are computed from the SSM/I 1987-2010 base period monthly means. Anomalies have been smoothed for display purposes.

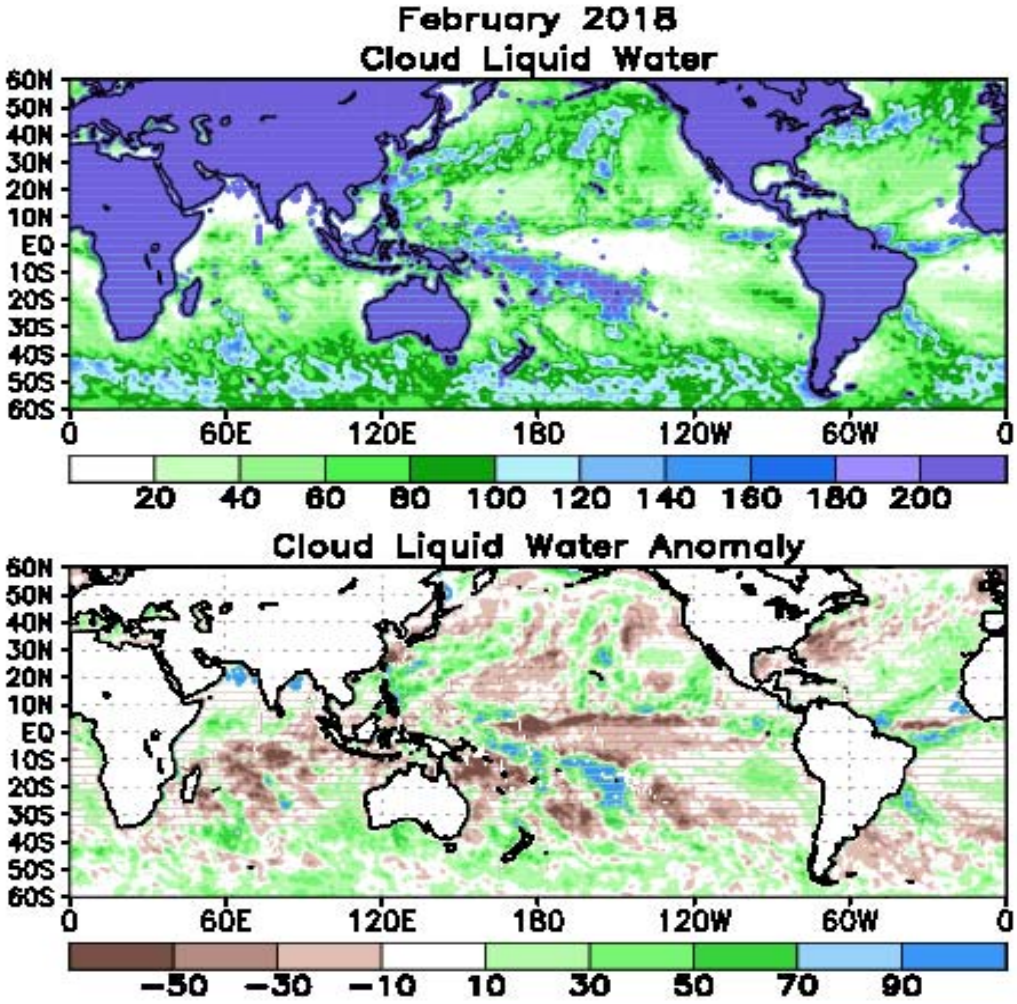


FIGURE T27. Mean (top) and anomalous (bottom) cloud liquid water (g $m^{-2}$) based on the Special Sensor Microwave/ Imager (SSM/I) (Weng et al 1997: *J. Climate*, **10**, 1086-1098). Anomalies are calculated from the 1987-2010 base period means.

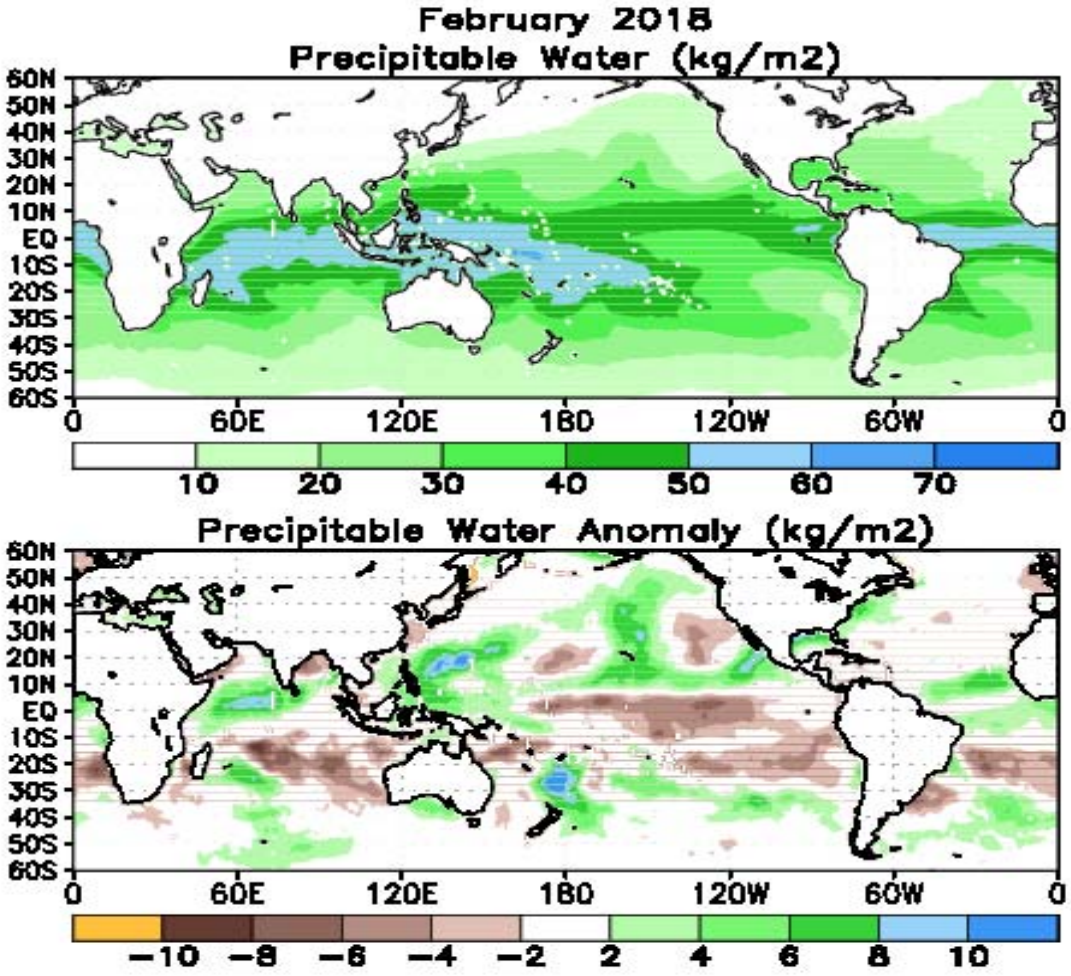


FIGURE T28. Mean (top) and anomalous (bottom) vertically integrated water vapor or precipitable water (kg $m^{-2}$) based on the Special Sensor Microwave/Imager (SSM/I) (Ferraro et. al, 1996: *Bull. Amer. Meteor. Soc.*, **77**, 891-905). Anomalies are calculated from the 1987-2010 base period means.

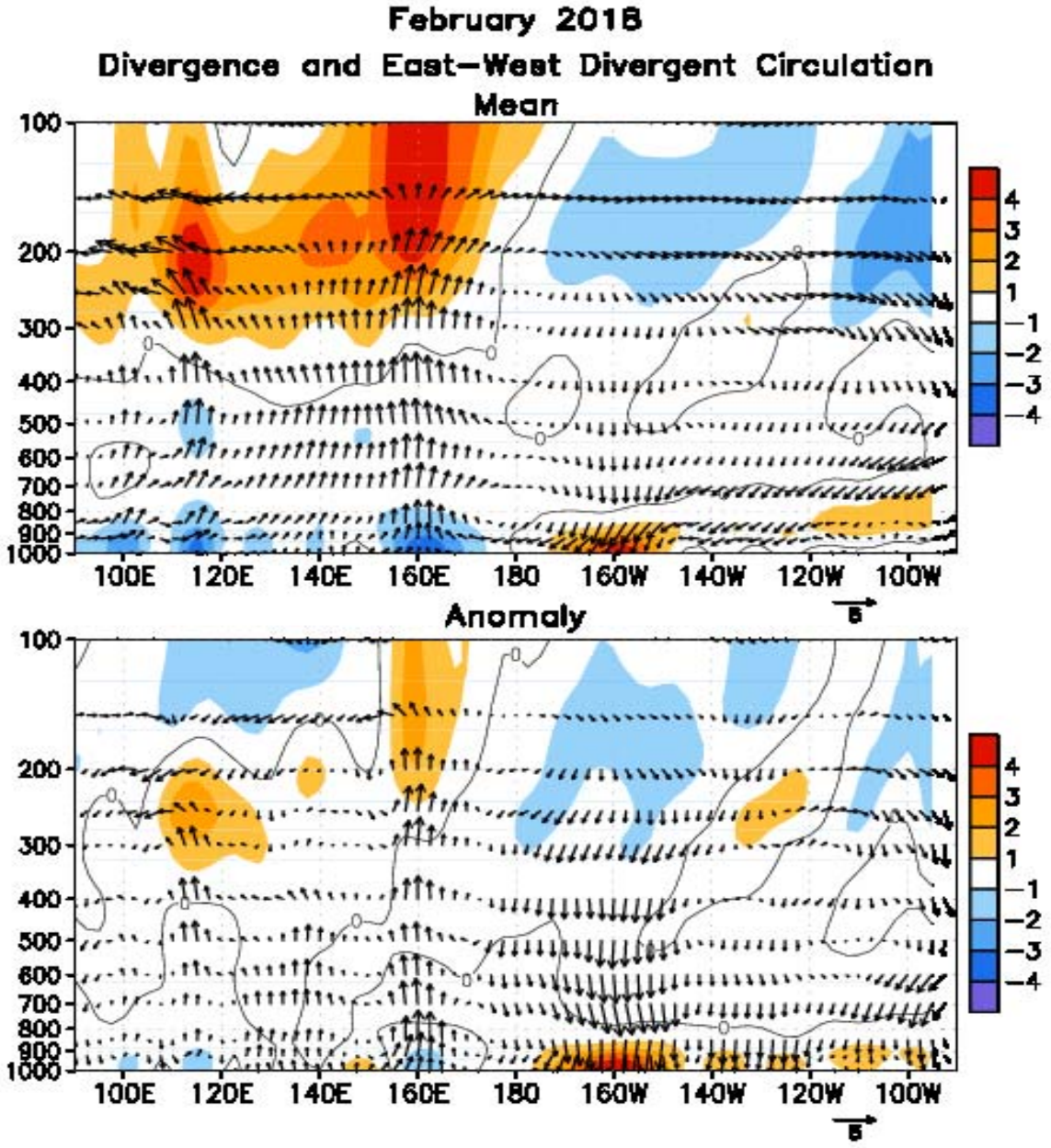


FIGURE T29. Pressure-longitude section (100E-80W) of the mean (top) and anomalous (bottom) divergence (contour interval is 1 x $10^{-6}$ $s^{-1}$) and divergent circulation averaged between 5N-5S. The divergent circulation is represented by vectors of combined pressure vertical velocity and the divergent component of the zonal wind. Red shading and solid contours denote divergence (top) and anomalous divergence (bottom). Blue shading and dashed contours denote convergence (top) and anomalous convergence (bottom). Anomalies are departures from the 1981-2010 base period monthly means.

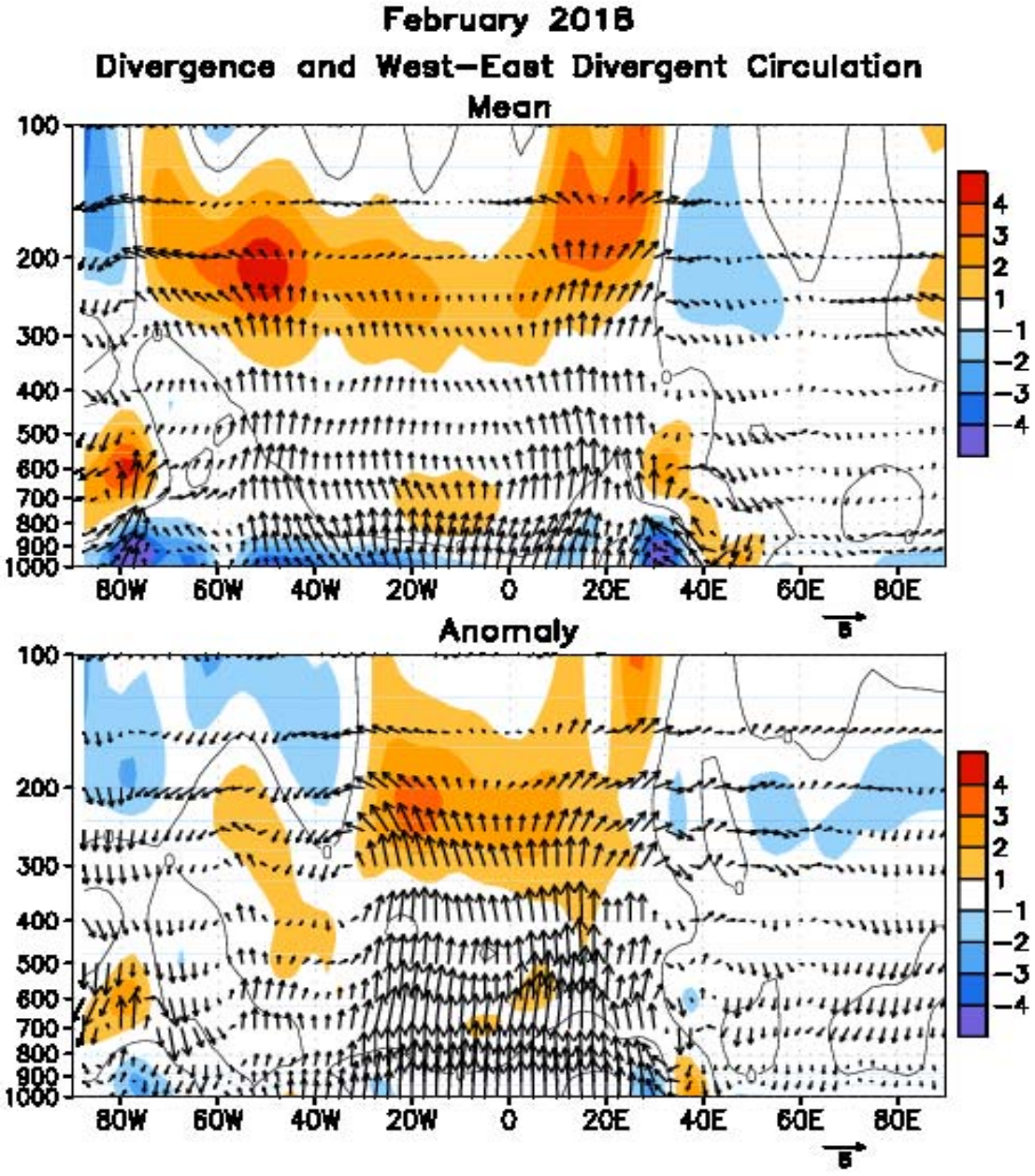


FIGURE T30. Pressure-longitude section (80W-100E) of the mean (top) and anomalous (bottom) divergence (contour interval is 1 x $10^{-6}$ $s^{-1}$) and divergent circulation averaged between 5N-5S. The divergent circulation is represented by vectors of combined pressure vertical velocity and the divergent component of the zonal wind. Red shading and solid contours denote divergence (top) and anomalous divergence (bottom). Blue shading and dashed contours denote convergence (top) and anomalous convergence (bottom). Anomalies are departures from the 1981-2010 base period monthly means.

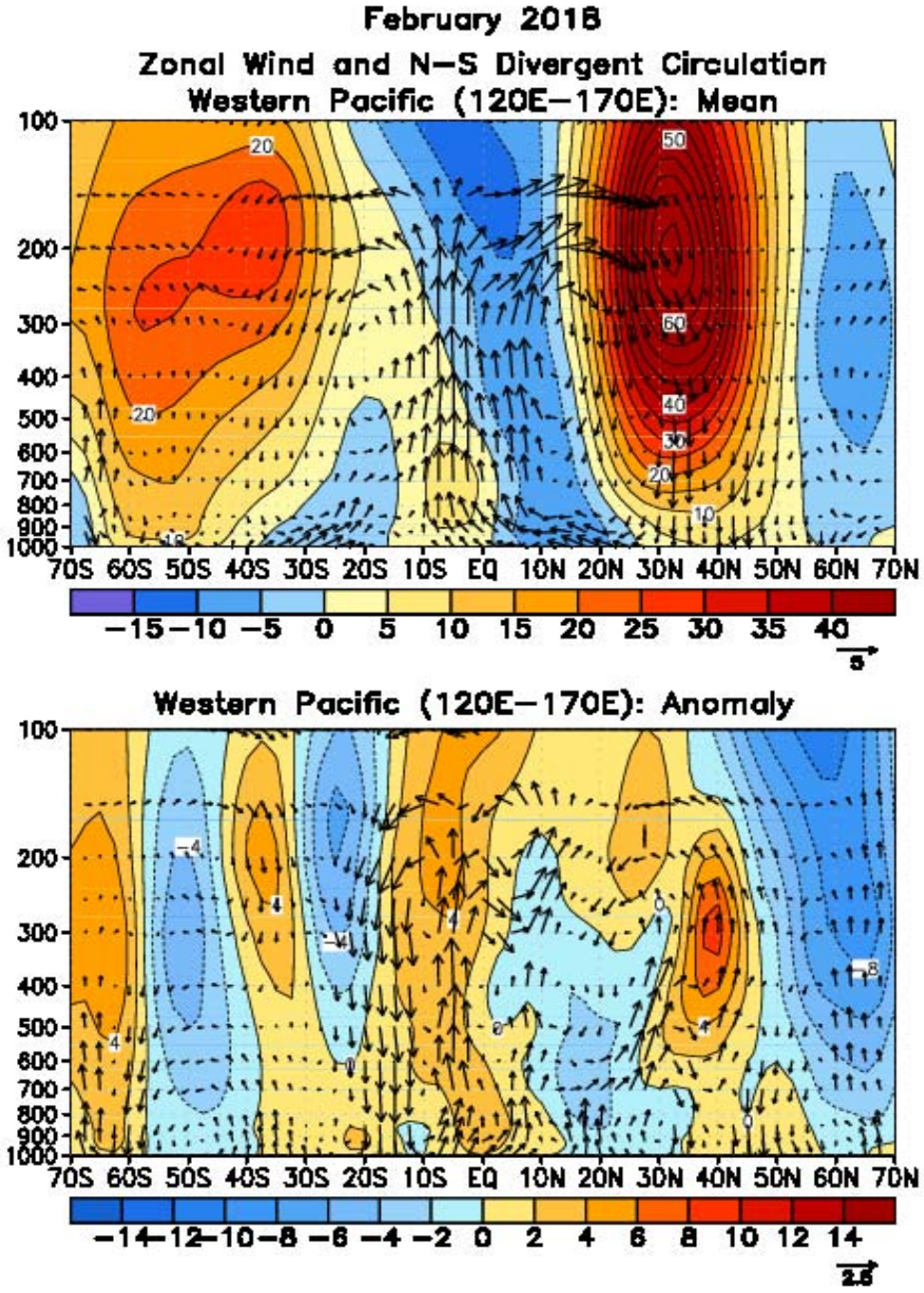


FIGURE T31. Pressure-latitude section of the mean (top) and anomalous (bottom) zonal wind (m $s^{-1}$) and divergent circulation averaged over the west Pacific sector (120E-170E). The divergent circulation is represented by vectors of combined pressure vertical velocity and the divergent component of the meridional wind. Red shading and solid contours denote a westerly (top) or anomalous westerly (bottom) zonal wind. Blue shading and dashed contours denote an easterly (top) or anomalous easterly (bottom) zonal wind. Anomalies are departures from the 1981-2010 base period monthly means.

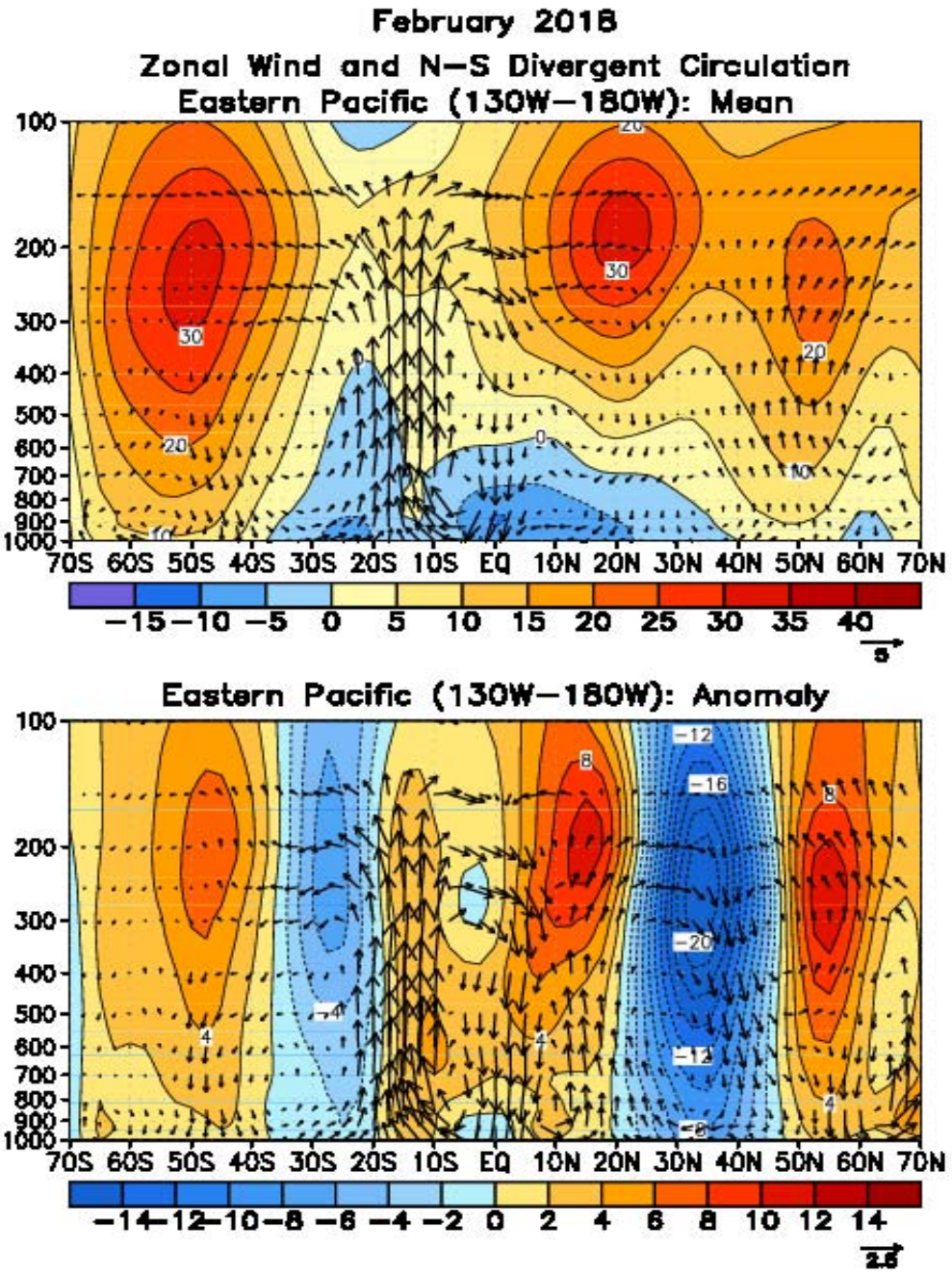


FIGURE T32. Pressure-latitude section of the mean (top) and anomalous (bottom) zonal wind (m $s^{-1}$) and divergent circulation averaged over the central Pacific sector (130W-180W). The divergent circulation is represented by vectors of combined pressure vertical velocity and the divergent component of the meridional wind. Red shading and solid contours denote a westerly (top) or anomalous westerly (bottom) zonal wind. Blue shading and dashed contours denote an easterly (top) or anomalous easterly (bottom) zonal wind. Anomalies are departures from the 1981-2010 base period monthly means.

Tropical Pacific Drifting Buoys R. Lumpkin/M. Pazos, AOML, Miami

During February 2018, 1459 satellite-tracked surface drifting buoys were reporting from the tropical Pacific. The drifter array revealed strong Tropical Instability Waves at 90-100W, and westward aomalies of ~20 cm/s at 130-140W, 10N. West of 160E near and south of the equator, four drifters indicated very strong (>40 cm/s) eastward anomalies.

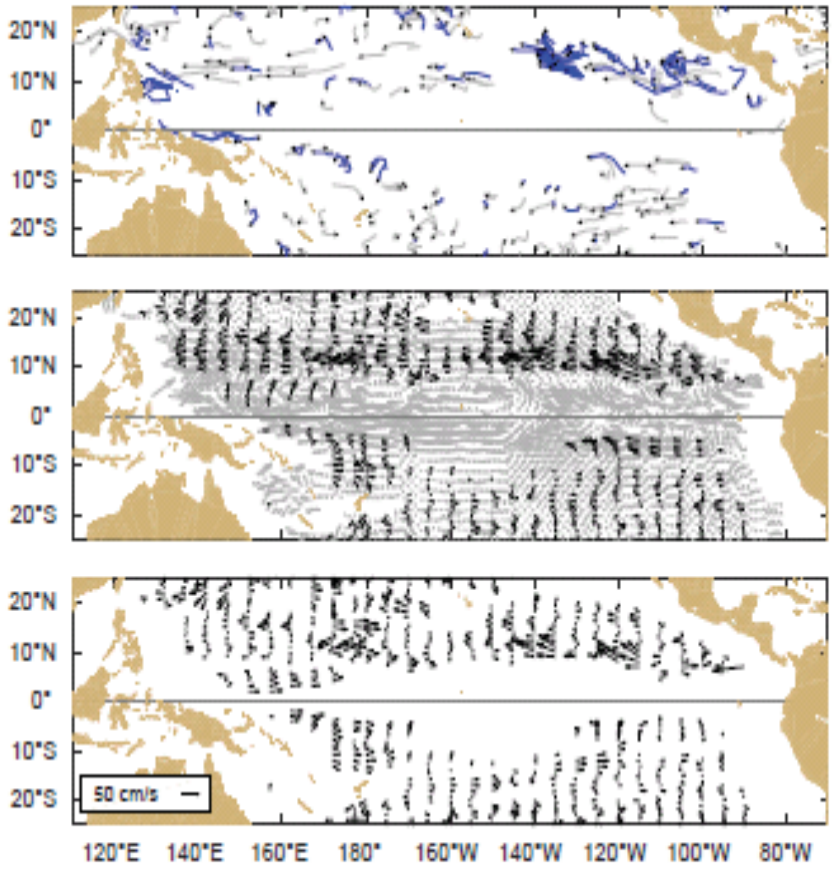


**Figure A1.1 Top:** Movements of drifting buoys in the tropical Pacific Ocean during February 2018. The linear segments of each trajectory represent a one week displacement. Trajectories of buoys which have lost their subsurface drogues are gray; those with drogues are black.
**Middle:** Monthly mean currents calculated from all buoys 1993-2002 (gray), and currents measured by the drogued buoys this month (black) smoothed by an optimal filter.
**Bottom:** Anomalies from the climatological monthly mean currents for this month.

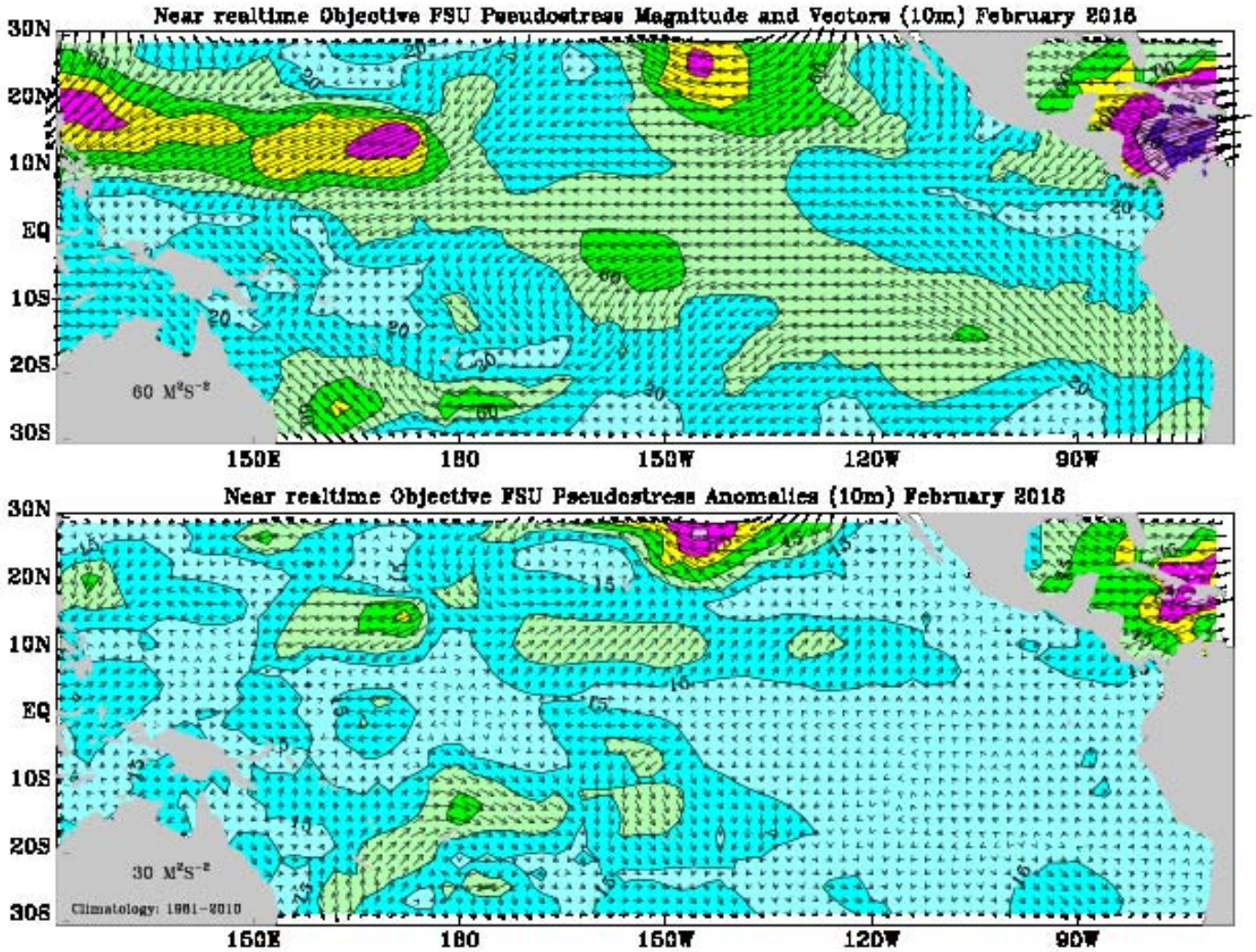


FSU SURFACE PSEUDO-STRESS VECTORS AND ANOMALIES: February 2018. Pseudo-stress vectors (top) are objectively analyzed from ship and buoy winds on a 2° grid. Ship and buoy data are independently weighted and the background field is created from the data. Contour interval of the vector magnitudes is 20 $M^2S^{-2}$. Anomalies (bottom) are departures from 1981-2010 mean. The contour interval is 15 $M^2S^{-2}$. For more information, please visit our web site at http://www.coaps.fsu.edu/RVSMDC/html/winds.shtml. Produced by Jeremy Ralph, Mark A. Bourassa, and Shawn R. Smith, Center for Ocean-Atmospheric Prediction Studies, Florida State University, Tallahassee, FL 32306-2840, USA.

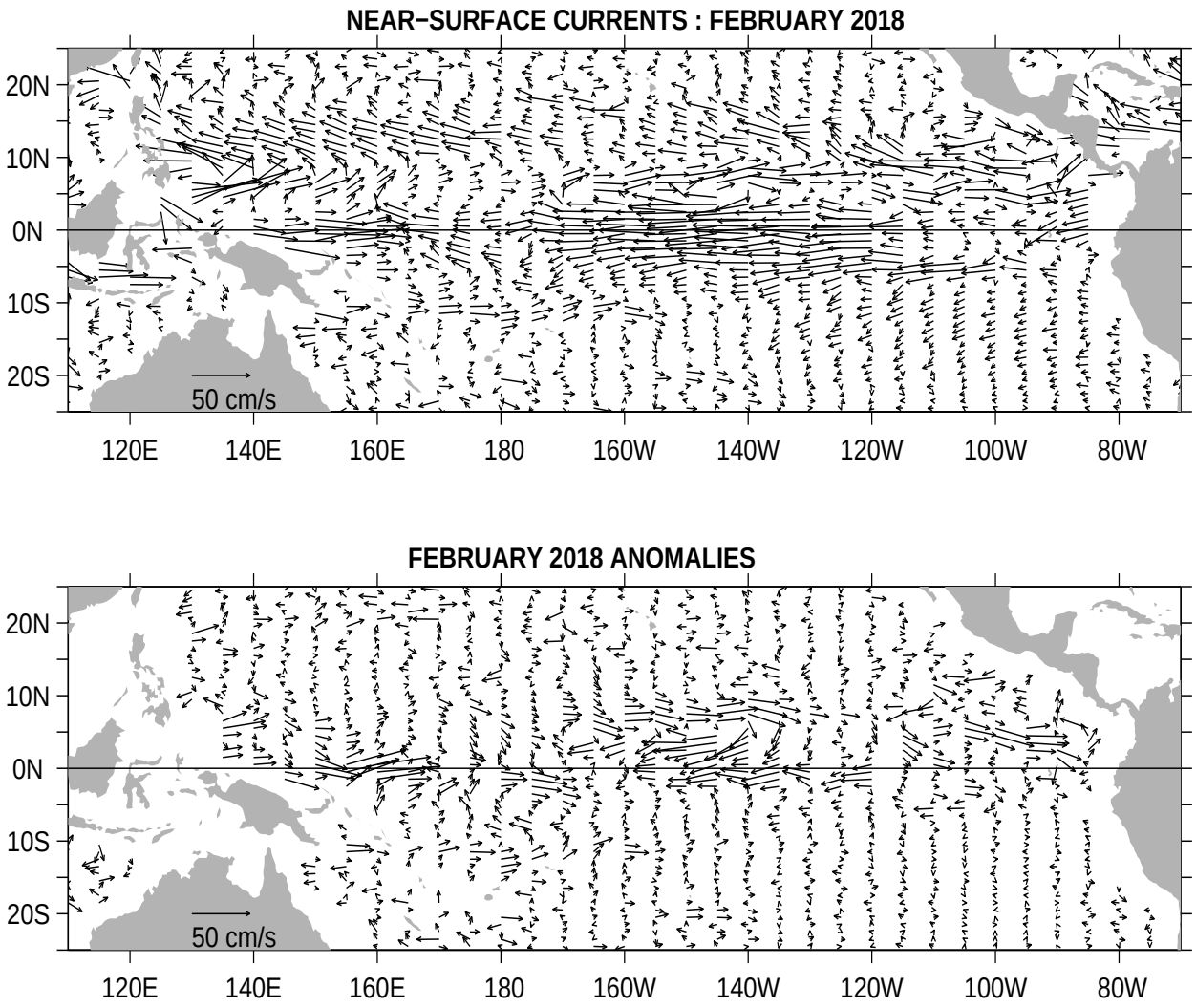


FIGURE A1.3. Ocean Surface Current Analysis-Real-time (OSCAR) for FEB 2018 (Bonjean and Lagerloef 2002, J. Phys. Oceanogr., Vol. 32, No. 10, 2938-2954; Lagerloef et al. 1999, JGR-Oceans, 104, 23313-23326). (top) Total velocity. Surface currents are calculated from satellite data including Jason sea level anomalies and NCEP winds. (bottom) Velocity anomalies. The subtracted climatology was based on SSM/I and QuickScat winds and Topex/ Poseidon and Jason from 1993-2003. See also http://www.oscar.noaa.gov.

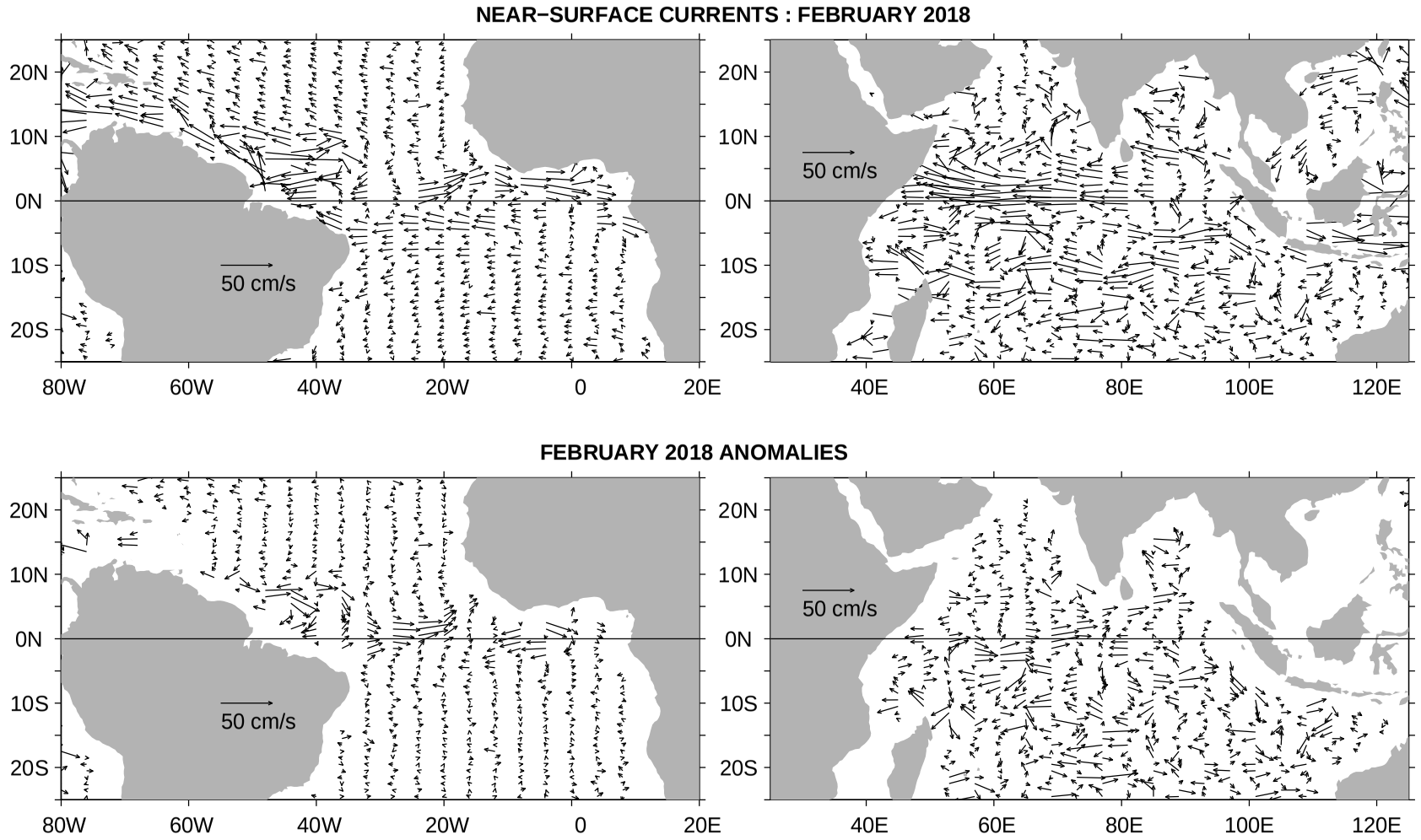


FIGURE A1.4. Ocean Surface Current Analysis-Real-time (OSCAR) for FEB 2018 (Bonjean and Lagerloef 2002, J. Phys. Oceanogr., Vol. 32, No. 10, 2938-2954; Lagerloef et al. 1999, JGR-Oceans, 104, 23313-23326). (top) Total velocity. Surface currents are calculated from satellite data including Jason sea level anomalies and NCEP winds. (bottom) Velocity anomalies. The subtracted climatology was based on SSM/I and QuickScat winds and Topex/Poseidon and Jason from 1993-2003. See also http://www.oscar.noaa.gov.

# Forecast Forum

The canonical correlation analysis (CCA) forecast of SST in the central Pacific (Barnett et al. 1988, *Science*, **241**, 192196; Barnston and Ropelewski 1992, *J. Climate*, **5**, 13161345), is shown in **Figs. F1 and F2.** This forecast is produced routinely by the Prediction Branch of the Climate Prediction Center. The predictions from the National Centers for Environmental Prediction (NCEP) Coupled Forecast System Model (CFS03) are presented in **Figs. F3 and F4a, F4b**. Predictions from the Markov model (Xue, et al. 2000: *J. Climate*, **13**, 849871) are shown in **Figs. F5 and F6.** Predictions from the latest version of the LDEO model (Chen et al. 2000: *Geophys. Res. Let*., **27**, 25852587) are shown in **Figs. F7 and F8**. Predictions using linear inverse modeling (Penland and Magorian 1993: *J. Climate*, **6**, 10671076) are shown in **Figs. F9 and F10.** Predictions from the Scripps / Max Planck Institute (MPI) hybrid coupled model (Barnett et al. 1993: *J. Climate*, **6**, 15451566) are shown in **Fig. F11.** Predictions from the ENSOCLIPER statistical model (Knaff and Landsea 1997, *Wea. Forecasting*, **12**, 633652) are shown in **Fig. F12.** Niño 3.4 predictions are summarized in **Fig. F13**, provided by the Forecasting and Prediction Research Group of the IRI.

The CPC and the contributors to the **Forecast Forum** caution potential users of this predictive information that they can expect only modest skill.

# ENSO Alert System Status: La Niña Advisory

# Outlook

A transition from La Niña to ENSO-neutral is most likely (~55% chance) during the March-May season, with neutral conditions likely to continue into the second half of the year.

# Discussion

During February 2018, La Niña weakened, but was still reflected by below-average sea surface temperatures (SSTs) in the east-central equatorial Pacific Ocean (Fig. T18). The monthly index values were -0.9C and -1.0C in the Niño-3.4 and Niño-3 regions, respectively, and were less negative in the surrounding Niño.4 and Niño1+2 regions (Table T2). While negative anomalies were maintained near the surface, the sub-surface temperature anomalies (averaged across 180°-100°W) warmed to near zero. This warming was due to the eastward propagation of above-average temperatures along the thermocline in association with a downwelling equatorial oceanic Kelvin wave (Fig. T17). The atmospheric anomalies typical of La Niña weakened considerably across the tropical Pacific. Con-

vection was suppressed near Indonesia and was only weakly enhanced over the far western Pacific (Fig. T25). Also, low-level wind anomalies were westerly over the western and central Pacific, while upper-level winds remained anomalously westerly over the eastern Pacific (Figs. T20, T21). Overall, the ocean and atmosphere system suggests La Niña is weakening.

Most models in the IRI/CPC plume predict La Niña will decay and return to ENSO-neutral during the Northern Hemisphere spring 2018 (Figs. F1-F13). The forecast consensus similarly favors a transition during the spring, with a continuation of ENSO-neutral conditions through the summer. In summary, a transition from La Niña to ENSO-neutral is most likely (~55% chance) during the March-May season, with neutral conditions likely to continue into the second half of the year.

Weekly updates of oceanic and atmospheric conditions are available on the Climate Prediction Center homepage (El Niño/La Niña Current Conditions and Expert Discussions).

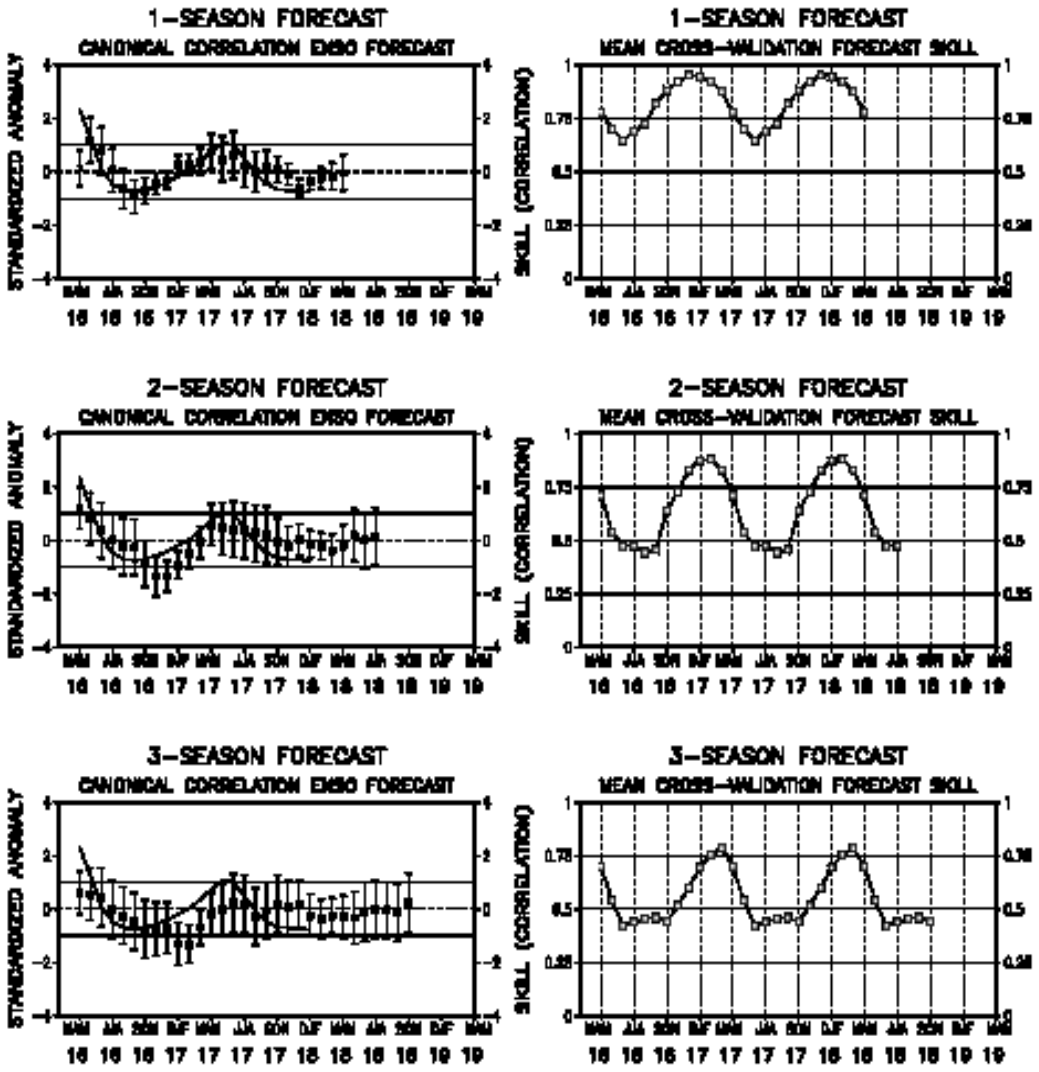


FIGURE F1. Canonical correlation analysis (CCA) sea surface temperature (SST) anomaly prediction for the central Pacific (5˚N to 5˚S, 120˚W to 170˚W (Barnston and Ropelewski, 1992, *J. Climate*, **5**, 1316-1345). The three plots on the left hand side are, from top to bottom, the 1-season, 2-season, and 3-season lead forecasts. The solid line in each forecast represents the observed SST standardized anomaly through the latest month. The small squares at the mid-points of the forecast bars represent the real-time CCA predictions based on the anomalies of quasi-global sea level pressure and on the anomalies of tropical Pacific SST, depth of the 20˚C isotherm and sea level height over the prior four seasons. The vertical lines represent the one standard deviation error bars for the predictions based on past performance. The three plots on the right side are skills, corresponding to the predicted and observed SST. The skills are derived from cross-correlation tests from 1956 to present. These skills show a clear annual cycle and are inversely proportional to the length of the error bars depicted in the forecast time series.

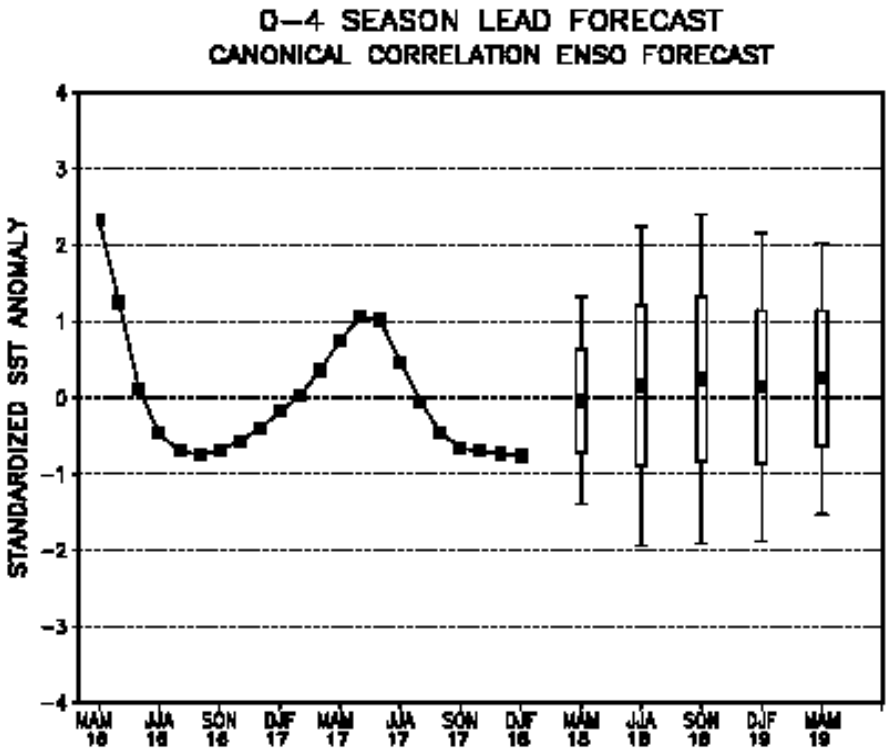


FIGURE F2. Canonical Correlation Analysis (CCA) forecasts of sea-surface temperature anomalies for the Nino 3.4 region (5N-5S, 120W-170W) for the upcoming five consecutive 3-month periods. Forecasts are expressed as standardized SST anomalies. The CCA predictions are based on anomaly patterns of SST, depth of the 20C isotherm, sea level height, and sea level pressure. Small squares at the midpoints of the vertical forecast bars represent the CCA predictions, and the bars show the one (thick) and two (thin) standard deviation errors. The solid continuous line represents the observed standardized three-month mean SST anomaly in the Nino 3.4 region up to the most recently available data.

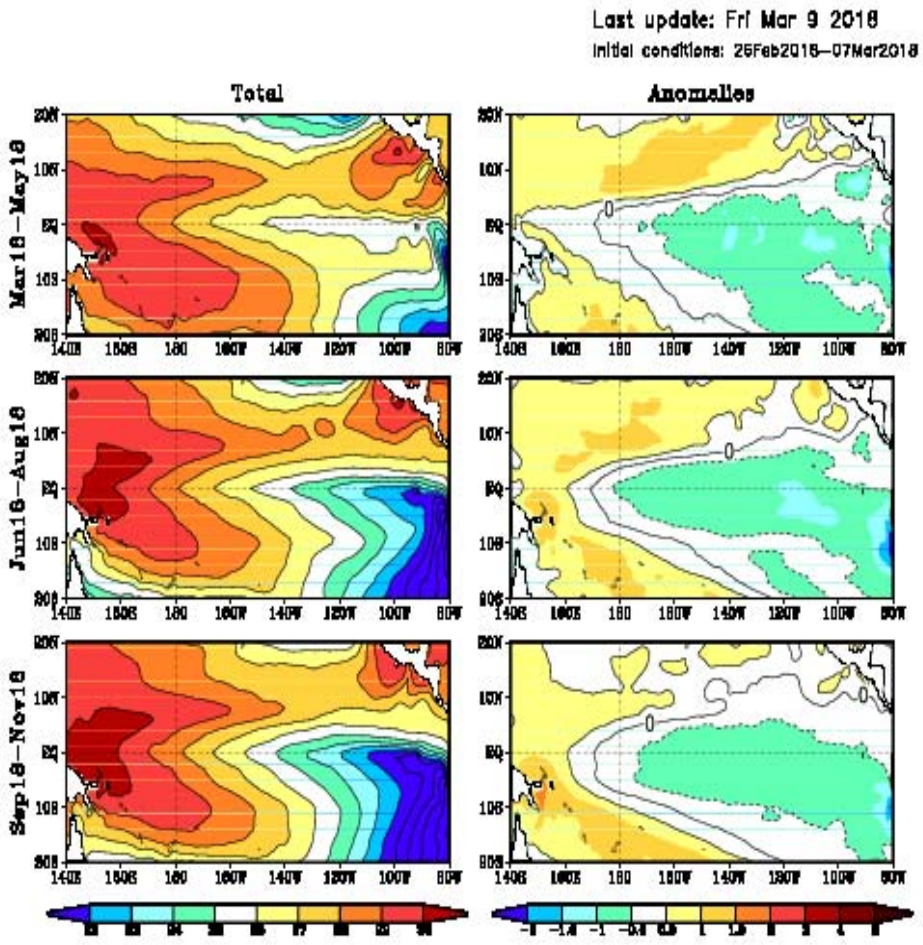


FIGURE F3. Predicted 3-month average sea surface temperature (left) and anomalies (right) from the NCEP Coupled Forecast System Model (CFS03). The forecasts consist of 40 forecast members. Contour interval is 1°C, with additional contours for 0.5°C and -0.5°C. Negative anomalies are indicated by dashed contours.

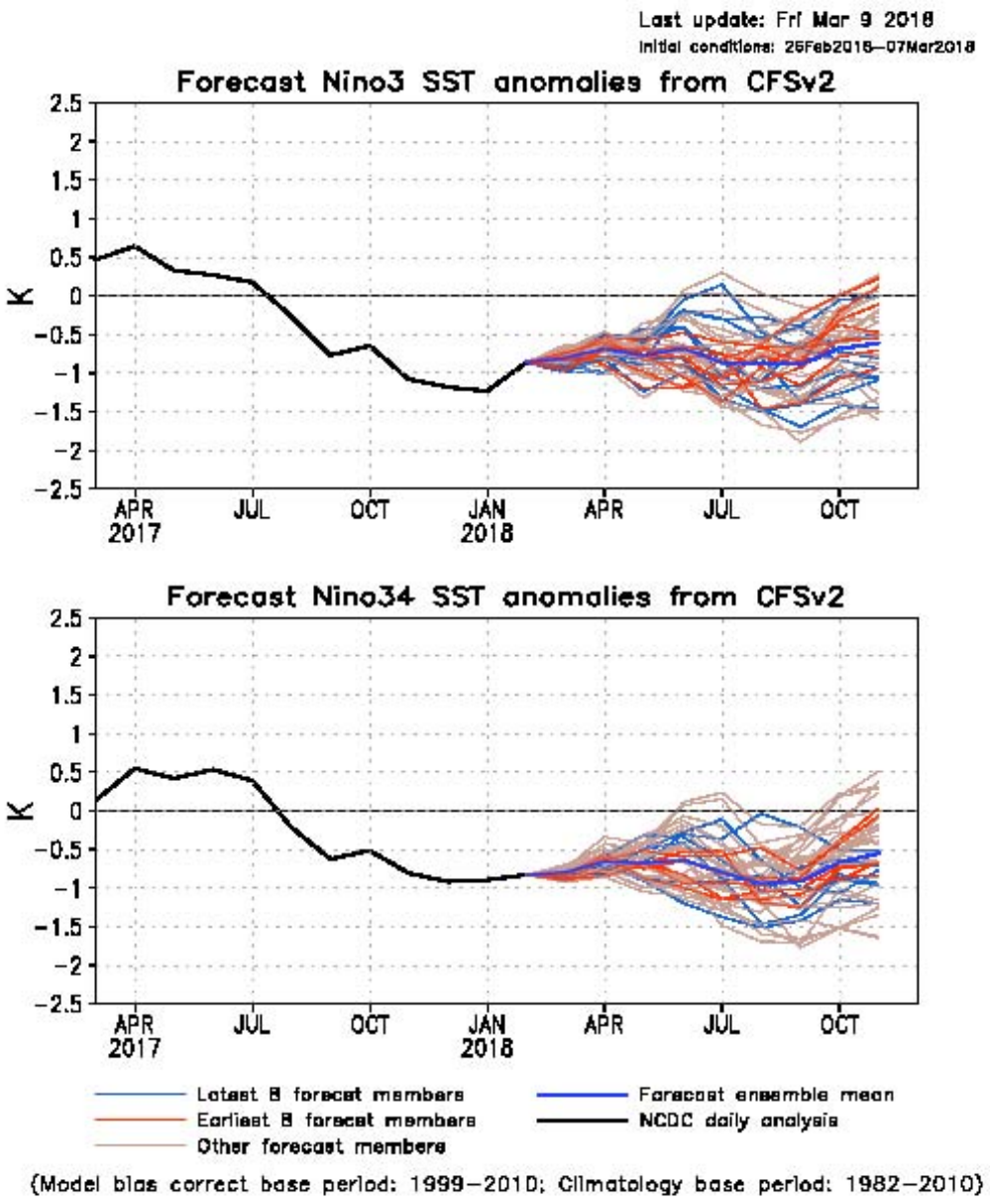


FIGURE F4. Predicted and observed sea surface temperature (SST) anomalies for the Nino 3 (top) and Nino 3.4 (bottom) regions from the NCEP Coupled Forecast System Model (CFS03). The forecasts consist of 40 forecast members. The ensemble mean of all 40 forecast members is shown by the blue line, individual members are shown by thin lines, and the observation is indicated by the black line. The Nino-3 region spans the eastern equatorial Pacific between 5N-5S, 150W-90W. The Nno 3.4 region spans the east-central equatorial Pacific between 5N-5S, 170W-120W.

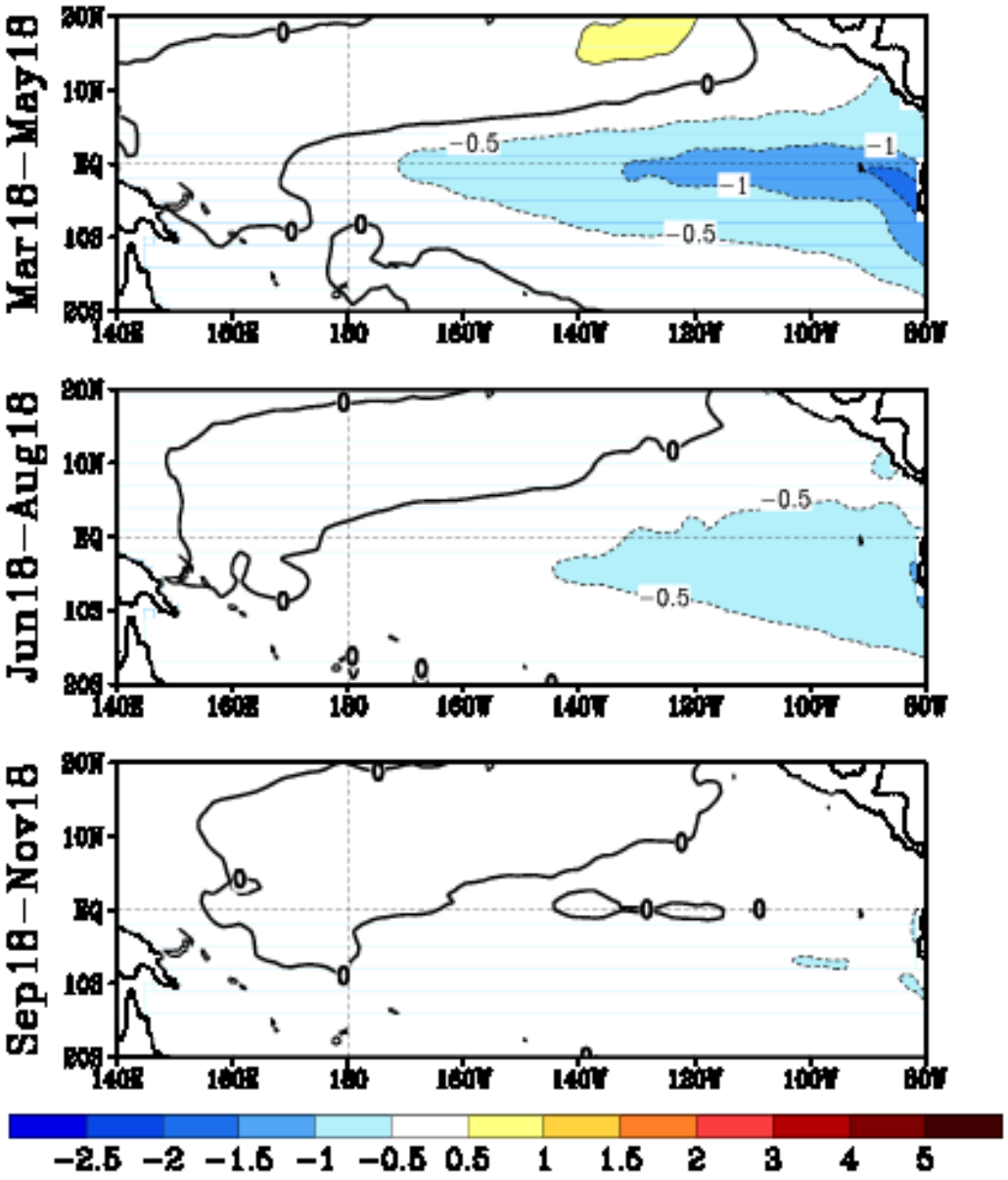


FIGURE F5. Predicted 3-month average sea surface temperature anomalies from the NCEP/CPC Markov model (Xue et al. 2000, *J. Climate*, **13**, 849-871). The forecast is initiated in FEB 2018 . Contour interval is 0.3C and negative anomalies are indicated by dashed contours. Anomalies are calculated relative to the 1971-2000 climatology.

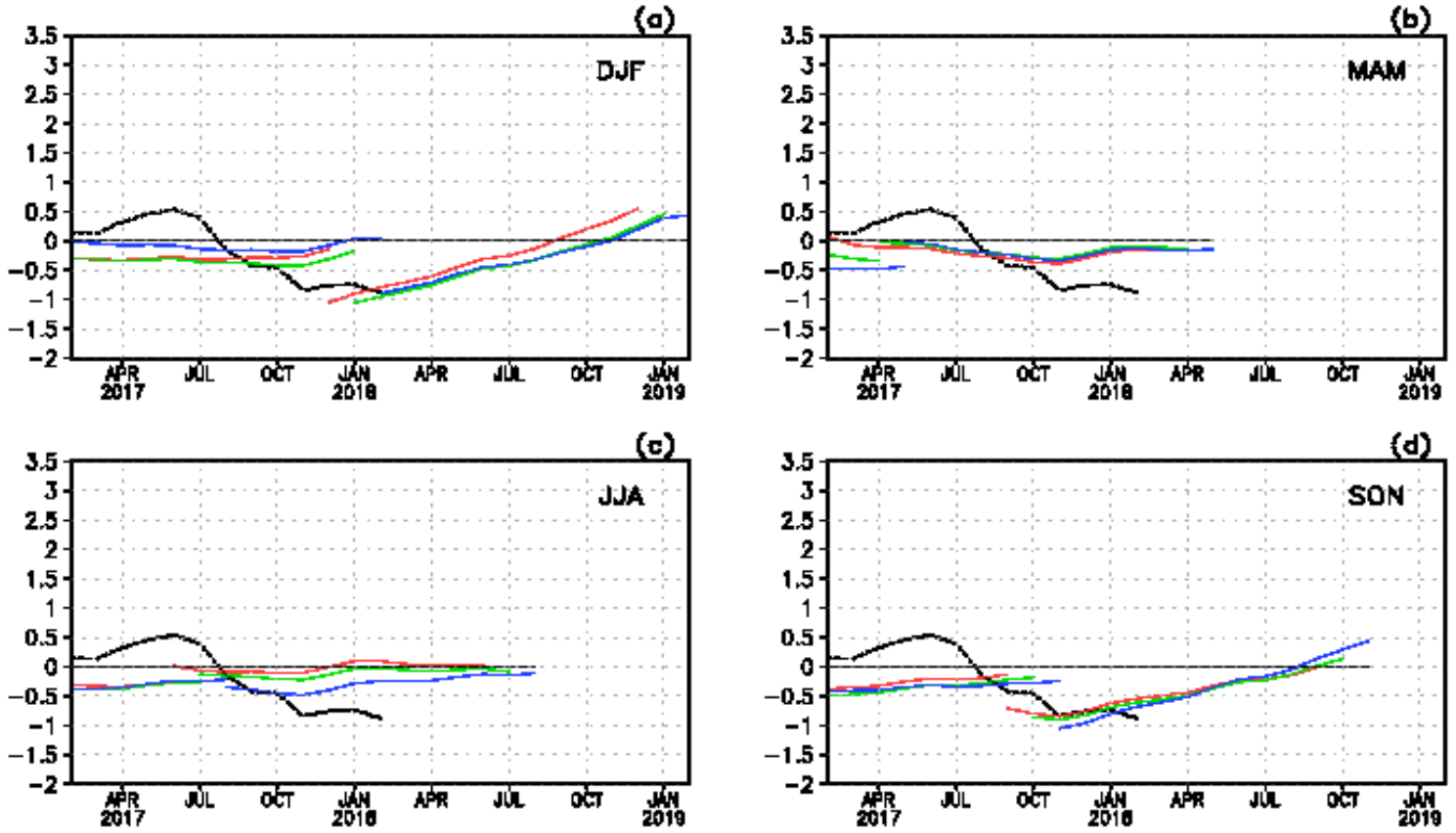


FIGURE F6. Time evolution of observed and predicted SST anomalies in the Nino 3.4 region (up to 12 lead months) by the NCEP/CPC Markov model (Xue et al. 2000, *J. Climate*, **13**, 849-871). Anomalies are calculated relative to the 1971-2000 climatology. Shown in each panel are the forecasts grouped by three consecutive starting months: (a) is for December, January, and February, (b) is for March, April, and May, (c) is for June, July, and August, and (d) is for September, October, and November. The observed Nino 3.4 SST anomalies are indicated by the black dashed lines. The Nino 3.4 region spans the east-central equatorial Pacific between 5N-5S, 170W-120W.

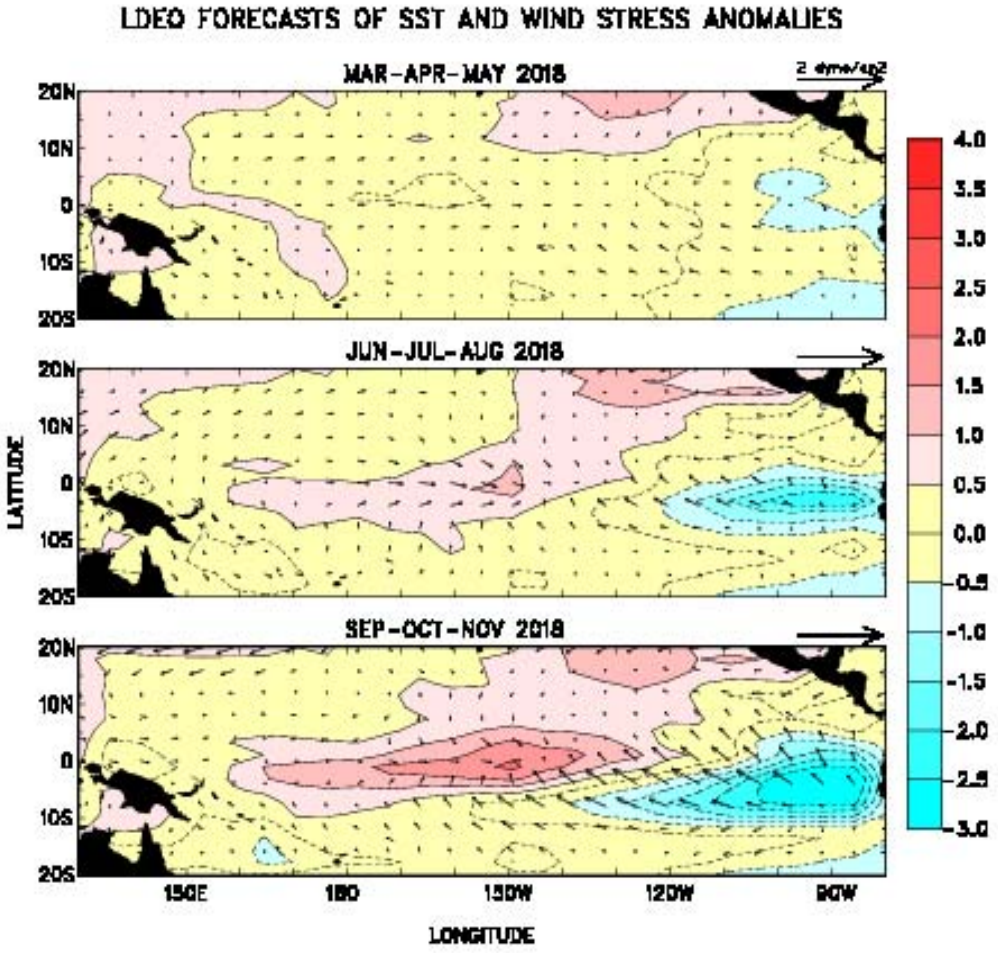


**FIGURE F7.** Forecasts of the tropical Pacific Predicted SST (shading) and vector wind anomalies for the next 3 seasons based on the LDEO model. Each forecast represents an ensemble average of 3 sets of predictions initialized during the last three consecutive months (see Figure F8).

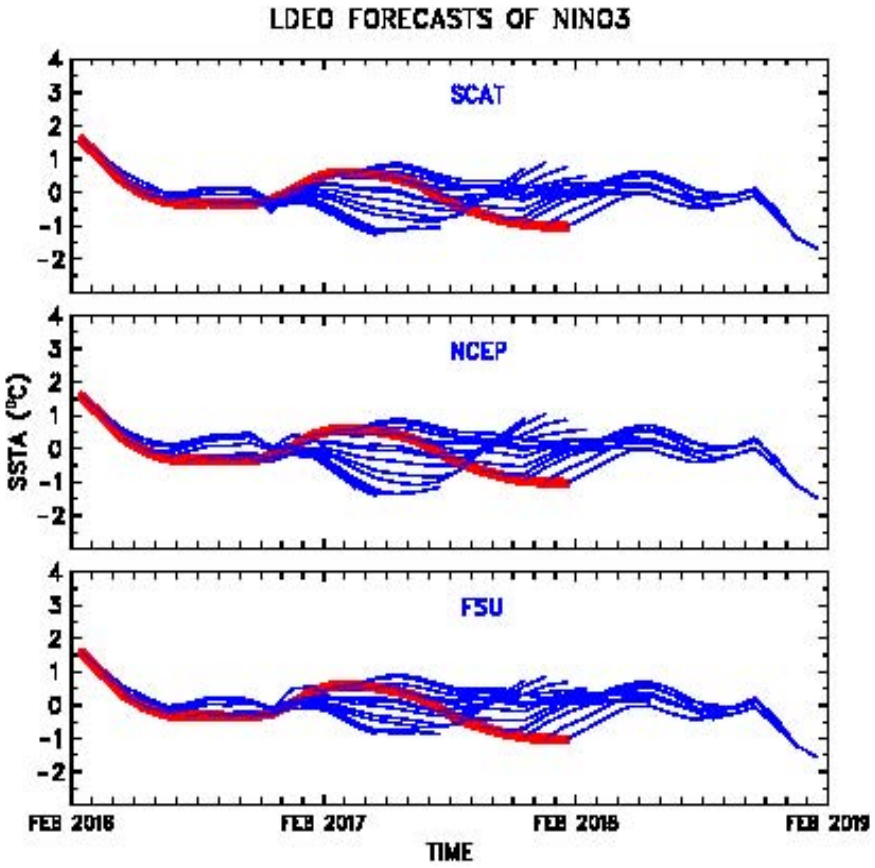


**FIGURE F8.** LDEO forecasts of SST anomalies for the Nino 3 region using wind stresses obtained from (top) QuikSCAT, (middle) NCEP, and (bottom) Florida State Univ. (FSU), along with SSTs (obtained from NCEP), and sea surface height data (obtained from TOPEX/POSEIDON) data. Each thin blue line represents a 12-month forecast, initialized one month apart for the past 24 months. Observed SST anomalies are indicated by the thick red line. The Nino-3 region spans the eastern equatorial Pacific between 5N-5S, 150W-90W.

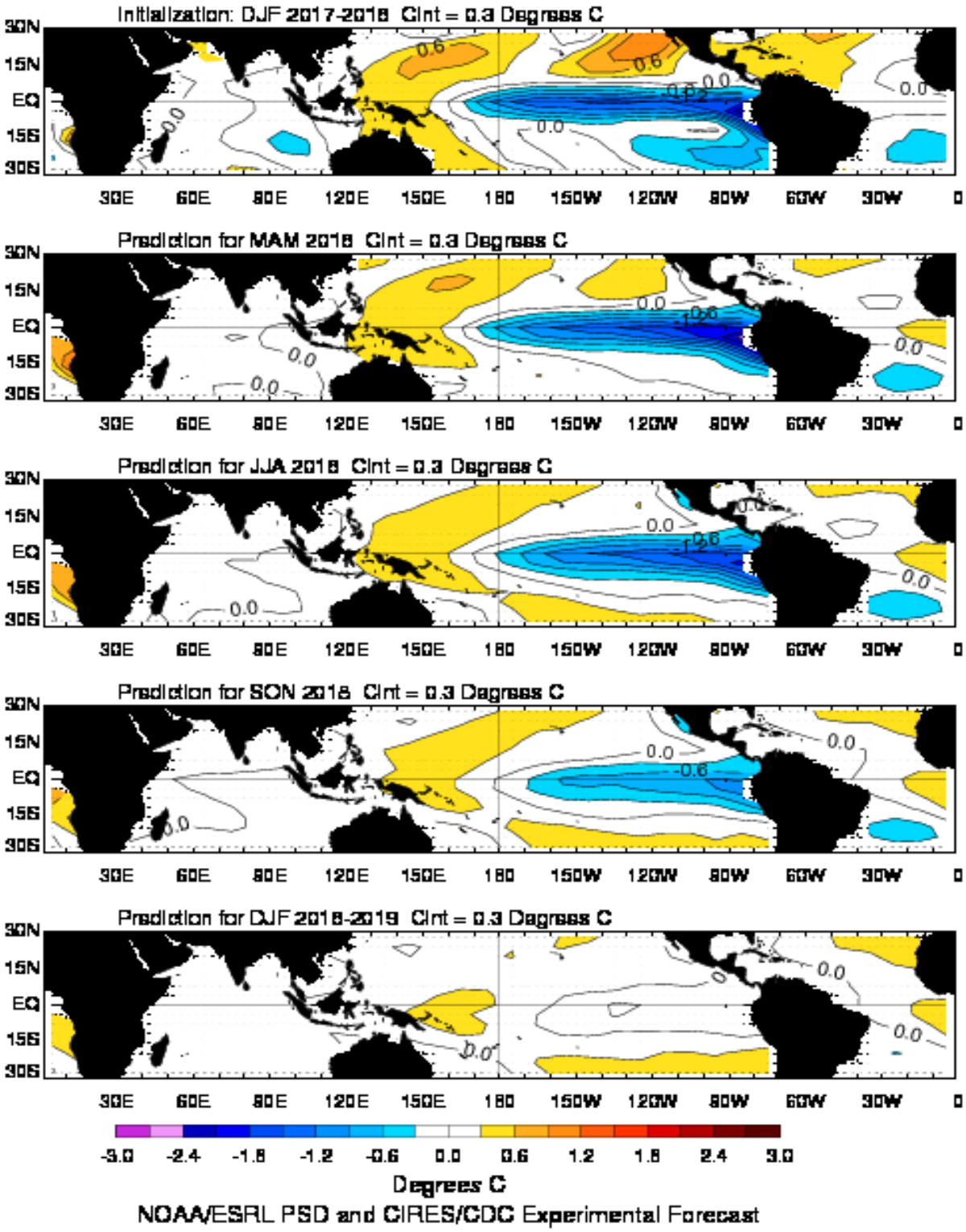


FIGURE F9. Forecast of tropical SST anomalies from the Linear Inverse Modeling technique of Penland and Magorian (1993: *J. Climate*, **6**, 1067-1076). The contour interval is 0.3C. Anomalies are calculated relative to the 1981-2010 climatology and are projected onto 20 leading EOFs.

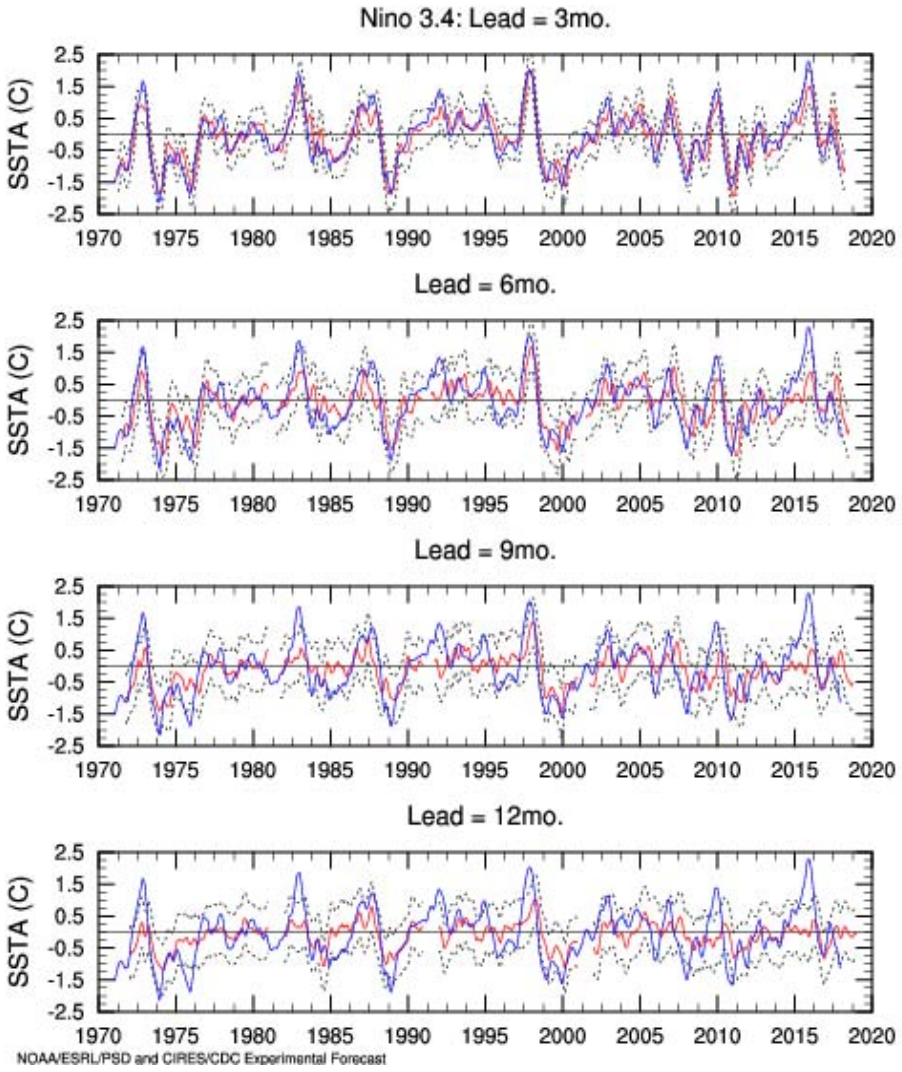


FIGURE F10. Predictions of Niño 3.4 SSTA (blue solid line) and verification (solid red line). The Niño3.4 Index was calculated in the area 6N-6S, 170W-120W. The 1980-2010 climatology was subtracted from ERSST data between 1950 and 2010, after which they were projected onto 20 EOFs containing 90% of thevariance. Significant 1950-2010 trends were subtracted from the corresponding PCs, the forecast was made on the detrended anomalies, after which the trend was added to the forecast. The dotted lines indicate the one standard deviation confidence interval for the forecasts based on a perfect adherence to assumption.

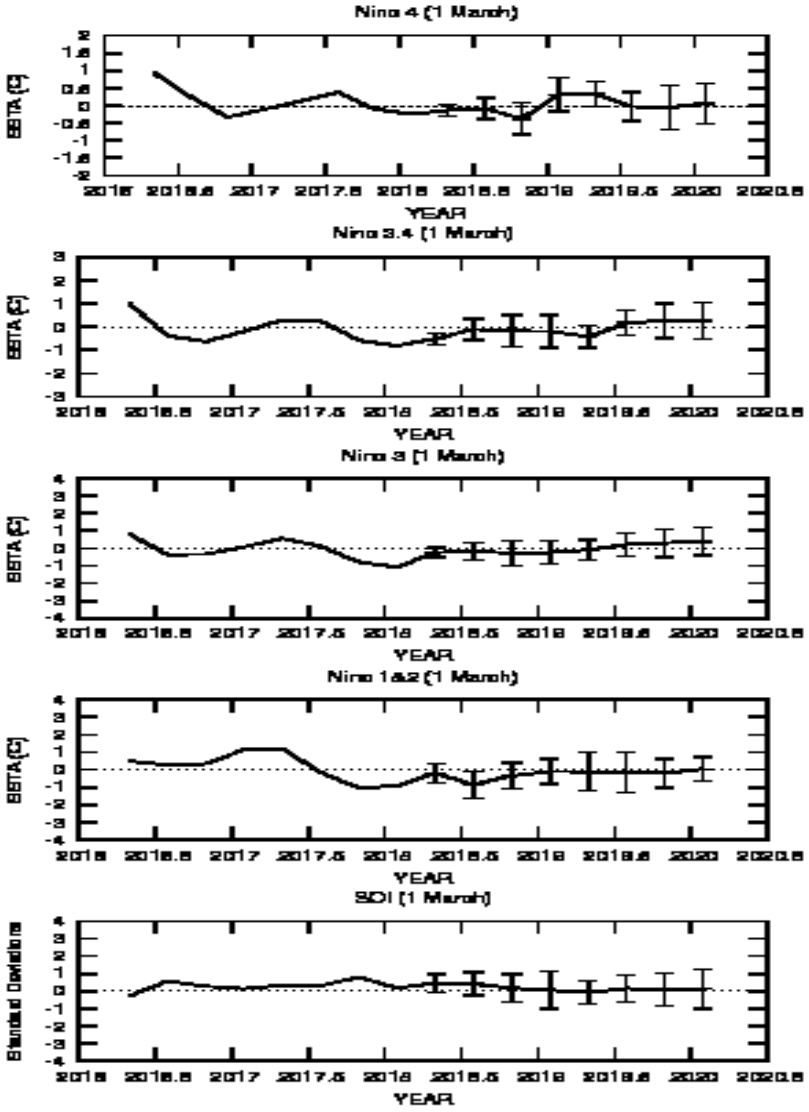


FIGURE F11. ENSO-CLIPER statistical model forecasts of three-month average sea surface temperature anomalies (green lines, deg. C) in (top panel) the Nino 4 region (5N-5S, 160E-150W), (second panel) the Nino 3.4 region (5N-5S, 170W-120W), (third panel) the Nino 3 region (5N-5S, 150W-90W), and (fourth panel) the Nino 1+2 region (0-10S, 90W-80W) (Knaff and Landsea 1997, *Wea. Forecasting*, **12**, 633-652). Bottom panel shows predictions of the three-month standardized Southern Oscillation Index (SOI, green line). Horizontal bars on green line indicate the adjusted root mean square error (RMSE). The Observed three-month average values are indicated by the thick blue line. SST anomalies are departures from the 1981-2010 base period means, and the SOI is calculated from the 1951-1980 base period means.

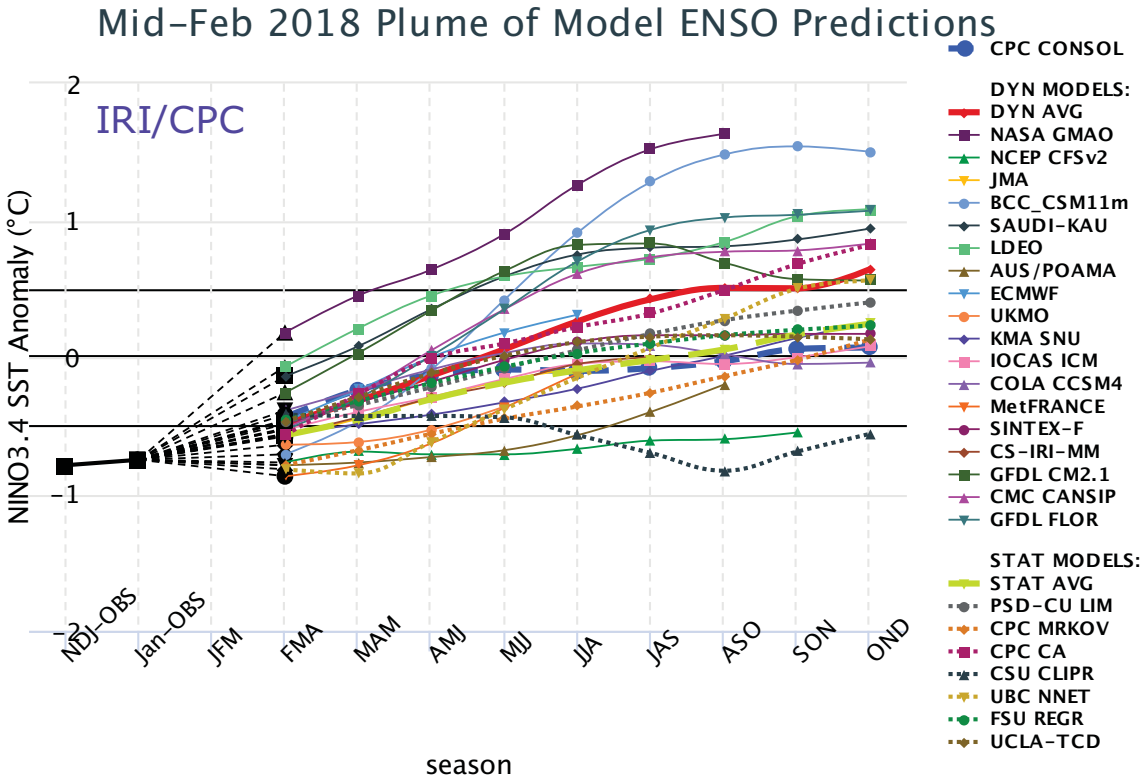


FIGURE F12. Time series of predicted sea surface temperature anomalies for the Nino 3.4 region (deg. C) from various dynamical and statistical models for nine overlapping 3-month periods. The Nino 3.4 region spans the east-central equatorial Pacific between 5N-5S, 170W-120W. Figure provided by the International Research Institute (IRI).

# Extratropical Highlights – February 2018

1. Northern Hemisphere

The 500-hPa circulation during February featured a highly amplified anomalous wave pattern (Fig. E9), and continued to be strongly influenced by La Niña and the Madden Julian Oscillation (MJO). Above-average heights were present over the high latitudes of the North Pacific, the eastern U.S., and large portions of the polar region, while below-average heights were present over most of Canada, the western U.S., and southern Europe.

This anomaly pattern projected onto several teleconnection patterns (Fig. E7, Table E1). It projected onto the positive phases of the North Atlantic Oscillation (NAO, +1.3) and the Tropical/ Northern Hemisphere pattern (TNH, +2.2). It also projected onto the negative phases of the Polar/ Eurasian pattern (-2.2), the east-Atlantic pattern (-1.4), and the east Atlantic/ Western Russian pattern (-1.4).

At 200-hPa, the circulation across the subtropical Pacific Ocean in both hemispheres reflected La Niña. The La Niña signal included highly amplified troughs east of the date line in both hemispheres, in association with the disappearance of deep tropical convection from the central equatorial Pacific (Fig. T25). The La Niña signal also included a focusing of the subtropical ridges over Australasia (Fig. T22), in association with enhanced convection over the western tropical Pacific, Indonesia, and the eastern Indian Ocean.

The main land-surface temperature signals during February included above-average temperatures across the southern and eastern U.S. and in the polar region, and below-average temperatures in the western Canada and western Europe (Fig. E1). The main precipitation signals included above-average totals in the central U.S. and southern Europe (Fig. E3).

a. North Pacific and North America

The 500-hPa circulation during February featured above-average heights over the high latitudes of the North Pacific, the Gulf of Alaska and the southeastern U.S., and below-average heights over Canada and the western U.S. (Fig. E9). This type of highly amplified wave pattern is typical of La Niña.

La Niña produces an enhanced subtropical ridge over southeastern Asia along with an amplified mid-Pacific trough (Fig. T22). These conditions act to retract westward the East Asian jet steam. This anomalous jet structure, in turn, acts to retract westward the mean downstream ridge and trough positions, resulting in the essence of the anomalous 500-hPa circulation pattern seen during February. This anomalous wave pattern projected strongly onto two teleconnection patterns which tend to be favored during La Niña winter; the positive phase of the TNH pattern and the negative phase of the PNA pattern (Fig. E7, Table E1).

This overall pattern contributed to anomalously warm surface temperatures in the eastern U.S.

and to anomalously cool temperatures in western Canada (Fig. E1). It also contributed to above-average precipitation in the central U.S. (Fig. E3). Area-averages totals in the Great Plains, Great Lakes, Midwest, and Ohio Valley regions in the upper 90th percentile of occurrences (Fig. E5).

b. Polar region

The mean February 500-hPa circulation during February featured an anomalous zonal wave-1 pattern, with above-average heights north of Eurasia and below-average heights extending from central Canada to Greenland (Fig. E9). This pattern appears to have reflected a downward extension of a stratospheric anomaly pattern that was prominent up to at least the 30 hPa level (Fig. S2).

At 500-hPa, this pattern projected strongly onto the negative phase of the Polar/ Eurasian pattern (-2.2). The anomalous southerly flow between the anomalous trough and the downstream anomalous ridge resulted in a massive influx of relatively mild air (and significantly warmer temperatures) into the polar region at levels extending from the surface (Fig. E8) to 500-hPa.

b. Europe

The circulation across the central North Atlantic and Europe reflected an anomalous zonal wave-4 pattern, with above-average heights over the west-central North Atlantic and Scandinavia, and below-average heights over Greenland and southern Europe (Fig E9). This pattern reflected an amplified jet stream over the western Atlantic (Fig. E10), along with a pronounced jet exit region and split-flow pattern across the eastern Atlantic and Europe. The northern branch of this split flow brought a large influx of milder air into the polar region. The southern branch contributed to increased storminess and above-average precipitation across southern Europe (Fig. E3). This marked the first time in more than a year that area-averaged precipitation was above average across southern Europe (Fig. E4).

2. Southern Hemisphere

The mean 500-hPa circulation during February featured above-average heights over the Indian Ocean and below-average heights over the high latitudes of the South Pacific Ocean (Fig. E15). At 200-hPa, the subtropical circulation featured an amplified trough over the central and eastern South Pacific Ocean, and ridge over western Australia (Fig. T22). This anomalous subtropical circulation is typical of La Niña.

The South African monsoon season runs from October to April. This area recorded above-average precipitation during February, with area-averaged totals in the upper 80th percentile of occurrences (Fig. E4). The most significant surpluses were observed in the northern and central portions of the monsoon region (Fig E3), where they helped to alleviate significant rainfall deficits which had accumulated over the last two months.

# TELECONNECTION INDICES

| Month | North Atlantic | | | North Pacific | | | EURASIA | | |
|---|---|---|---|---|---|---|---|---|---|
| | NAO | EA | WP | EP-NP | PNA | TNH | EATL/ WRUS | SCAND | POLEUR |
| FEB 18 | 1.3 | -1.4 | 0.4 | 0.2 | -1.7 | 2.2 | -1.4 | 0.4 | -2.2 |
| JAN 18 | 1.2 | 0.5 | 0.4 | 0.7 | -0.1 | -0.3 | -1.6 | 0.4 | -1.5 |
| DEC 17 | 0.7 | -0.5 | 0.3 | --- | 0.6 | 1.0 | -1.6 | -0.5 | -1.9 |
| NOV 17 | -0.1 | 0.1 | 0.7 | 0.4 | -2.0 | --- | -1.2 | -0.1 | -2.2 |
| OCT 17 | 0.7 | 0.6 | 0.7 | -0.6 | -0.3 | --- | -0.0 | 0.3 | -1.2 |
| SEP 17 | -0.5 | 1.6 | -1.2 | -0.5 | -0.3 | --- | -2.5 | 0.5 | -1.7 |
| AUG 17 | -1.5 | 2.0 | -1.4 | -1.6 | 0.2 | --- | -2.9 | -1.6 | 1.8 |
| JUL 17 | 1.3 | 1.8 | 0.5 | 0.0 | 1.3 | --- | -0.6 | 0.0 | -0.1 |
| JUN 17 | 0.4 | 2.0 | -0.8 | 0.5 | 1.2 | --- | 0.3 | -1.4 | -0.1 |
| MAY 17 | -1.7 | 0.5 | 0.7 | -0.7 | -0.2 | --- | 1.5 | 0.9 | 0.5 |
| APR 17 | 1.7 | -0.6 | -0.4 | 1.0 | 0.1 | --- | 0.7 | -1.4 | -1.4 |
| MAR 17 | 0.4 | 1.0 | -2.1 | -1.0 | -0.0 | --- | -1.0 | -1.0 | 0.7 |
| FEB 17 | 0.7 | 0.6 | -0.1 | 0.2 | -0.1 | -0.1 | 1.1 | 0.7 | -0.4 |

TABLE E1-Standardized amplitudes of selected Northern Hemisphere teleconnection patterns for the most recent thirteen months (computational procedures are described in Fig. E7). Pattern names and abbreviations are North Atlantic Oscillation (NAO); East Atlantic pattern (EA);West Pacific pattern (WP); East Pacific - North Pacific pattern (EP-NP); Pacific/North American pattern (PNA); Tropical/Northern Hemisphere pattern (TNH);East Atlantic/Western Russia pattern (EATL/WRUS-called Eurasia-2 pattern by Barnston and Livezey, 1987, *Mon. Wea. Rev.*, **115**, 1083-1126); Scandanavia pattern (SCAND-called Eurasia-1 pattern by Barnston and Livezey 1987); and Polar Eurasia pattern (POLEUR). No value is plotted for calendar months in which the pattern does not appear as a leading mode.

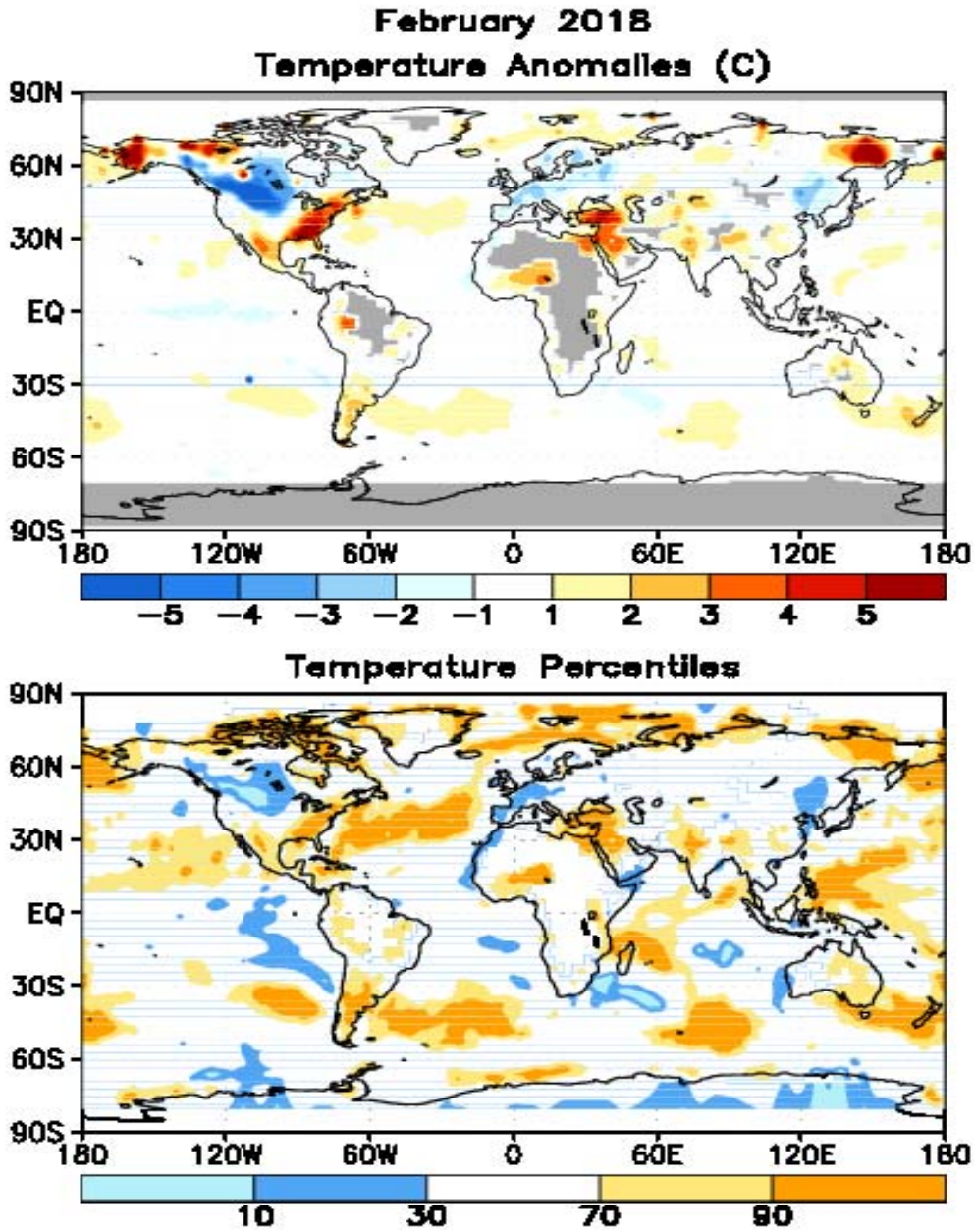


FIGURE E1. Surface temperature anomalies (°C, top) and surface temperature expressed as percentiles of the normal (Gaussian) distribution fit to the 1981–2010 base period data (bottom) for FEB 2018. Analysis is based on station data over land and on SST data over the oceans (top). Anomalies for station data are departures from the 1981–2010 base period means, while SST anomalies are departures from the 1981–2010 adjusted OI climatology. (Smith and Reynolds 1998, *J. Climate*, **11**, 3320-3323). Regions with insufficient data for analysis in both figures are indicated by shading in the top figure only.

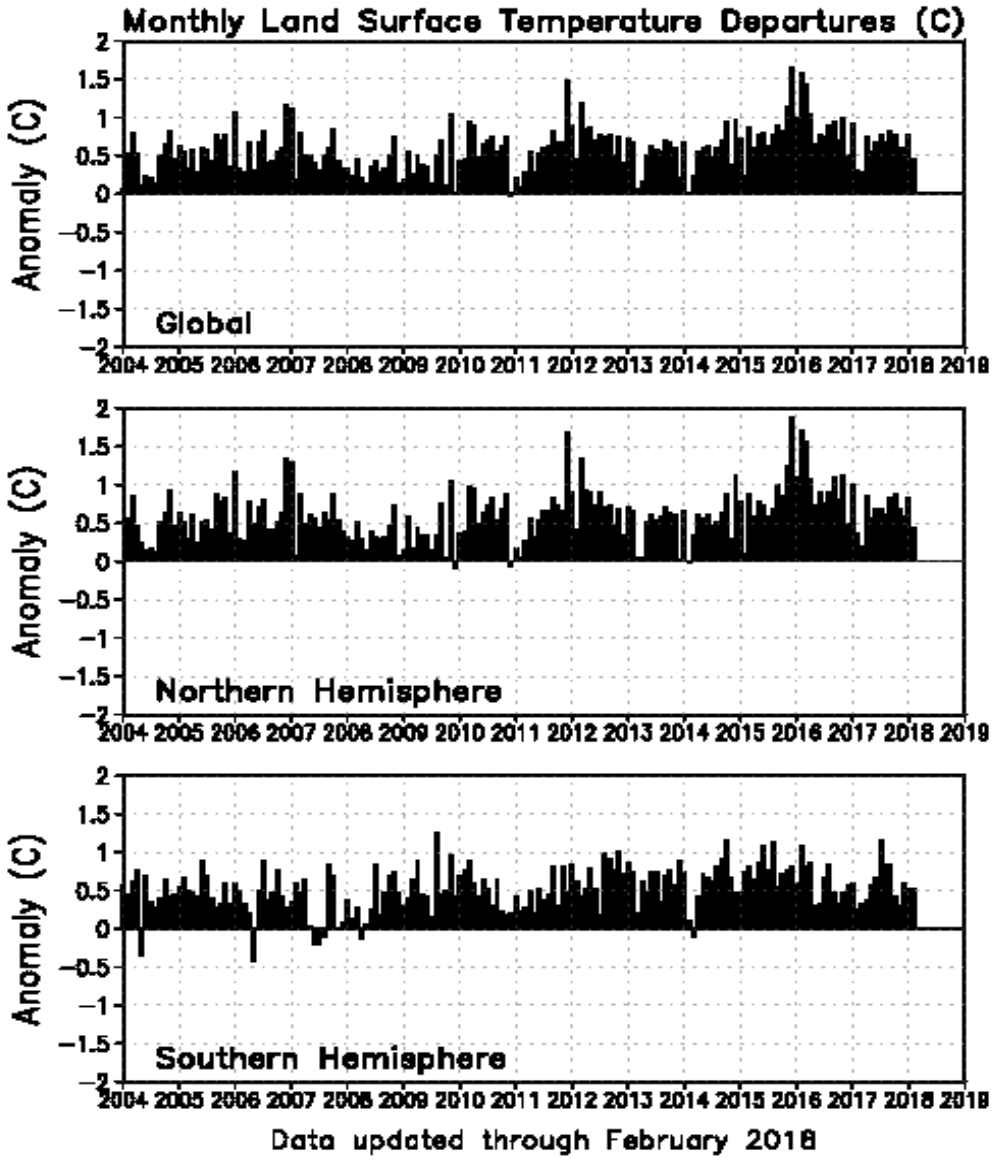


FIGURE E2. Monthly global (top), Northern Hemisphere (middle), and Southern Hemisphere (bottom) surface temperature anomalies (land only, ˚C) from January 1990 - present, computed as departures from the 1981–2010 base period means.

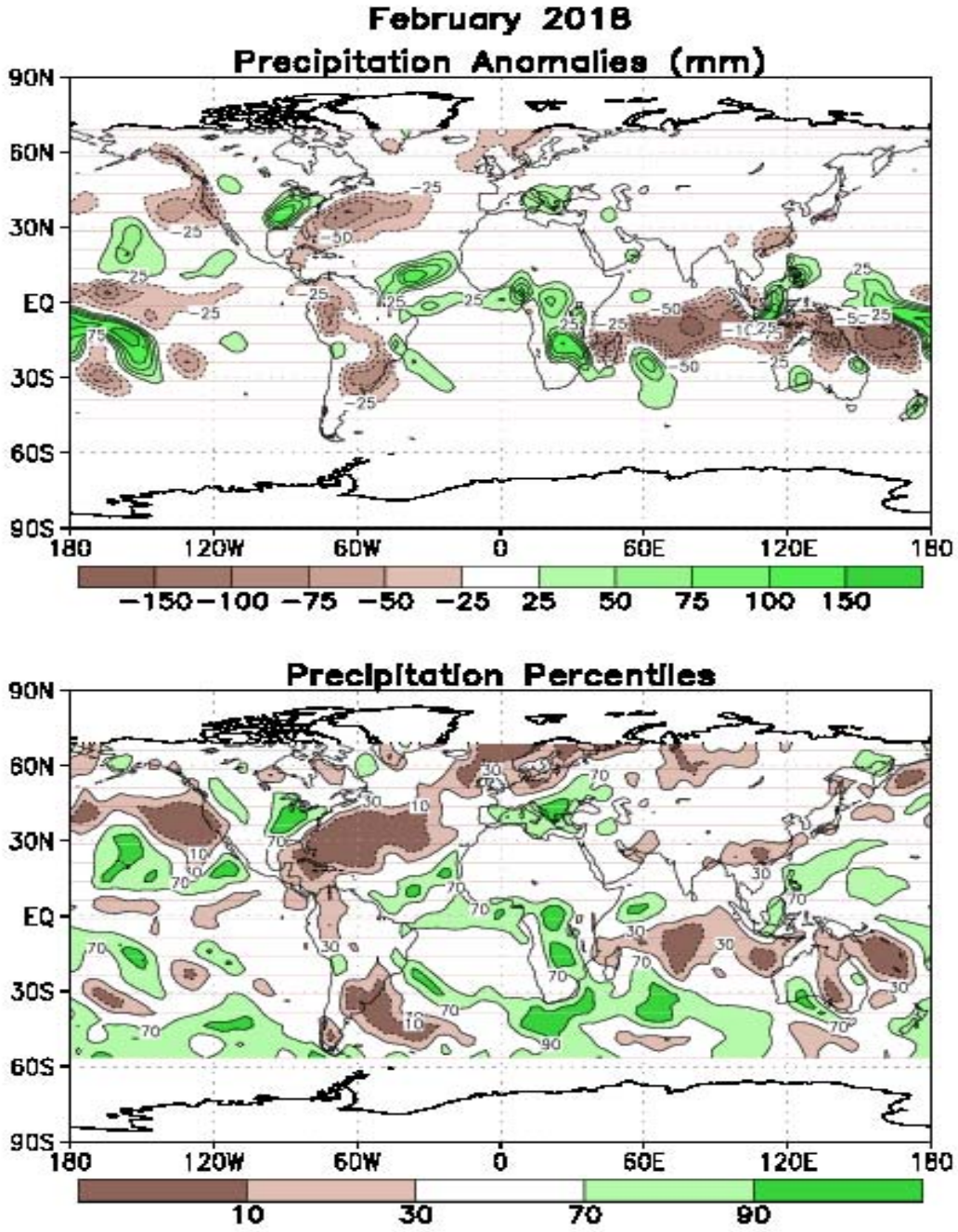


FIGURE E3. Anomalous precipitation (mm, top) and precipitation percentiles based on a Gamma distribution fit to the 1981–2010 base period data (bottom) for FEB 2018. Data are obtained from a merge of raingauge observations and satellite-derived precipitation estimates (Janowiak and Xie 1999, *J. Climate*, **12**, 3335–3342). Contours are drawn at 200, 100, 50, 25, -25, -50, -100, and -200 mm in top panel. Percentiles are not plotted in regions where mean monthly precipitation is <5mm/month.

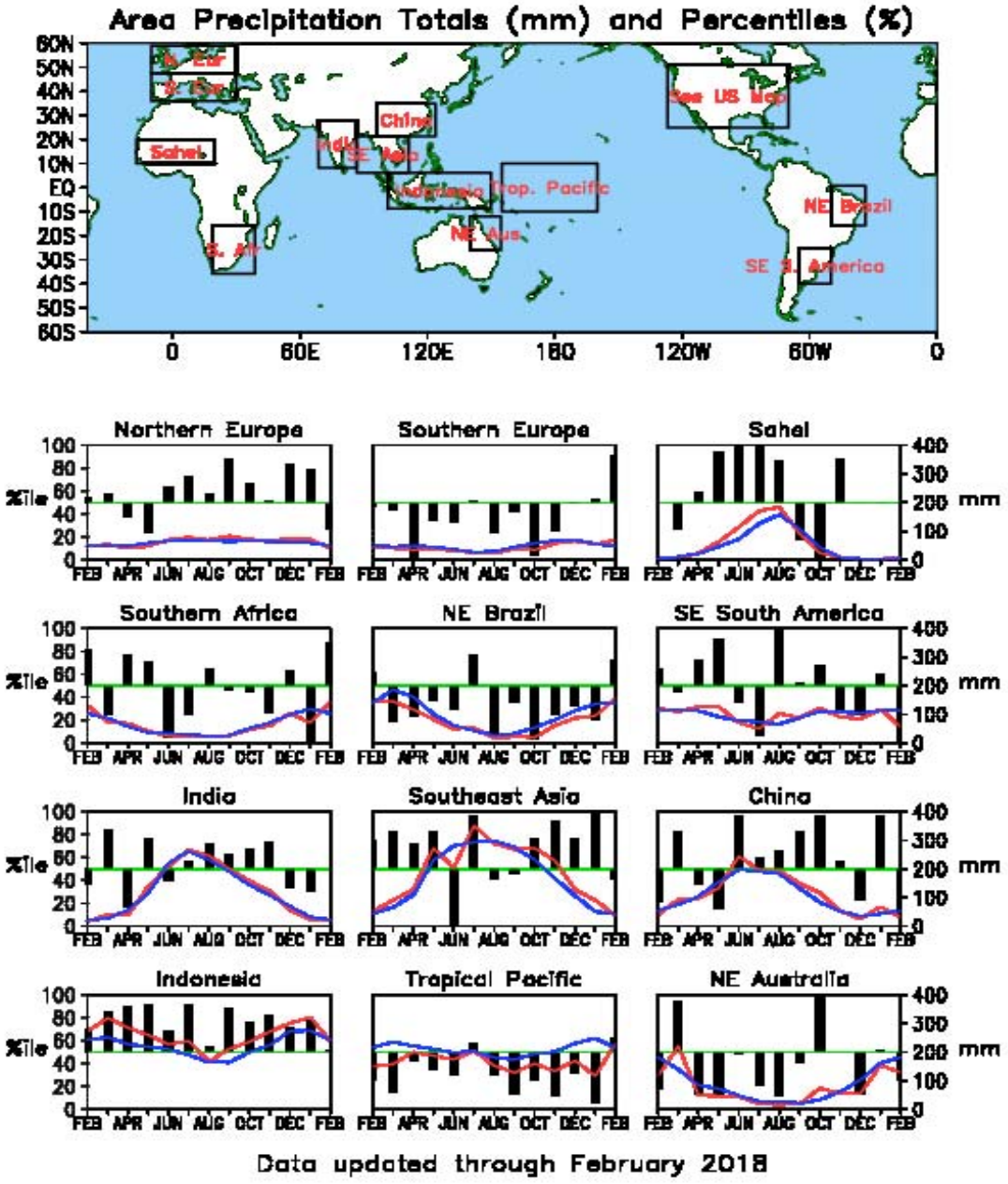


FIGURE E4. Areal estimates of monthly mean precipitation amounts (mm, solid lines) and precipitation percentiles (%, bars) for the most recent 13 months obtained from a merge of raingauge observations and satellite-derived precipitation estimates (Janowiak and Xie 1999, *J. Climate*, **12**, 3335–3342). The monthly precipitation climatology (mm, dashed lines) is from the 1981–2010 base period monthly means. Monthly percentiles are not shown if the monthly mean is less than 5 mm.

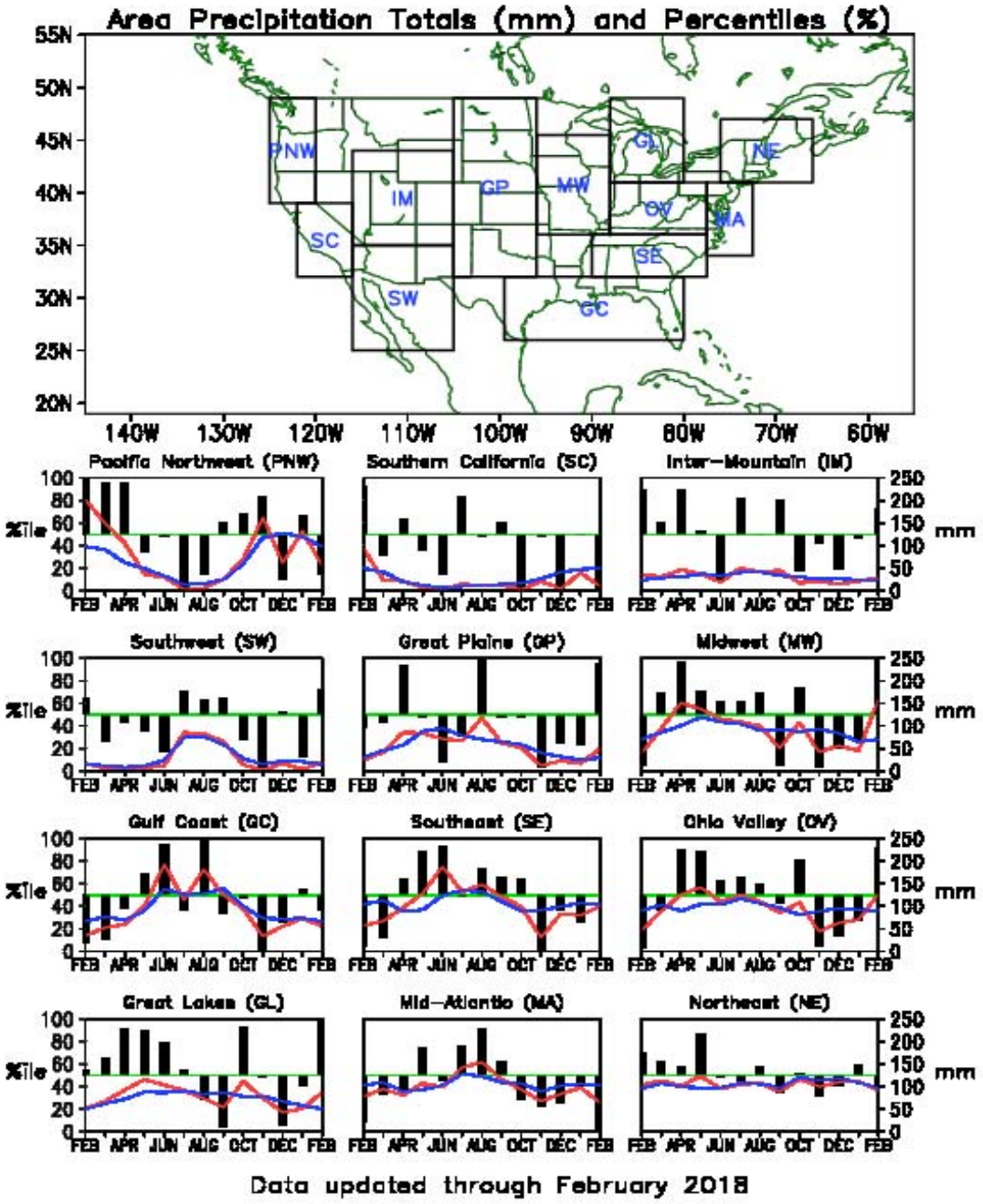


FIGURE E5. Areal estimates of monthly mean precipitation amounts (mm, solid lines) and precipitation percentiles (%, bars) for the most recent 13 months obtained from a merge of raingauge observations and satellite-derived precipitation estimates (Janowiak and Xie 1999, *J. Climate*, **12**, 3335–3342). The monthly precipitation climatology (mm, dashed lines) is from the 1981–2010 base period monthly means. Monthly percentiles are not shown if the monthly mean is less than 5 mm.

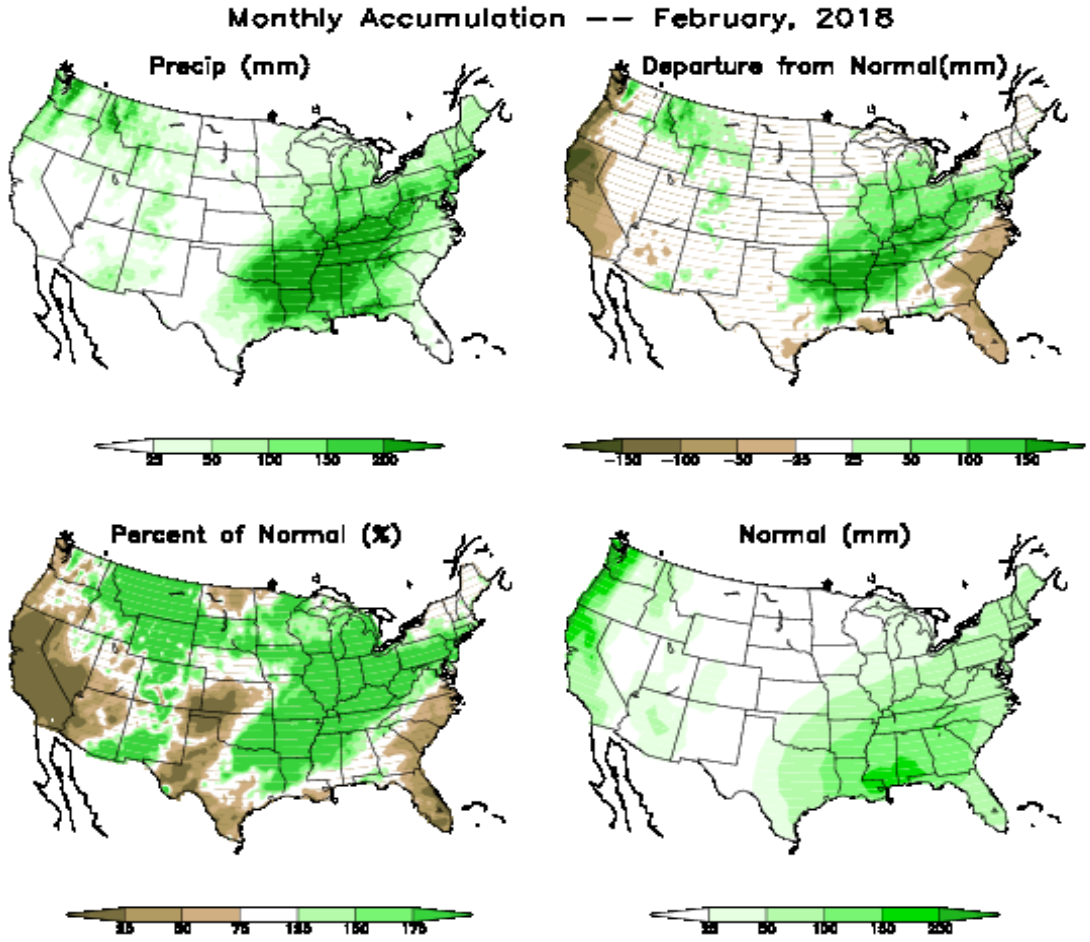


FIGURE E6. Observed precipitation (upper left), departure from average (upper right), percent of average (lower left), and average precipitation (lower right) for FEB 2018. The units are given on each panel. Base period for averages is 1981–2010. Results are based on CPC's U. S. daily precipitation analysis, which is available at http://www.cpc.ncep.noaa.gov/prodcuts/precip/realtime.

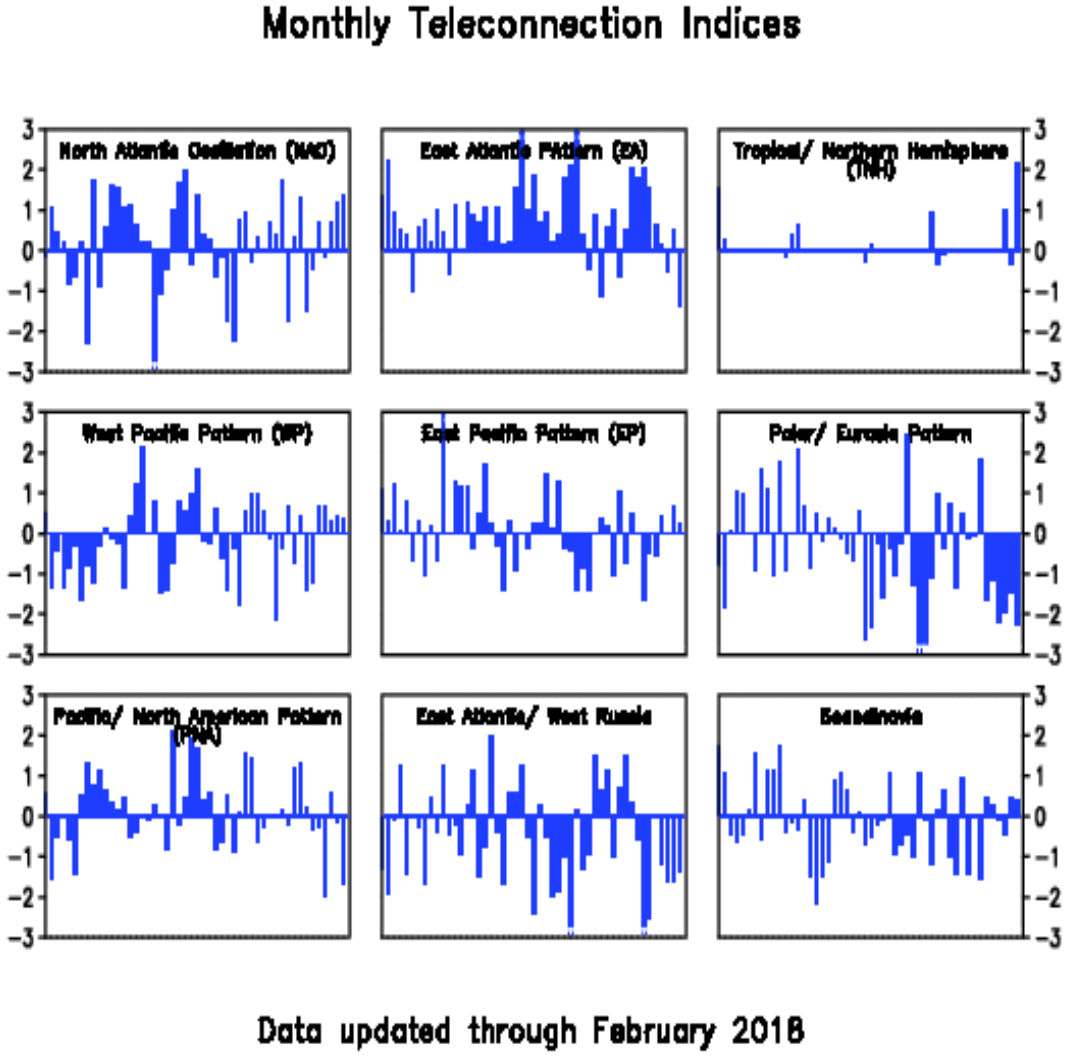


FIGURE E7. Standardized monthly Northern Hemisphere teleconnection indices. The teleconnection patterns are calculated from a Rotated Principal Component Analysis (RPCA) applied to monthly standardized 500-hPa height anomalies during the 1981-2010 base period. To obtain these patterns, ten leading un-rotated modes are first calculated for each calendar month by using the monthly height anomaly fields for the three-month period centered on that month: [i.e., The July modes are calculated from the June, July, and August standardized monthly anomalies]. A Varimax spatial rotation of the ten leading un-rotated modes for each calendar month results in 120 rotated modes (12 months x 10 modes per month) that yield ten primary teleconnection patterns.The teleconnection indices are calculated by first projecting the standardized monthly anomalies onto the teleconnection patterns corresponding to that month (eight or nine teleconnection patterns are seen in each calendar month). The indices are then solved for simultaneously using a Least-Squares approach. In this approach, the indices are the solution to the Least-Squares system of equations which explains the maximum spatial structure of the observed height anomaly field during the month. The indices are then standardized for each pattern and calendar month independently. No index value exists when the teleconnection pattern does not appear as one of the ten leading rotated EOF's valid for that month.

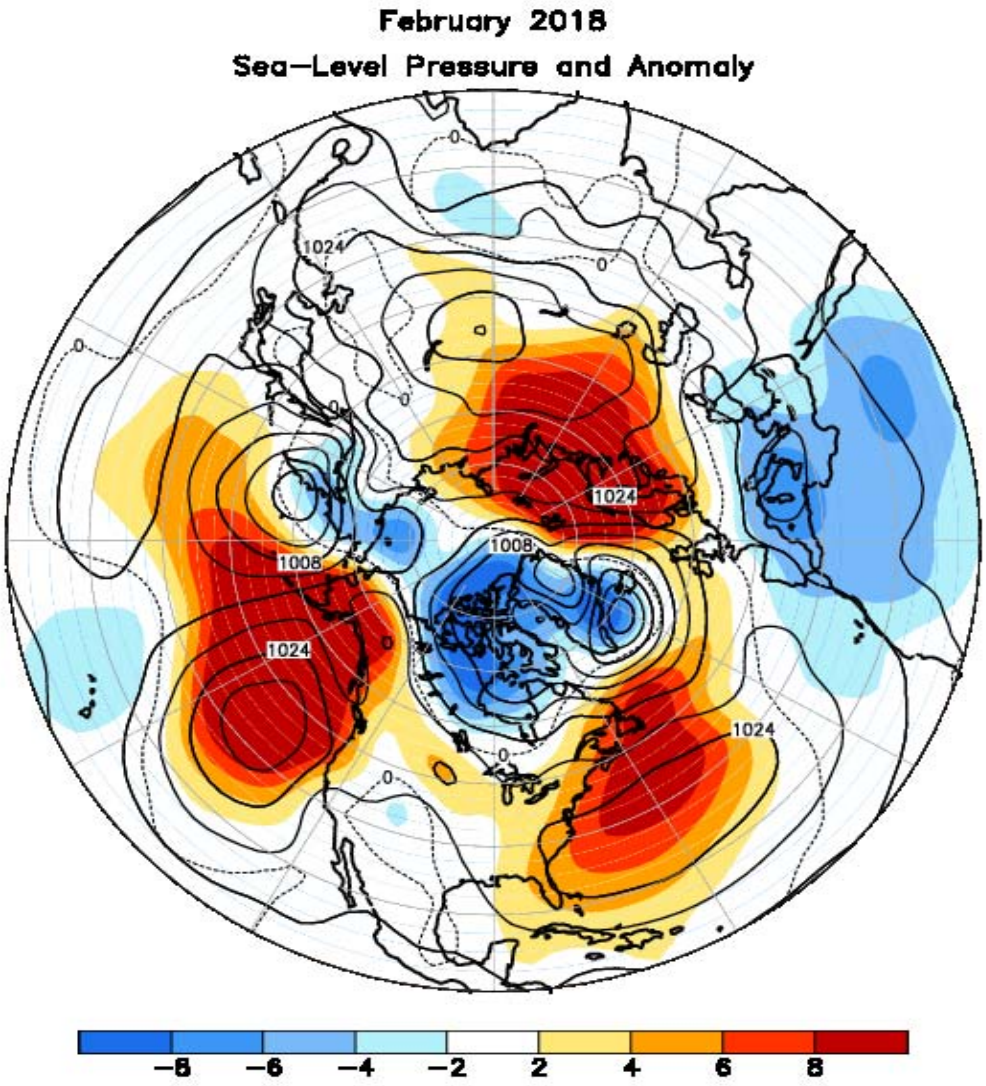


FIGURE E8. Northern Hemisphere mean and anomalous sea level pressure (CDAS/Reanalysis) for FEB 2018. Mean values are denoted by solid contours drawn at an interval of 4 hPa. Anomaly contour interval is 2 hPa with values less (greater) than -2 hPa (2 hPa) indicated by dark (light) shading. Anomalies are calculated as departures from the 1981-2010 base period monthly means.

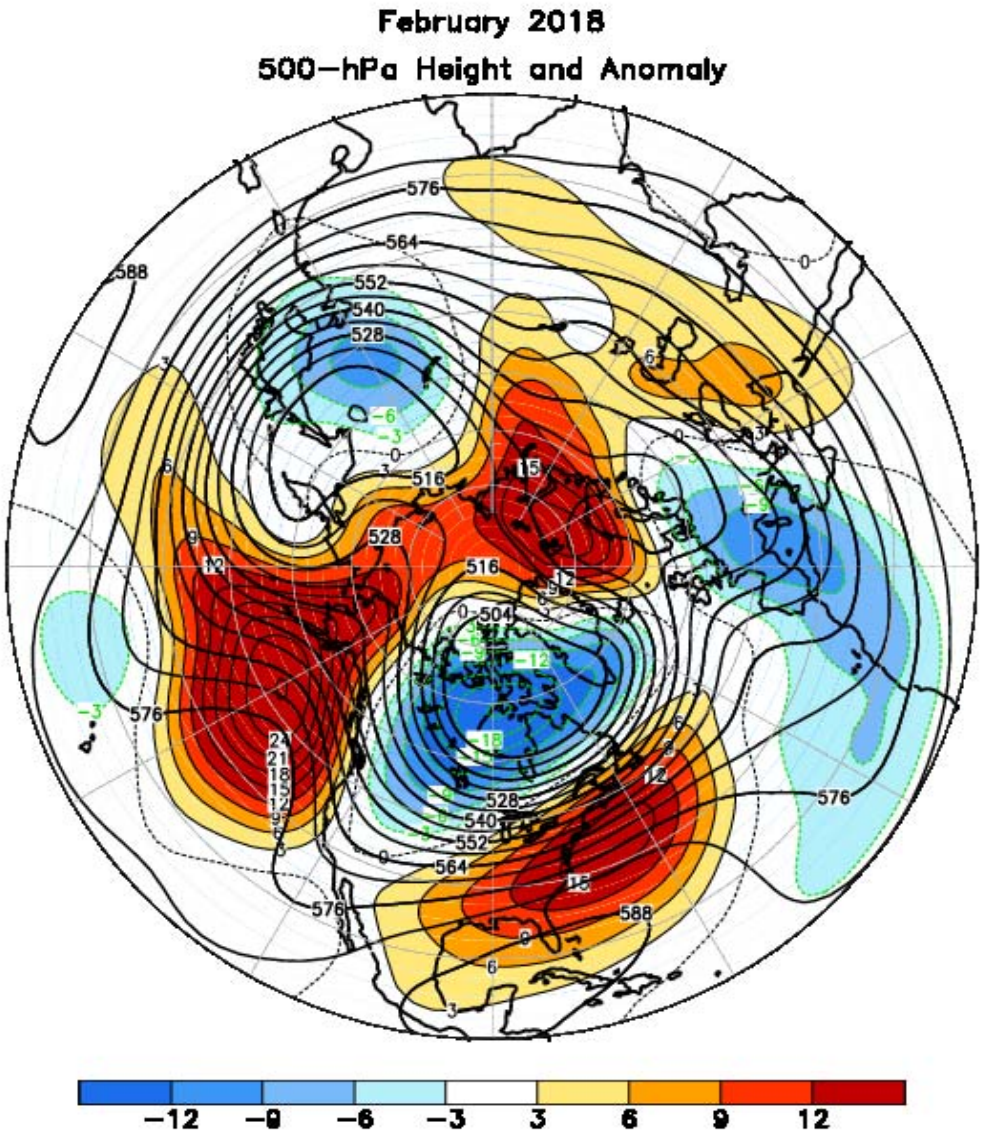


FIGURE E9. Northern Hemisphere mean and anomalous 500-hPa geopotential height (CDAS/Reanalysis) for FEB 2018. Mean heights are denoted by solid contours drawn at an interval of 6 dam. Anomaly contour interval is 3 dam with values less (greater) than -3 dam (3 dam) indicated by dark (light) shading. Anomalies are calculated as departures from the 1981-2010 base period monthly means.

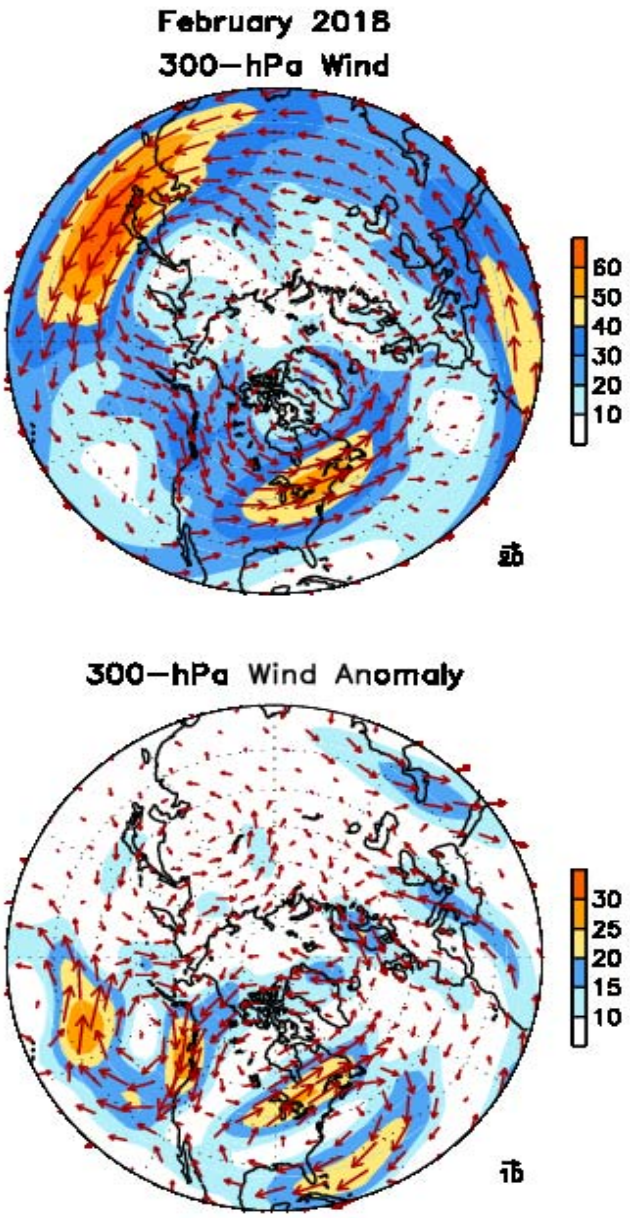


FIGURE E10. Northern Hemisphere mean (left) and anomalous (right) 300-hPa vector wind (CDAS/Reanalysis) for FEB 2018. Mean (anomaly) isotach contour interval is 10 (5) $ms^{-1}$. Values greater than 30 $ms^{-1}$ (left) and 10 $ms^{-1}$ (rights) are shaded. Anomalies are departures from the 1981-2010 base period monthly means.

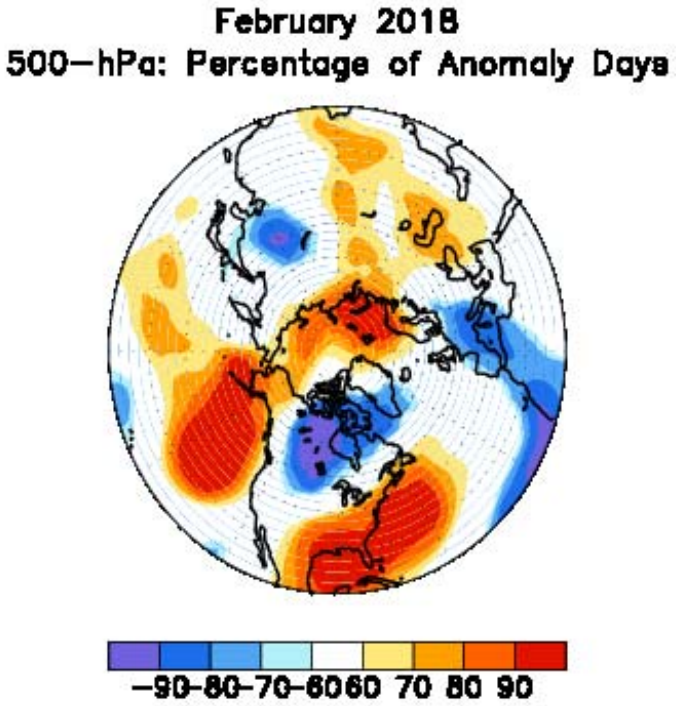


FIGURE E11. Northern Hemisphere percentage of days during FEB 2018 in which 500-hPa height anomalies greater than 15 m (red) and less than -15 m (blue) were observed. Values greater than 70% are shaded and contour in-

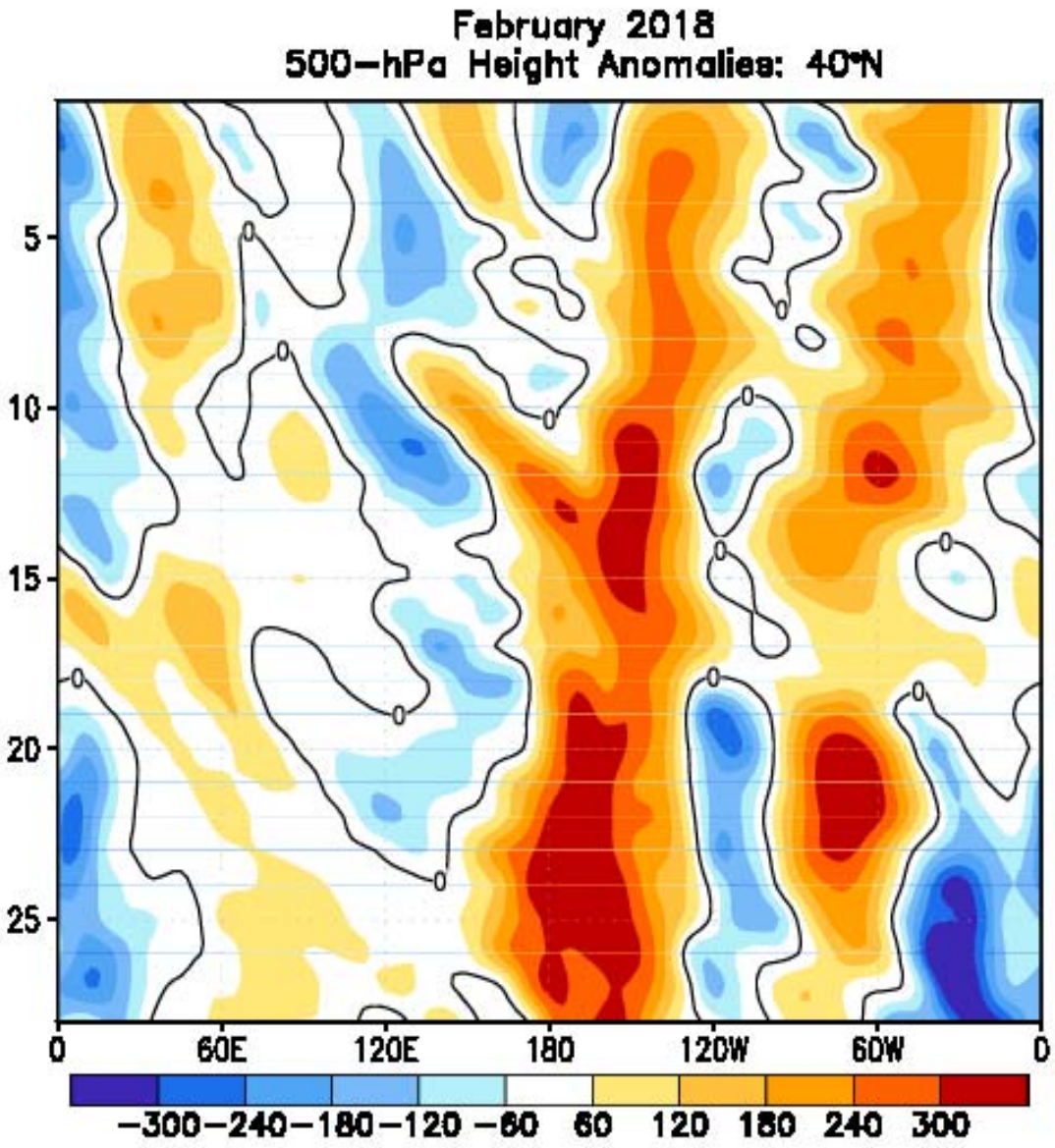


FIGURE E12. Northern Hemisphere: Daily 500-hPa height anomalies for FEB 2018 averaged over the 5° latitude band centered on 40°N. Positive values are indicated by solid contours and dark shading. Negative values are indicated by dashed coutours and light shading. Contour interval is 60 m. Anomalies are departures from the 1981-2010 base period daily means.

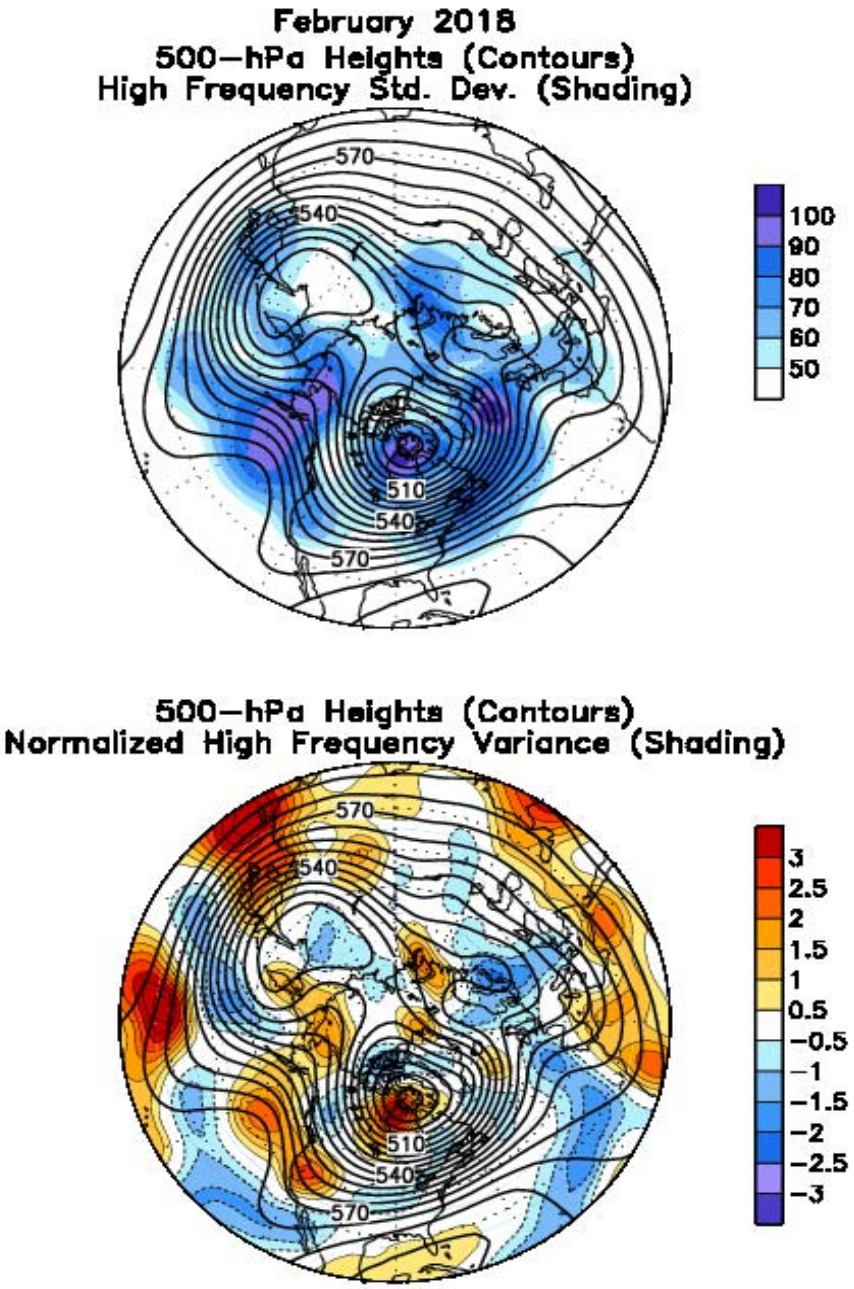


FIGURE E13. Northern Hemisphere 500-hPa heights (thick contours, interval is 6 dam) overlaid with (Top) Standard deviation of 10-day high-pass (HP) filtered height anomalies and (Bottom) Normalized anomalous variance of 10-day HP filtered height anomalies. A Lanczos filter is used to calculate the HP filtered anomalies. Anomalies are departures from the 1981-2010 daily means.

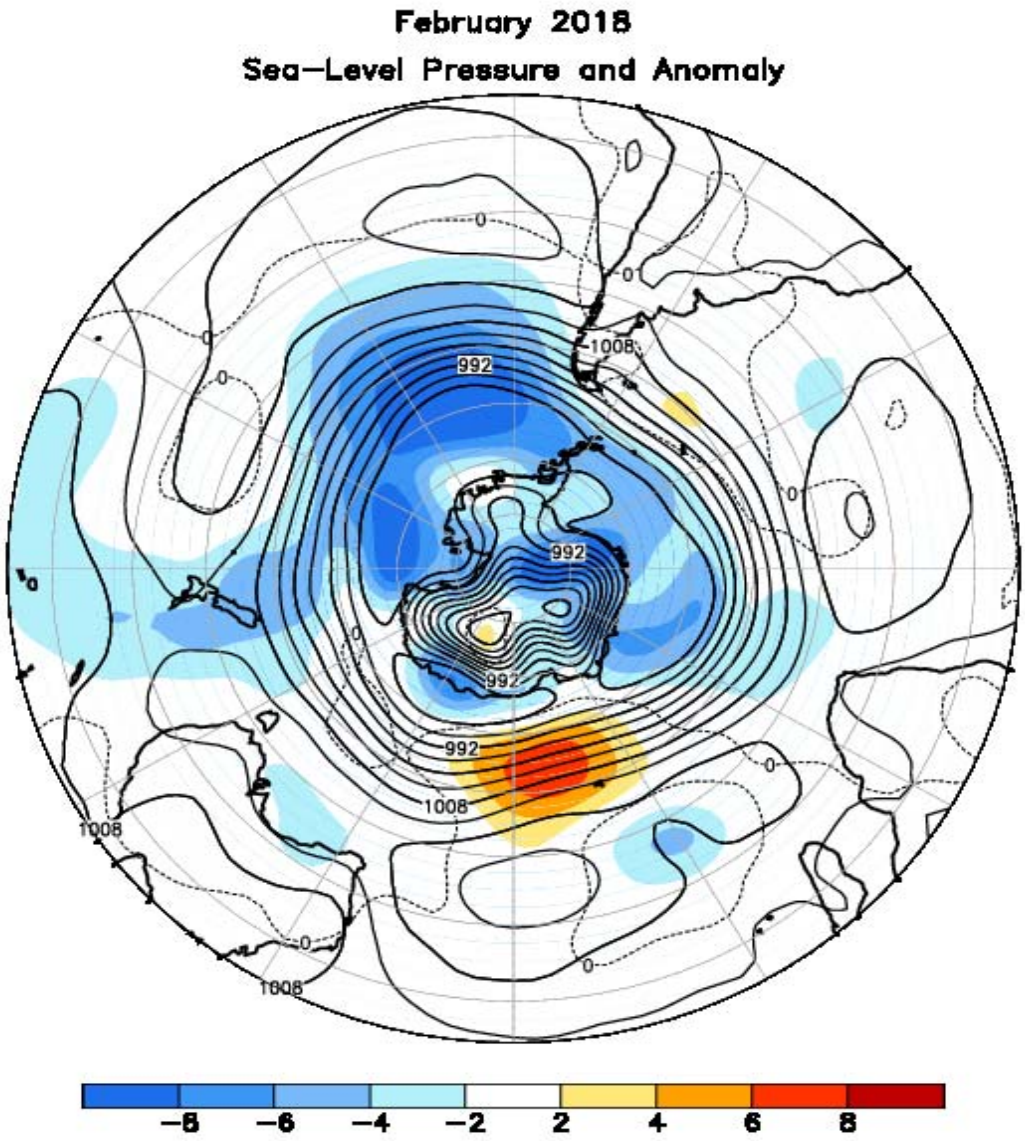


FIGURE E14. Southern Hemisphere mean and anomalous sea level pressure(CDAS/Reanalysis) for FEB 2018. Mean values are denoted by solid contours drawn at an interval of 4 hPa. Anomaly contour interval is 2 hPa with values less (greater) than -2 hPa (2 hPa) indicated by dark (light) shading. Anomalies are calculated as departures from the 1981-2010 base period monthly means.

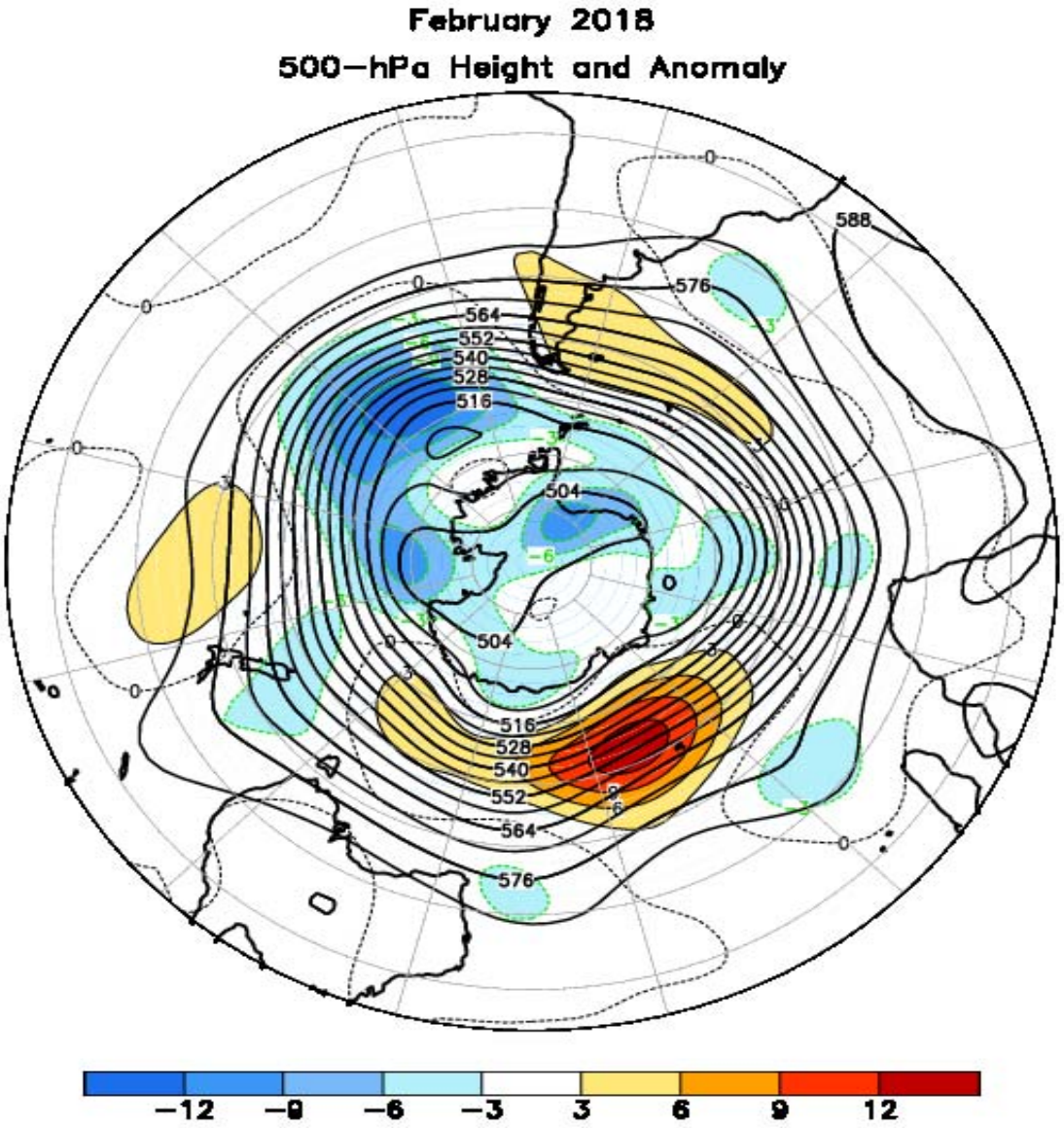


FIGURE E15. Southern Hemisphere mean and anomalous 500-hPa geopotential height (CDAS/Reanalysis) for FEB 2018. Mean heights are denoted by solid contours drawn at an interval of 6 dam. Anomaly contour interval is 3 dam with values less (greater) than -3 dam (3 dam) indicated by dark (light) shading. Anomalies are calculated as departures from the 1981-2010 base period monthly means.

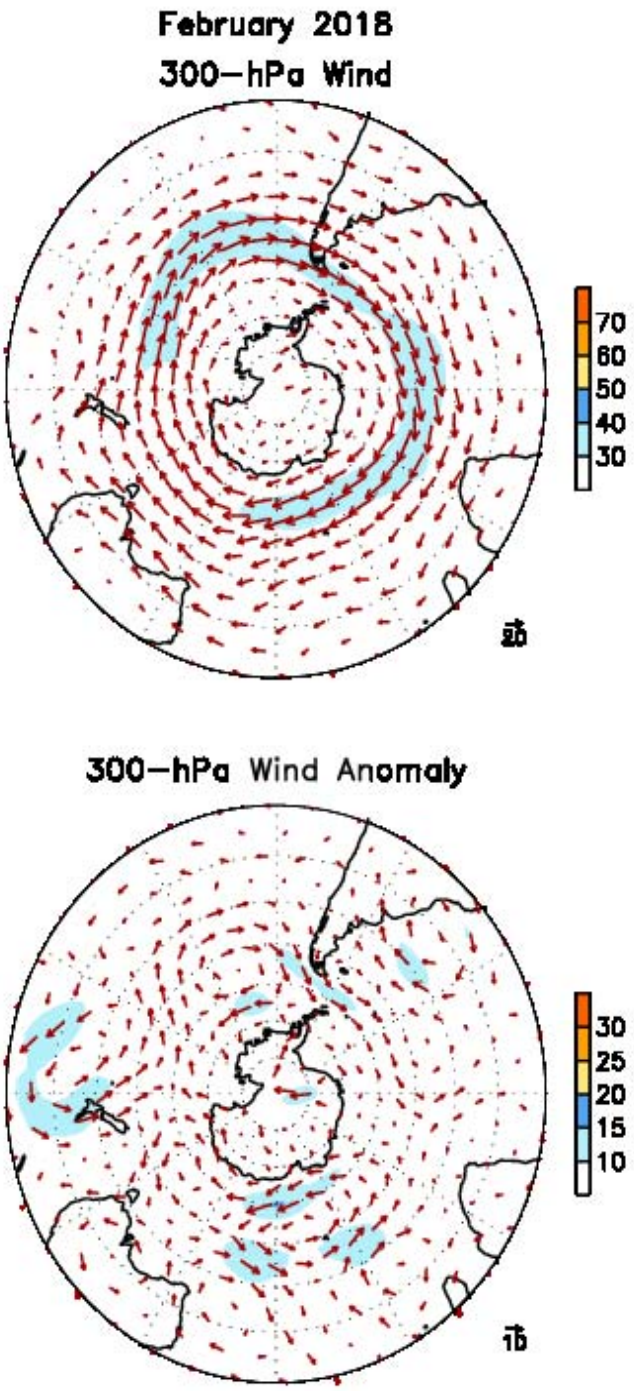


FIGURE E16. Southern Hemisphere mean (left) and anomalous (right) 300-hPa vector wind (CDAS/Reanalysis) for FEB 2018. Mean (anomaly) isotach contour interval is 10 (5) $ms^{-1}$. Values greater than 30 $ms^{-1}$ (left) and 10 $ms^{-1}$ (rights) are shaded. Anomalies are departures from the 1981-2010 base period monthly means.

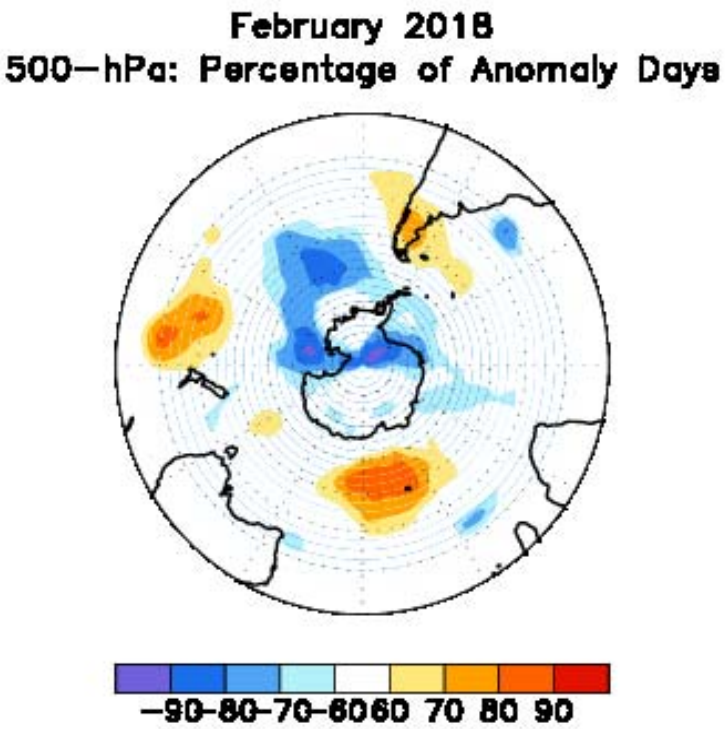


FIGURE E17. Southern Hemisphere percentage of days during FEB 2018 in which 500-hPa height anomalies greater than 15 m (red) and less than -15 m (blue) were observed. Values greater than 70% are shaded and contour in-

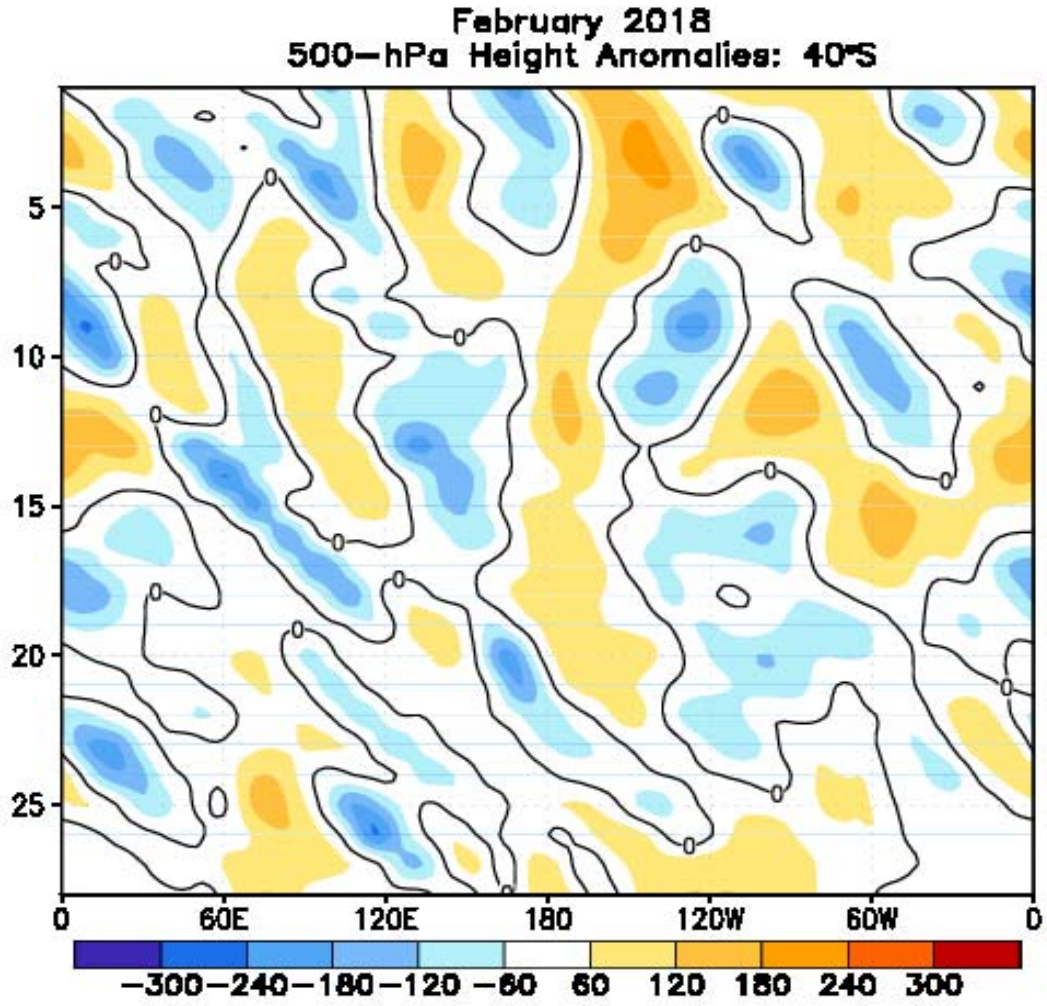


FIGURE E18. Southern Hemisphere: Daily 500-hPa height anomalies for FEB 2018 averaged over the 5° latitude band centered on 40°S. Positive values are indicated by solid contours and dark shading. Negative values are indicated by dashed coutours and light shading. Contour interval is 60 m. Anomalies are departures from the 1981-2010 base period daily means.

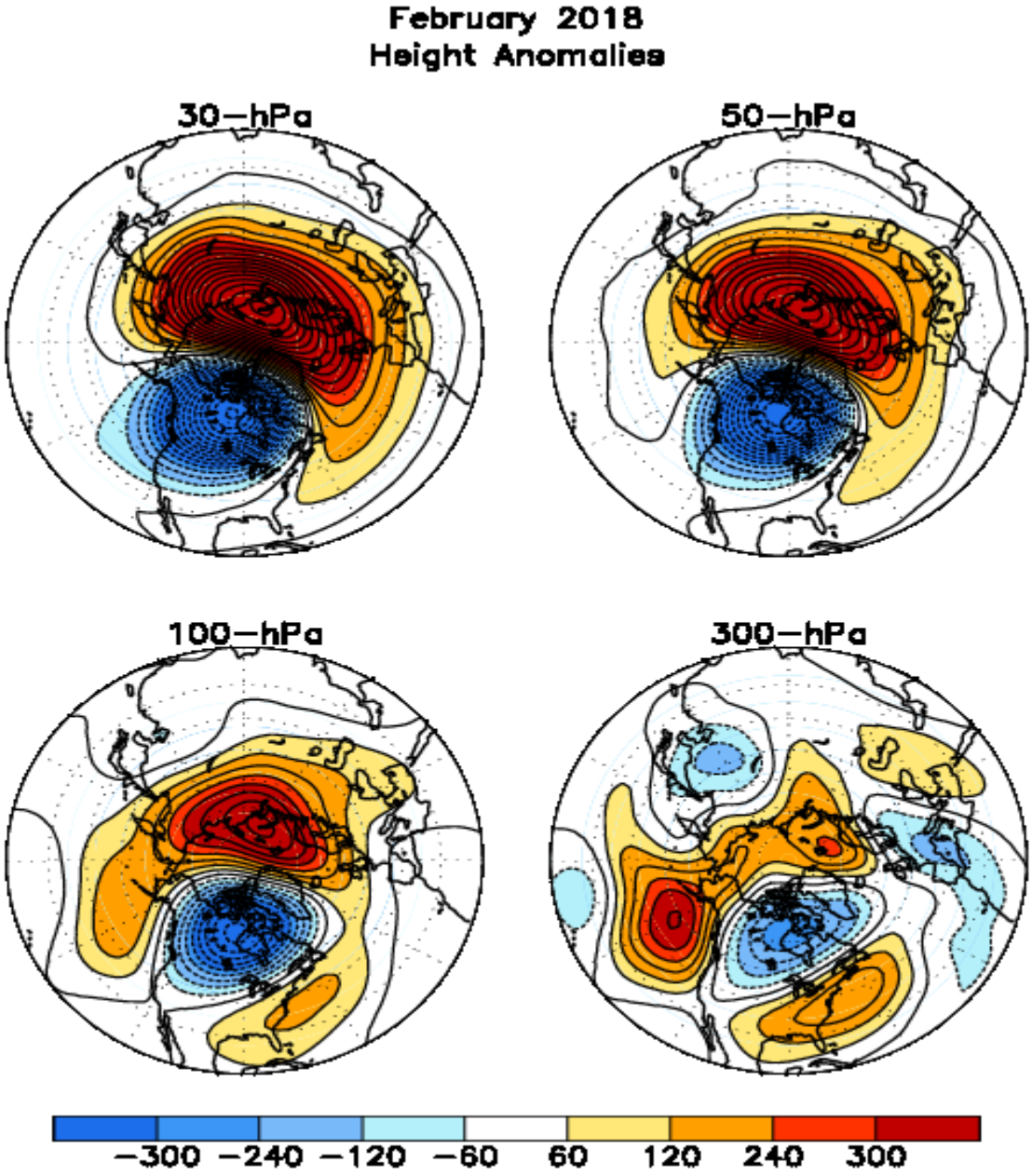


FIGURE S1. Stratospheric height anomalies (m) at selected levels for FEB 2018. Positive values are indicated by solid contours and dark shading. Negative values are indicated by dashed contours and light shading. Contour interval is 60 m. Anomalies are calculated from the 1981-2010 base period means. Winter Hemisphere is shown.

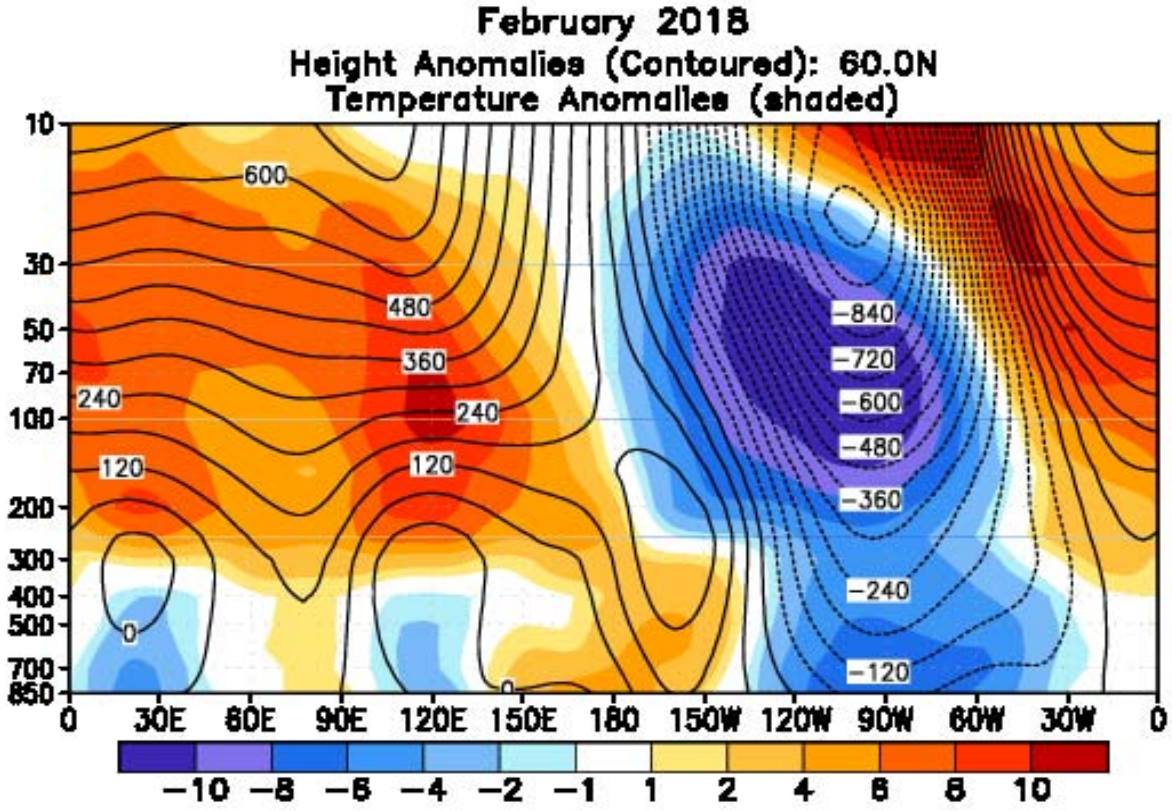


FIGURE S2. Height-longitude sections during FEB 2018 for height anomalies (contour) and temperature anomalies (shaded). In both panels, positive values are indicated by solid contours and dark shading, while negative anomalies are indicated by dashed contours and light shading. Contour interval for height anomalies is 60 m and for temperature anomalies is 2°C. Anomalies are calculated from the 1981-2010 base period monthly means. Winter Hemisphere is shown.

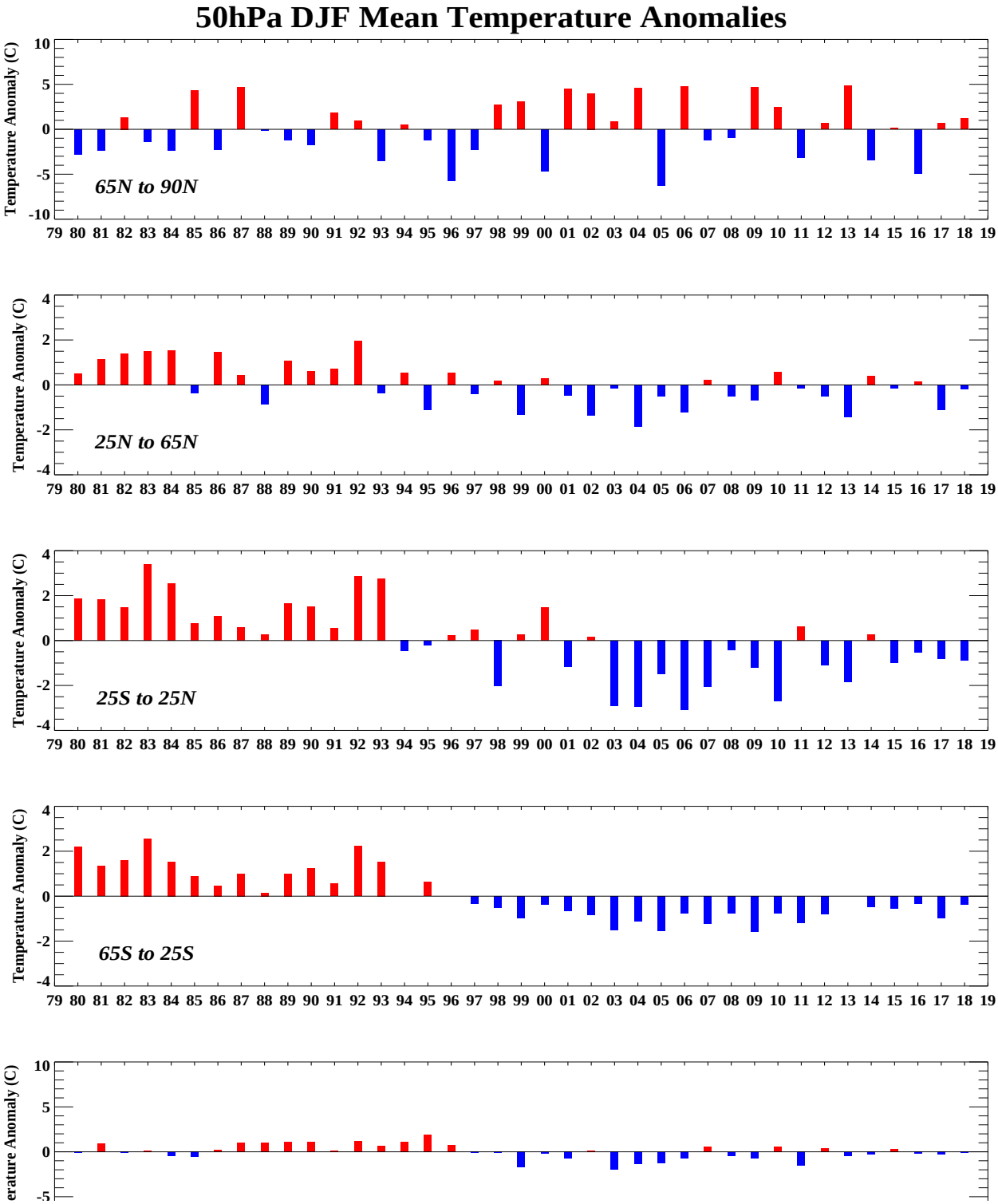


FIGURE S3. Seasonal mean temperature anomalies at 50-hPa for the latitude bands 65°–90°N, 25°–65°N, 25°N–25°S, 25°–65°S, 65°–90°S. The seasonal mean is comprised of the most recent three months. Zonal anomalies are taken from the mean of the entire data set.

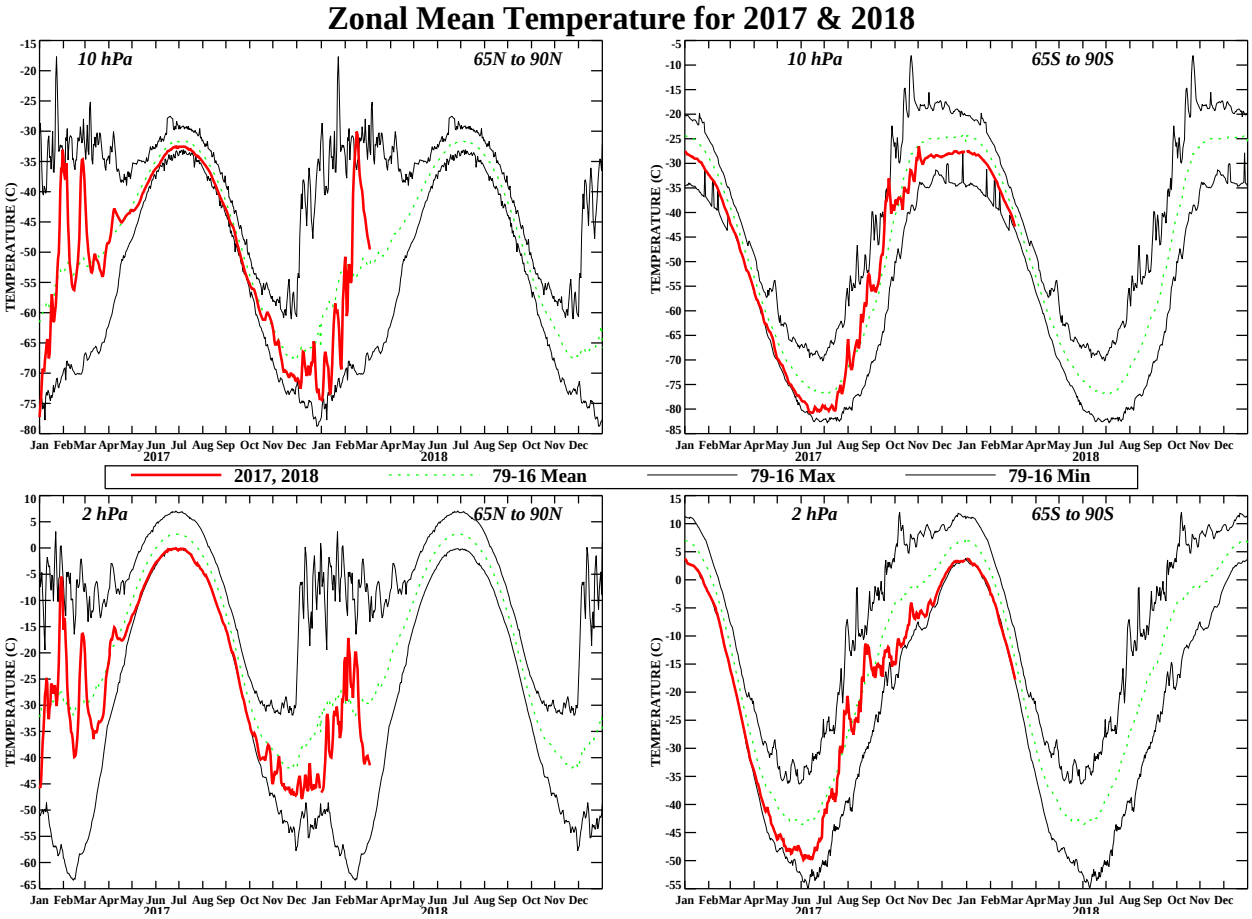


FIGURE S4. Daily mean temperatures at 10-hPa and 2-hPa (thick line) in the region 65°–90°N and 65°–90°S for the past two years. Dashed line depicts the 1981-2010 base period daily mean. Thin solid lines depict the daily extreme maximum and minimum temperatures.

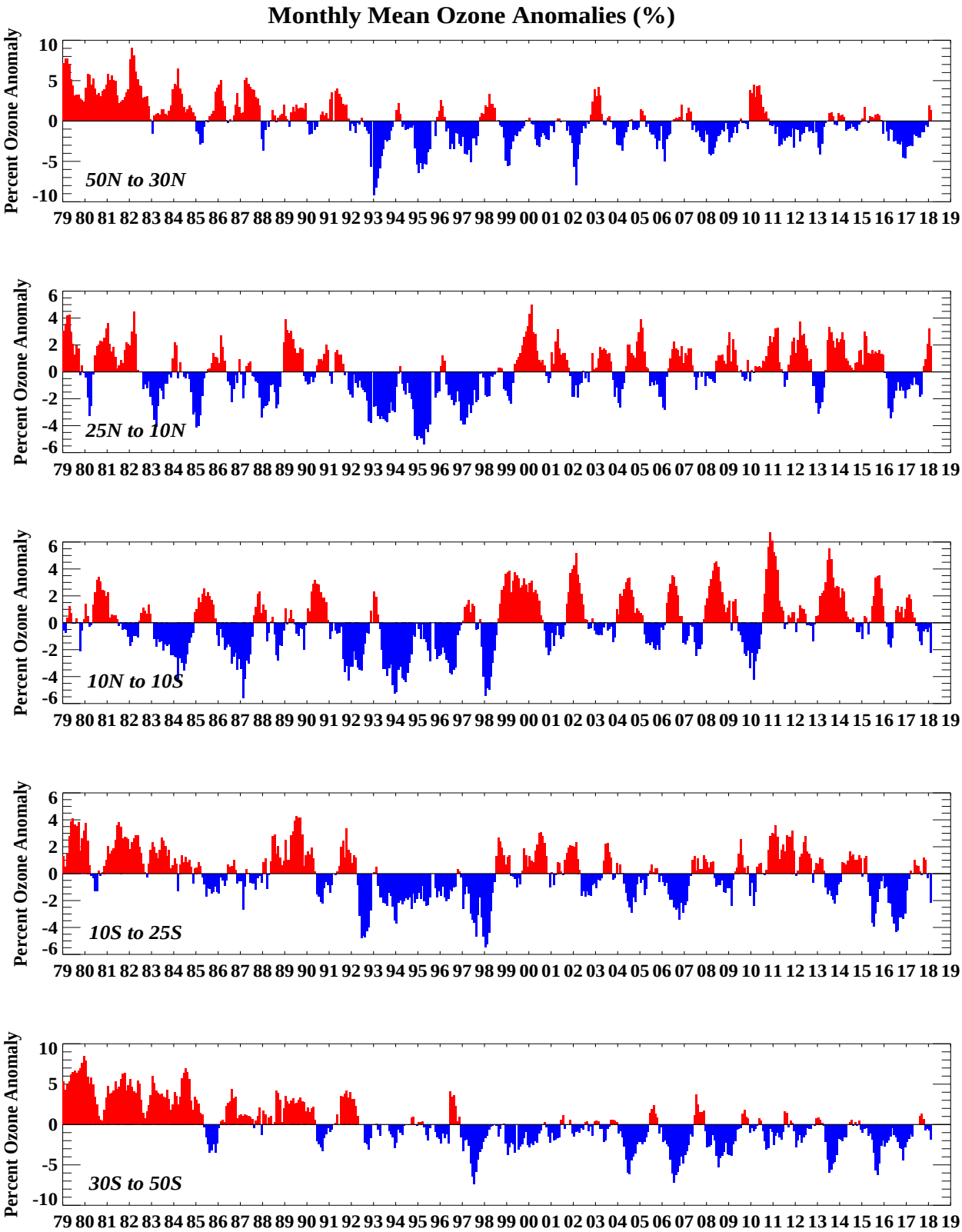


FIGURE S5. Monthly ozone anomalies (percent) from the long term monthly means for five zones: 50N-30N (NH mid-latitudes), 25N-10N (NH tropical surf zone), 10N-10S (Equatorial-QBO zone), 10S-25S (SH tropical surf zone), and 30S-50S (SH mid-latitudes). The long term monthly means are determined from the entire data set

## FEBRUARY PERCENT DIFF (2018 - AVG[79-86])

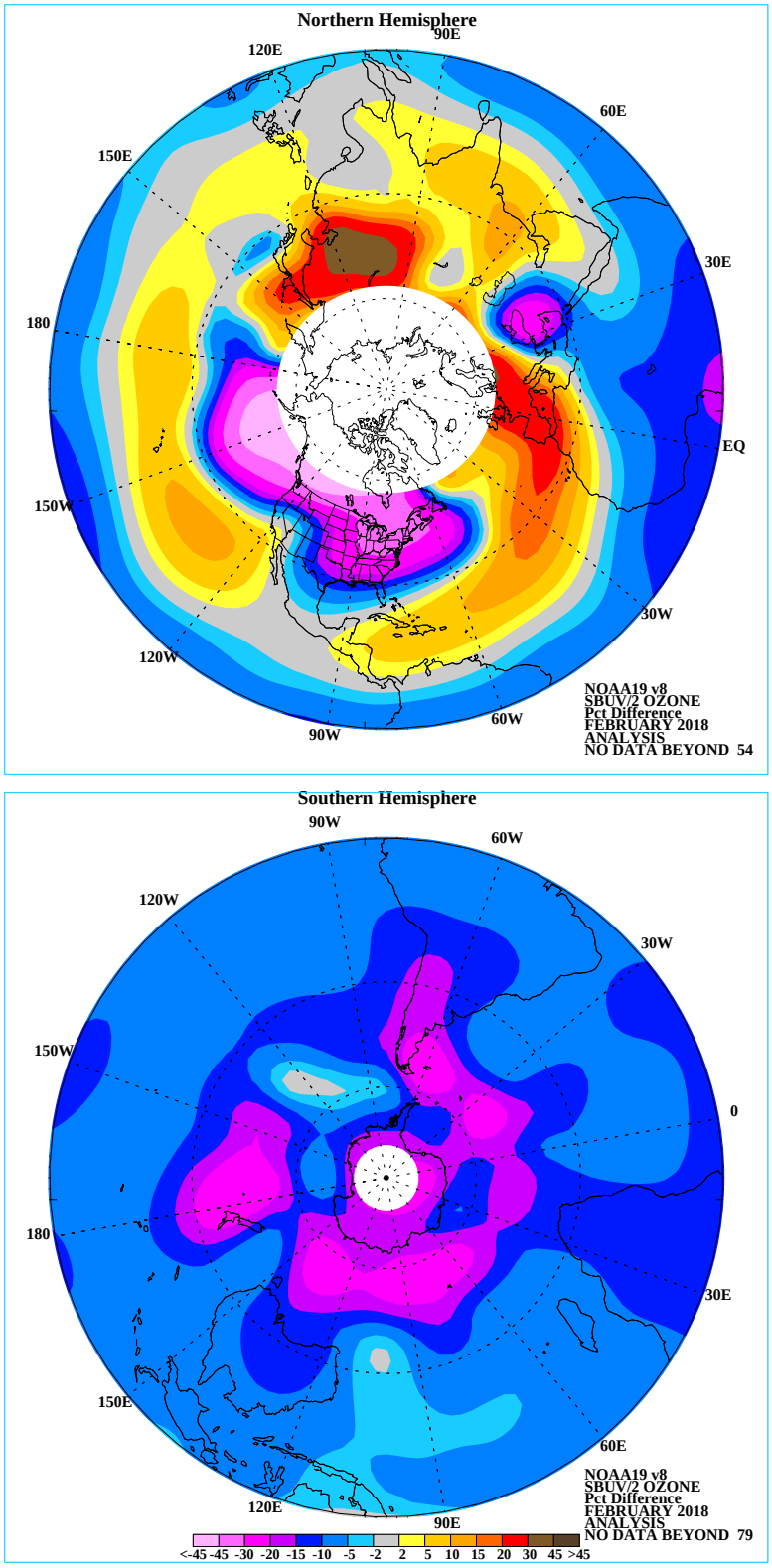


FIGURE S6. Northern (top) and Southern (bottom) Hemisphere total ozone anomaly (percent difference from monthly mean for the period 1979-1986). The region near the winter pole has no SBUV/2 data.

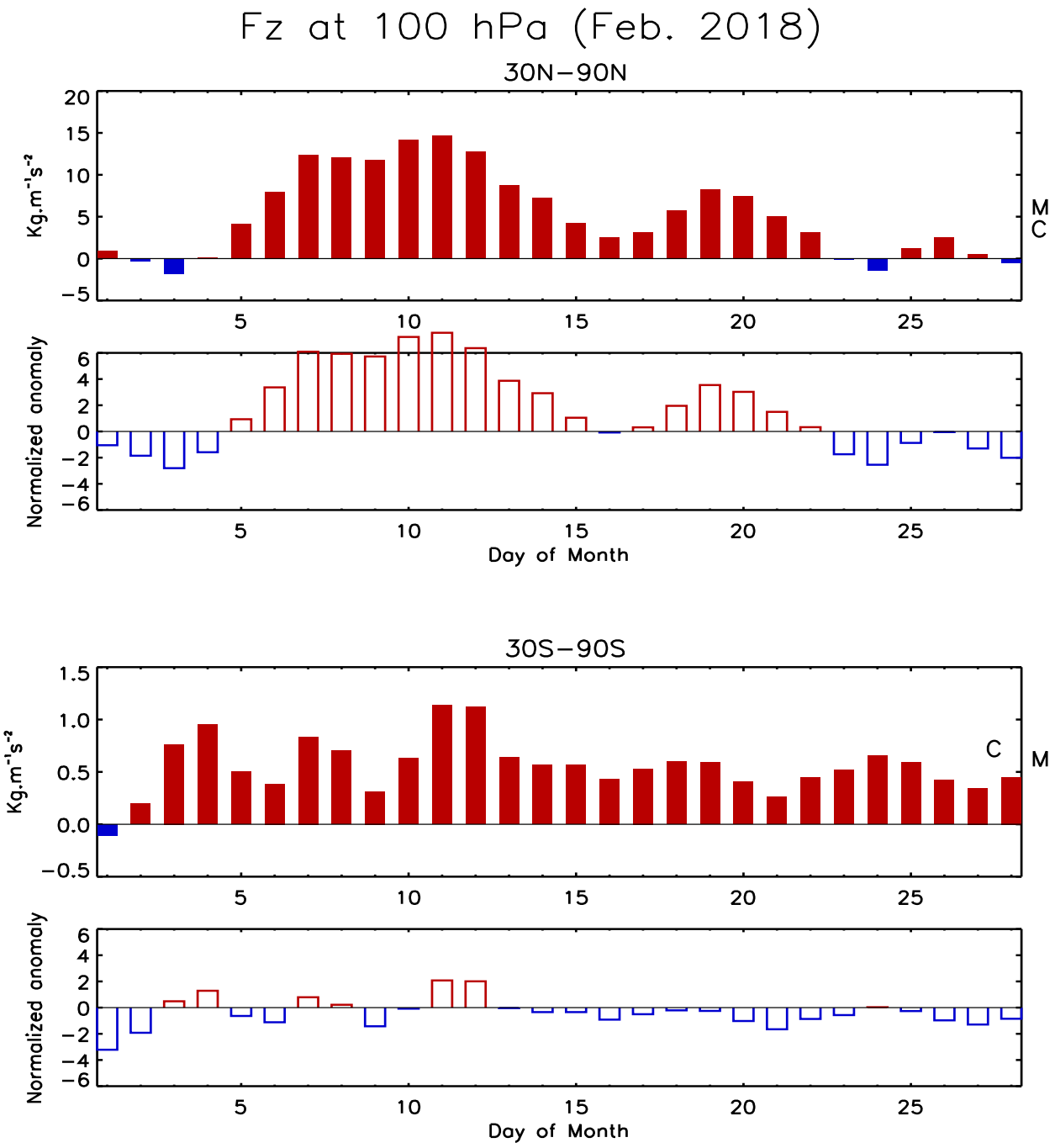


FIGURE S7. Daily vertical component of EP flux (which is proportional to the poleward transport of heat or upward transport of potential energy by planetary wave) at 100 hPa averaged over (top) 30°N–90°N and (bottom) 30°S–90°S for FEB 2018. The EP flux unit (kg $m^{-1}$ $s^{-2}$) has been scaled by multiplying a factor of the Brunt Vaisala frequency divided by the Coriolis parameter and the radius of the earth. The letter 'M' indicates the current monthly mean value and the letter 'C' indicates the climatological mean value. Additionally, the normalized departures from the monthly climatological EP flux values are shown.

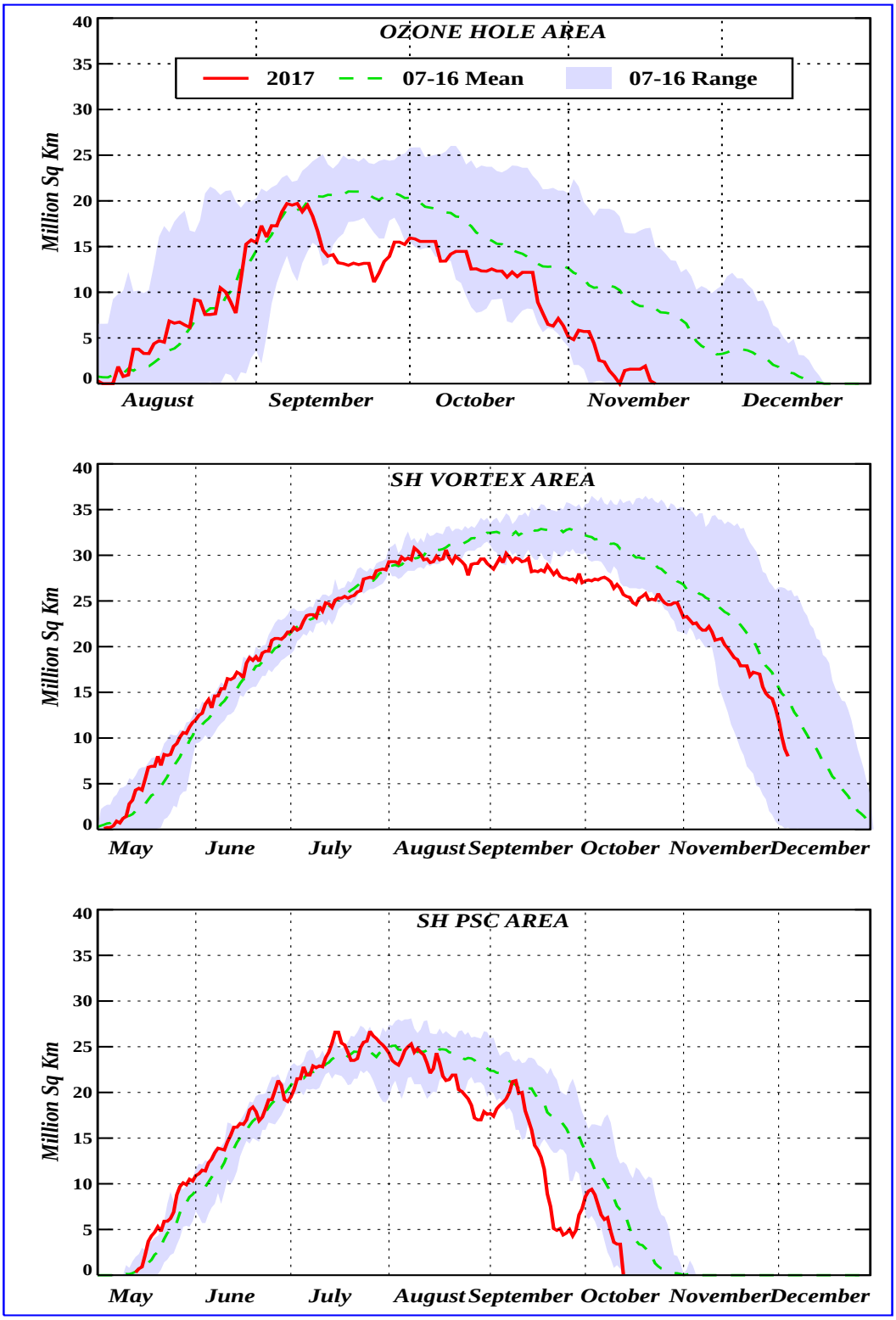


FIGURE S8. Daily time series showing the size of the SH polar vortex (representing the area enclosed by the 32 PVU contour on the 450K isentropic surface), and the areal coverage of temperatures < -78C on the 450K isentropic surface.

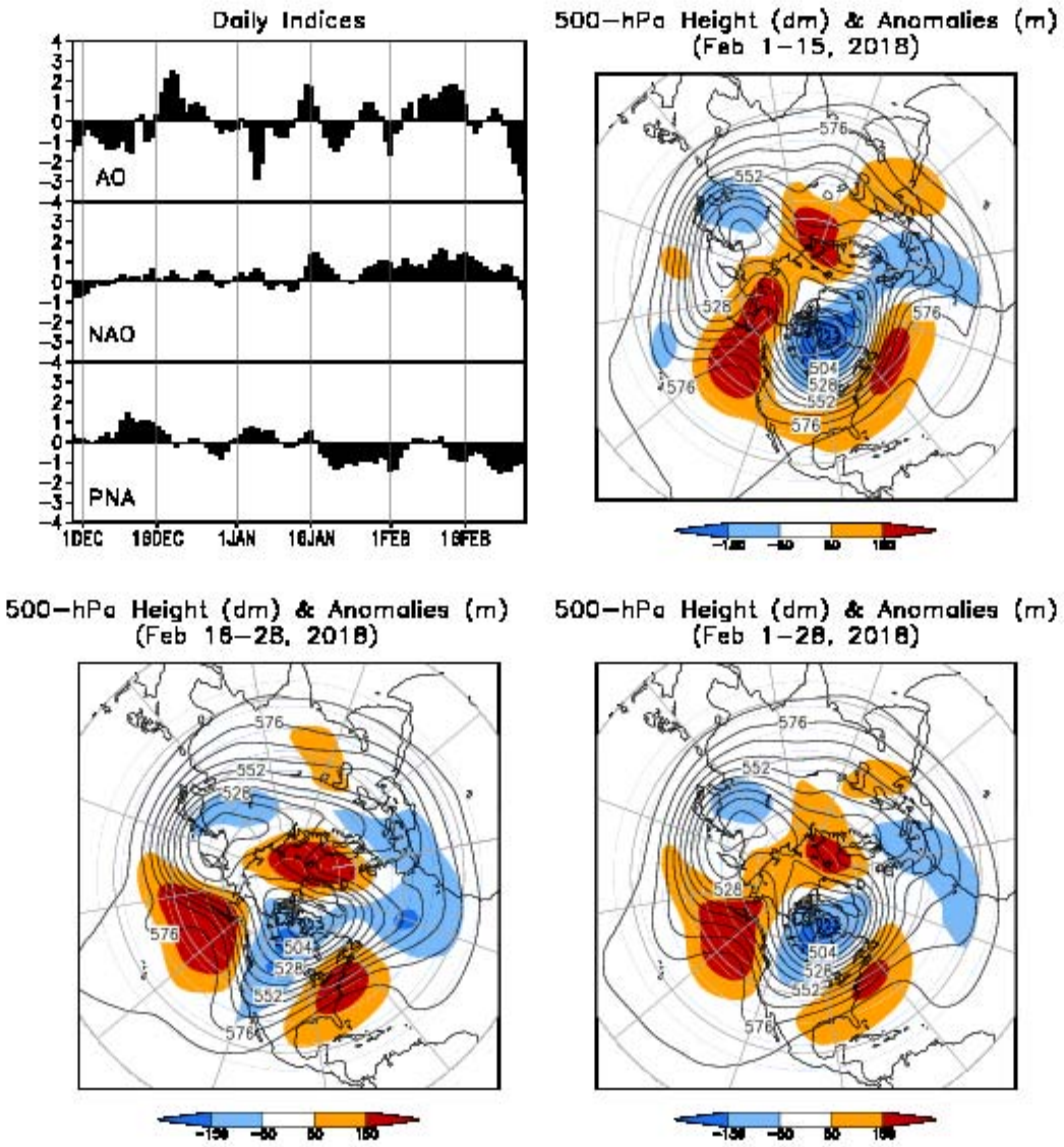


FIGURE A2.1. (a) Daily amplitudes of the Arctic Oscillation (AO) the North Atlantic Oscillation (NAO), and the Pacific-North American (PNA) pattern. The pattern amplitudes for the AO, (NAO, PNA) are calculated by projecting the daily 1000-hPa (500-hPa) height anomaly field onto the leading EOF obtained from standardized time- series of daily 1000-hPa (500-hPa) height for all months of the year. The base period is 1981–2010.

(b-d) Northern Hemisphere mean and anomalous 500-hPa geopotential height (CDAS/Reanalysis) for selected periods during FEB 2018 are shown in the remaining 3 panels. Mean heights are denoted by solid contours drawn at an interval of 8 dam. Dark (light) shading corresponds to anomalies greater than 50 m (less than -50 m). Anomalies are calculated as departures from the 1981-2010 base period daily means.

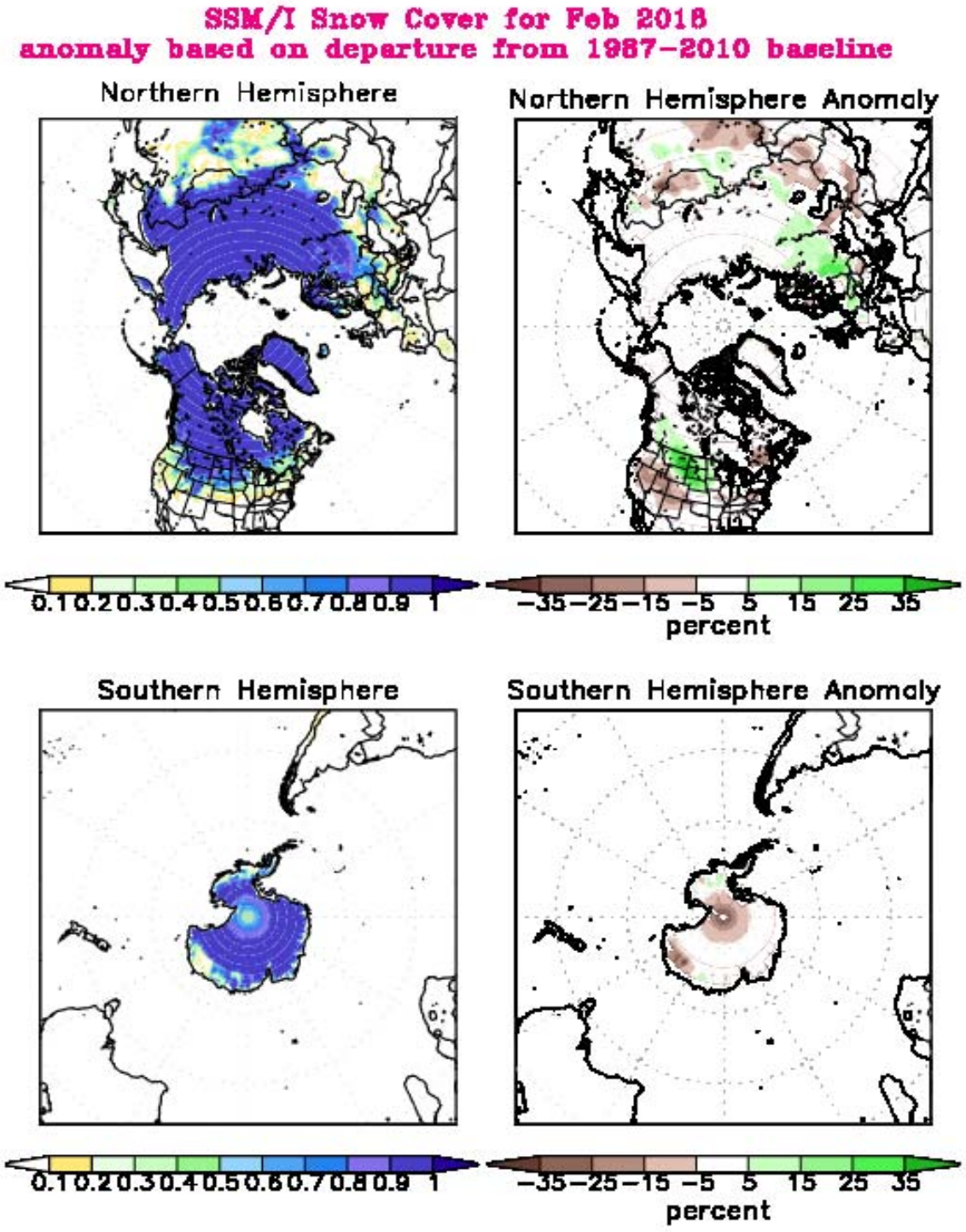


FIGURE A2.2. SSM/I derived snow cover frequency (%) (left) and snow cover anomaly (%) (right) for the month of FEB 2018 based on 1987 - 2010 base period for the Northern Hemisphere (top) and Southern Hemisphere (bottom). It is generated using the algorithm described by Ferraro et. al, 1996, Bull. Amer. Meteor. Soc., vol 77, 891-905.